Pressure Development in Dust Explosions

An experimental study in the 20-liter Siwek sphere and a 0.5 m^3 non-standardized vessel

Camilla Engström Skavland

A thesis submitted in partial fulfilment of the requirements
for the degree of *Master of Science* in the subject of
Physics; Process Safety Technology

Department of Physics and Technology

University of Bergen

Bergen, Norway

June 2018

Abstract

This thesis describes an experimental investigation of pressure development in dust explosions, using two different volumes. The 20-liter Siwek sphere is a standard explosion test apparatus used for determining maximum pressures and maximum rate of pressure rise of an explosion. The other vessel, with a volume of 0.5 m^3 is built from scratch for the same purpose.

The aim is to see whether the same explosion properties are obtained in the two vessels. The scaling law ('cube-root law') at which one determines the severity of an explosion and evaluate mitigation safety measures after, is said to be independent of vessel size. One could therefore expect the same explosion severities in both vessels. Conversely, it is known that several parameters such as chemical composition, particle size distribution and turbulence level will influence a dusts' explosion violence.

Organic dust holding two different moisture contents as well as aluminum dust were tested in both vessels in accordance to the European Standard, and evaluated. In addition, results acquired by GexCon AS from a 25 m^3 vessel were considered and compared to the explosion properties obtained in this work.

It was relevant to investigate validity of the 'cube-root law' with regard to combustion of dusts where thermal radiation is thought to be important, which is typical for aluminum. Thermal radiation can heat up particles faster and farther away from the reaction zone than thermal convection. This may lead to an increase of flame propagation velocity with radius, and thus the explosion violence will indeed be affected by vessel size.

The results showed some deviations in explosion violence when increasing the vessel volume, as did different particle size distributions. However, large discrepancies were observed when altering moisture content and turbulence levels at the time of ignition. Thus, the K_{St}-value seems to be an approximate measure of explosion violence, and should not be blindly trusted when designing mitigation safety measures in the industry.

Preface

The present work is a master thesis submitted as a part of a Master of Science degree in the subject of Process Safety Technology at the department of Physics and Technology at the University of Bergen. The experimental work was carried out at CexCon AS' facilities at Fantoft, Bergen. The work started in the fall of 2017 and was completed in June 2018.

Acknowledgements

Firstly, I would like to thank the University of Bergen and my supervisor Bjørn J. Arntzen for giving me the opportunity to conduct an experimental thesis, and GexCon AS for letting me use their facilities, equipment and brainpower. It has been more challenging and motivating than I could ever have imagined.

I would also like to thank my external supervisor Ivar B. Kalvatn for eye-opening discussions and outstanding guidance during this whole year. His patience has been golden in times when mine has been absent.

Thanks to the mechanics at the workshop at the Department of Physics and Technology for providing me with specially designed equipment necessary for conducting the experiments. To Kjetil L. Olsen and Morten N. Holme for being at disposal for whatever it might be, and to Brian Wilkins for sharing his thoughts and enthusiasm.

Finally yet importantly, my awesome friends who always cheers me on. For sending me encouraging snaps and sarcastic memes, for feeding me and motivating me with a glass of wine (or 5) when times get rough, and for just always being there whenever I need it.

Bergen, June 2018

Camilla Engström Skavland

Table of Contents

List of tables

List of figures

Nomenclature

Abbreviations

BNC	Bayonet Neill–Concelman connector
CFD	Computational Fluid Dynamics
EU	European Union
EN	International Standard
EES	European Economic Area
FLACS	Flame ACceleration Simulator
ISO	International Organization for Standardization
LFL	Lower Flammability Limit
NI	National Instruments
PHRD	Protractor-operated High Rate Discharge
SMD	Sauter Mean Diameter
UFL	Upper Flammability Limit

Latin symbols

A	Area	m^2
A_v	Required vent area	m^2
d_i	Diameter of distribution i	m
d_{50}	Mass median diameter	m
$d_{3,2}$	Sauter mean diameter	m
E_f	Venting efficiency	
E_i	Ignition energy	J
F	View factor	
h	Height	m
I	Intensity	$W \cdot m^{-2}$
k	Correction factor	
K_{St}	Explosibility of dust	$m \cdot bar \cdot s^{-1}$
L/D	Length-to-diameter of the enclosure	
m	Mass of given species	kg
M	Average molecular weight of a given species	kg
n	Number of moles	
p_{ci}	Pressure due to chemical igniters	bar
p_{ex}	Explosion pressure	bar
p_i	Initial pressure	bar
p_{max}	Maximum explosion overpressure	bar
p_{red}	Strength of enclosure	bar
$p_{red,max}$	Maximum reduced explosion overpressure	bar
p_{stat}	Static activation overpressure of the venting device	bar
P	Absolute pressure	bar
$P(t)$	Absolute pressure as a function of time	bar
p_1	Lower pressure point	bar
p_2	Upper pressure point	bar
r	Reflection coefficient	
R	The universal gas constant	$J \cdot mol^{-1} \cdot s^{-1}$
r_o	Chamber radius	m

r_{flame}	Radial position of the flame front	m
$r(t)$	Radius of fireball	m
S_b	Flame speed	$m \cdot s^{-1}$
S_e	Velocity due to expansion of burnt mixture	$m \cdot s^{-1}$
S_f	Flame front speed	$m \cdot s^{-1}$
S_n	Velocity due to change in number of molecules	$m \cdot s^{-1}$
S_u	Burning velocity	$m \cdot s^{-1}$
t	Time	s
T	Absolute temperature	K
T	Absolute temperature of radiating body	K
T_b	Absolute temperature of the burnt gas	K
Ti	Initial absolute temperature	K
T_o	Absolute temperature of absorbing body	K
t_1	Lower time point	s
t_2	Upper time point	s
V	Volume	m^3
$V(t)$	Fractional volume occupied by fireball with respect to time	
$(dp/dt)_{max}$	Maximum rate of explosion pressure rise	$bar \cdot s^{-1}$

Greek symbols

α	Absorption coefficient	
ϵ	Emissivity constant	
ρ_b	Density of burned gas	$kg \cdot m^{-3}$
ρ_u	Density of unburned gas	$kg \cdot m^{-3}$
σ	Stefan Boltzmann's constant	$W \cdot m^{-2} \cdot K^{-4}$
τ	Transmission coefficient	

1 Introduction

1.1 Motivation

Dust explosions present a hazard whenever combustible material is present as fine powder, and can be dispersed in air to form an explosive dust-air cloud in a partly confined or confined volume, and there is an ignition source present. Hence, dust explosions pose a hazard to both personnel and equipment in industries that produce, transport or handle combustible dusts.

Eckhoff (2003) [1] explains that any solid material that can burn in air will do so with a violence and speed that increases with increasing degree of subdivision. Figure 1.1 illustrates three different combustion rates; (a) a piece of wood that burns slowly and is increasing its heat over a long period of time. In (b) the log is cut into several small pieces, the combustion rate increases and the ignition of the wood has become easier. If the log is cut into small particles and the particles are suspended in a sufficiently large volume of air, the combustion rate will be very fast, and the energy required for ignition is very small. Such a burning dust cloud is illustrated in (c) and is a dust explosion [1].

(a) *(b)* *(c)*

Figure 1.1: *Illustration of how the combustion rate of a given rate of combustible solid increases with increasing subdivision, from Eckhoff [1].*

The concept of dust explosions

A dust cloud is a mechanical suspension; a system of fine particles dispersed by turbulence, illustrated in Figure 1.2. When such a dust cloud of combustible material and adequate mass is present in a volume that is confined, or partly confined, and there is an ignition source present, the possibility of a dust explosion exists.

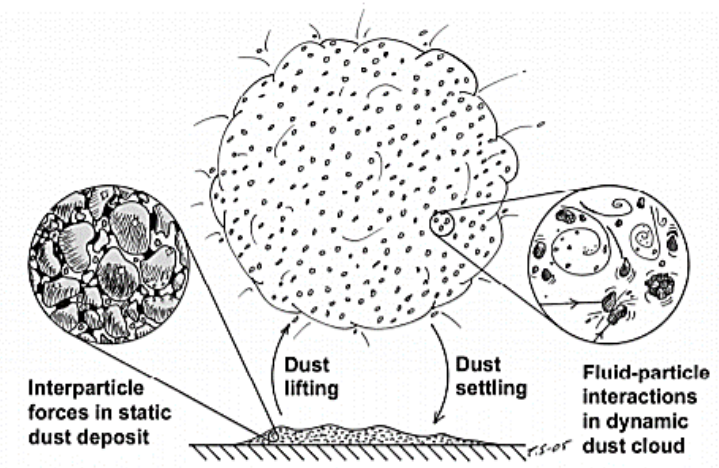

Figure 1.2: *Dust clouds are mechanical suspensions, from Skjold et al. [2].*

The difference between a fire and a dust explosion is illustrated by the fire triangle and explosion pentagon in Figure 1.3.

The fuel can be any solid material that is divided into small particles (in the order of 0.1 mm or less) which is able to react exothermically with an oxidizer, usually air. Flammable dust clouds, i.e. a mixture between dust and oxidizer which is inside a flammable range, are often found inside process equipment, where there is a natural high degree of confinement. In such geometries a release of chemical energy due to a combustion process will contribute to a rapid increase in pressure, which potentially can result in damaging structures and causing fires.

Because material properties have a strong effect on the reactivity of dust cloud, safety parameters, such as the explosion pressure, maximum rate of pressure rise and explosion violence must be tested with representative samples in standardized equipment [3].

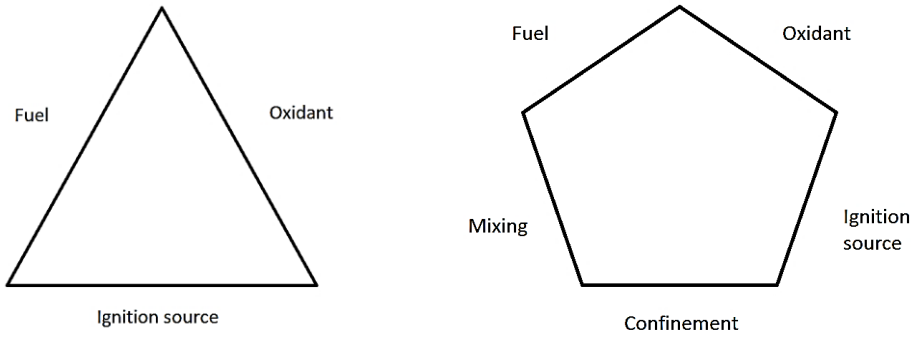

(a) *(b)*

Figure 1.3*: (a) The fire triangle and (b) the explosion pentagon.*

Similar to the combustion process of gases, a dust explosion generally involves oxide formation:

$$Fuel + oxygen \rightarrow oxide + heat \qquad (1.1)$$

But metal powders can also react with carbon dioxide or nitrogen to develop heat for the explosion [4].

Frequency of dust explosions

Far from all dust explosion events are reported in the media, especially not the minor ones. Consequently the historical and statistical reports of dust explosion frequencies are only indicative. Eckhoff [1] examined the detail of 75 dust explosions which occurred in the U.S. between 1900 and 1956, while Jeske and Beck (1989) studied 426 dust explosions from 1965 to 1985. The two studies indicates that only about 15% of occurring dust explosions are recorded [4]. This means that the real number of dust explosions that take place are six times higher than the number of reported accidents.

In later years the understanding of the hazard of dust explosions have grown, but it still occur multiple explosion incidents each week. Dusts that are involved in recorded accidents are both organic, such as fish meal and flour dust, as well metal dusts. The losses from the explosions vary from financial damages only, to much more severe consequences. In April of 2016 an oregano spice explosion occurred in the facilities of High Quality Organics in Nevada, damaging only the hopper that the explosion occurred in. A sugar dust explosion occurred 8 years earlier at the Imperial Sugar Company in Georgia, causing 14 fatalities and 38 injuries [5].

In 2017 a total of 68 dust explosions and 169 fires related to combustible dusts occurred [6]. In accidents where combustible dusts was not the main fuel is classified as "related incidents" by the Combustible Dust Incident Report. An overview of incidents, injuries and fatalities are displayed in Table 1.1.

Table 1.1: *Overview of recorded incidents in 2017, from Combustible Dust Incident Report [6].*

	Combustible Dust Incidents			Related Incidents
	North America	International	Global	Global
Fires	123	37	169	35
Explosions	32	36	68	41
Injuries	61	102	163	441
Fatalities	6	7	13	342

Even though we have come a long way towards understanding the mechanisms of dust explosions, they still present a hazard to both man, environment and equipment.

Prevention and mitigation of dust explosions

The information in this section is collected from *Dust explosion causation, prevention and mitigation: An overview* by Amyotte and Eckhoff [7] unless stated otherwise.

Risk may be defined as the most likely consequence of a hazard, combined with the likelihood or probability of it occurring. There are two strategies for reducing the risk of dust explosions: either we must reduce the probability of a dust explosion occurring, also called prevention, or we must reduce the consequences of a dust explosion when it occurs; mitigation.

Even though dust explosions are more complicated than gas explosions, i.e. the explosion pentagon versus the fire triangle, it is still relevant to eliminate either the ignition source, the combustible material, or the oxygen (inerting) to avoid a dust explosion. This is a probability reducing measure. The explosion pentagon can be used to identify consequence reducing measures, such as venting and isolation. Evidently it is desired that dust explosions are

prevented rather than mitigated, but both measures are likely to be required for a given installation. Dust explosion mitigation and prevention can be organized from most to least effective in terms of measures related to inherent safety, engineered safety and procedural safety.

Probability reducing measures

Inherent safety seeks to remove the hazard itself and involves four principles: Minimization, which includes limitation or removal of dust deposits. Substitution, e.g. replacing the current material with a less reactive dust. Moderation, including altering the composition of a dust by adding inertants or diluting the substance. And finally, simplification; which involves elimination of problems by initial design rather than adding equipment to deal with such problems.

Consequence reducing measures

Engineered safety involves supplement of safety devices at the end of the design, like an automatic dust explosion suppression system. Engineered safety can be divided into two categories; passive and active engineered safety. Passive engineered safety would be physical barriers, explosion venting panels and all other equipment that does not require any activation beyond the initiating event (e.g. dust explosion overpressure) to serve their purpose. Active engineered safety on the other hand, require some kind of detection and activation to execute their function. Such equipment include automatic explosion suppression systems and mechanical isolation valves.

Procedural safety measures control hazards through personnel education and procedures. Such measures include removal of ignition sources from areas where there could be formation of explosible dust clouds, and grounding to provide shock protection.

Although this thesis will not investigate inerting, it is noteworthy that this method of dust explosion mitigation/prevention could be classified either as inherent or active engineering safety depending on the method of use. A collection of means of preventing and mitigating dust explosions can be seen in Table 1.2.

Table 1.2: *Means of preventing and mitigating dust explosions, from Eckhoff [1].*

Prevention		**Mitigation**
Preventing ignition sources, such as:	**Preventing explosible dust cloud:**	
• Smouldering combustion in dust • Open flames • Hot surfaces • Electric sparks/arcs and electrostatic discharges • Heat from mechanical impact	• Dust concentration outside combustible range • Inerting by adding inter gas (N_2, CO_2, Ar,…) • Inerting by adding inert dust (e.g. rock dust) • Intrinsic inerting	• Pressure resistant equipment • Venting • Isolation (sectioning) • Automatic suppression • Partial inerting • Good housekeeping (dust removal/cleaning)

Industries in the EU and EES that are handling potentially explosive atmospheres are required to perform systematic safety work to improve and protect the health and safety of their workers. These regulations and requirements are regulated by the EU Directive 99/92/EC [8]. The Directive emphasizes that in order to prevent and protect against explosions, the employers are to take measures, either technical, organizational or both, to prevent the formation of explosive atmospheres, to avoid the presence of ignition sources or if all goes wrong; to mitigate the effects of the explosion with the health and safety of the workers in mind [8].

Going forth in this work, only consequence reducing measures will be considered. Pressure resistant vessels, explosion venting, isolation and suppression are all mitigation measures and are all dependent on the K_{St}-value. The explosibility is a critical input value when it comes to determining how sturdy equipment should be, or how large the vent area in a vessel would have to be in order to get sufficient pressure release during an explosion.

Domino effect

The satisfactory dust concentration for an explosion to occur outside process vessels are rarely found, hence most dust explosions are initiated inside process equipment (such as mills, hoppers, silos, dryers, and mixers). These are called *primary explosions*. When such an explosion occurs, it may cause the vessel to rupture if it has insufficient pressure release. As important as it is to prevent primary dust explosions, it is just as, if not more, important to reduce the risk of the first explosion causing a series of other explosions; i.e. to prevent 'domino effect'.

If a primary explosion occurs, the following blast wave and flame can stir up a layer of settled dust lying nearby, forming another explosible dust cloud and ignite it as illustrated in Figure 1.4. These *secondary explosions* tend to be even more violent than the primary explosions, and it is therefore crucial to avoid them [4].

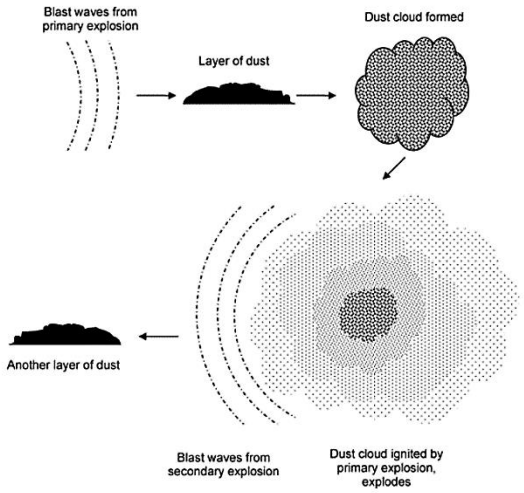

Figure 1.4: *Domino effect in dust explosions, from Abbasi and Abbasi [4].*

Determination of explosion violence

There are large variations in the ignition sensitivity of various combustible dusts, and thereby large variations in their explosion rate. Different standardized tests are developed to determine various parameters of combustible dusts. An important safety characteristic is the explosivity, or the explosion violence of a dust, denoted K_{St}. The K_{St}-value is considered to be constant for a given dust [9], independent of vessel size, and is central in the process of determining mitigation measures when facing a dust explosion. The scaling law in which the K_{St}-value is obtained is called the 'cube-root law' [10]. Dusts are divided into dust explosion classes after their explosion characteristic. The larger the K_{St} the grater the severity of the explosion, ref. Table 1.2.

Table 1.3: *Definition of dust explosion classes, from U.S. Department of Labor [11].*

Dust explosion class	K_{St} **[m·bar/s]**	**Characteristics**
St 0	0	Non-explosible
St 1	$0 < K_{St} \leq 200$	Weak to moderately explosible
St 2	$200 < K_{St} \leq 300$	Strongly explosible
St 3	$300 < K_{St}$	Very strongly explosible

When calculating the K_{St}-value the maximum rate of pressure rise, $(\mathrm{d}p/\mathrm{d}t)_{\max}$, is necessary. A typical pressure-time curve is illustrated in Figure 1.5.

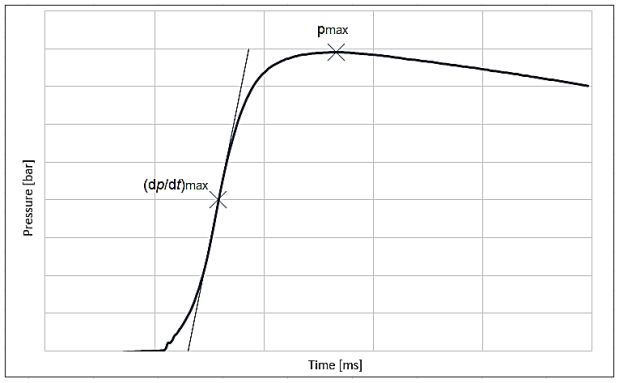

Figure 1.5: *Pressure-time history for a typical explosion test.*

Designing vent areas

Explosion venting is a protective measure for enclosures where intolerable high explosion overpressures are prevented. Weak areas in the walls of the vessel open at an early stage of the explosion, the burning and/or unburnt material and combustion products are released and the overpressure inside the enclosure is reduced. When determining the value of the maximum reduced explosion overpressure, $p_{red,max}$, generated inside the vessel by the vented explosion, the vent area is the most important factor [12]. The basic principle of explosion venting is illustrated in Figure 1.6.

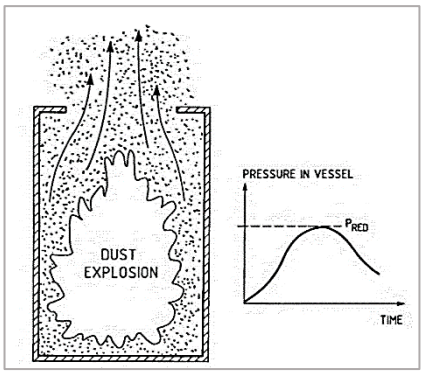

Figure 1.6: *The basic principle of explosion venting, from Eckhoff [1].*

The required area of the vent opening depends on several parameters:

i) Enclosure volume (V)
ii) Strength of enclosure (p_{red})
iii) Static activation overpressure of the venting device (p_{stat})
iv) Maximum explosion overpressure (p_{max})
v) The rate of pressure rise $(\mathrm{d}p/\mathrm{d}t)_{\max}$
vi) Atmospheric conditions
vii) Length-to-diameter of enclosure, L/D

When calculating the size of vent areas for vessels and equipment where dust explosions might occur, the K_{St}-value, or the given explosion class for the dust is used. This poses an issue, when considering that the value may not be constant for a given dust. Therefore, when conducting standardized tests, the explosion severity may be under- or overestimated. As a result of this, as will the explosion hazard, and thereby one would obtain vent areas that are too small or unnecessary large, respectively.

Vent areas for vessels where dust explosions might occur, can be calculated according to the European Standard (EN 14491) [12].

The effects of thermal radiation

All matter with a temperature greater than absolute zero is known to emit thermal radiation due to the thermal motion of the atoms and molecules in the matter. How much a matter or dust radiates, will affect the heat transfer in the combustion zone, the burning rate, and thereby the explosion violence [13]. Since thermal radiation is proportional to the fourth power of the temperature, the overall increase of explosion violence for a radiating dust can be substantial. Yet, the 'cube-root law' does not take this into account, thus making thermal radiation an ambiguous parameter.

1.2 Aim of current work

To prevent lives from being lost and damage being done to environment and infrastructure, it is relevant to investigate whether the 'cube-root-law' is valid. Explosivities obtained in the standard 20-liter Siwek sphere are used when designing risk reducing measures and equipment such as vent areas for industrial sized enclosures. The aim is to examine if changing the volume alters the K_{St}-value when testing aluminum dust in accordance with the standard. In addition the effect of particle size and moisture content will be examined and furthermore the ignition delay time, i.e. the turbulence at the time of ignition will be considered.

Is it possible that the standardized method is not satisfactory, and that the K_{St}-value is indeed dependent of volume, dust properties and the cloud formation process?

2 Theory and previous work

2.1 Definitions and Basic Concepts

2.1.1 Combustion

The information in this section is collected from *Combustion* by Warnatz et al. [14] unless stated otherwise.

Three components are necessary for a combustion to take place; fuel, oxygen and an ignition source, as illustrated in Figure 1.3 (a). To initiate combustion, the fuel and oxygen need to be ignited. Ignition occurs when the heat generation rate in the volume, or in some part of the volume, exceeds the rate of heat loss from the volume. As the temperature continues to rise, it will eventually reach a point where the diffusion of reactants controls the heat rate generation, and a stable state of decomposition is established. The basic principle of ignition is illustrated in Figure 2.1.

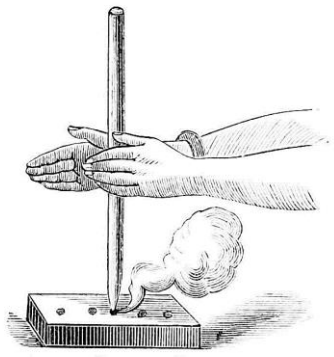

***Figure 2.1**: Man has used the basic knowledge of ignition since the beginning of time, from Youmans [15].*

As described, in a combustion process, fuel and oxidizer are mixed and burned. The process can be simplified to:

$$Fuel + oxygen \rightarrow H_2O + CO_2 \qquad (2.1)$$

Combustion is divided into two main categories based upon whether the fuel and oxidizer is mixed first and then burned (*premixed*) or whether combustion and mixture occur simultaneously (*non-premixed*). Further subdivision is based on whether the fluid flow is laminar or turbulent. An overview can be seen in Table 2.1.

Table 2.1: *Basic flame types, from Warnatz et al. [14].*

Fuel/Oxidizer Mixing	Fluid Motion	Examples
Premixed	Turbulent	Spark-ignited gasoline engine
		Low NOx stationary gas turbine
	Laminar	Flat flame
		Bunsen burner
Non-premixed	Turbulent	Diesel engine
		Pulverized coal combustion
	Laminar	Wood fire
		Candle

A third system also needs to be considered; intermediate systems, such as partially premixed combustion and premixed combustion with non-premixed substructures. The latter represents a *dust explosion*.

2.1.2 Factors influencing ignition sensitivity and explosion violence of dust clouds

A dust cloud is affected by several factors. The most important are gathered from Eckhoff (2003) and discussed here:

1. *Chemical composition of the dust, including its moisture content.*

   Dust chemistry affects both thermodynamics and kinetics, which is related to the amount of heat liberated during combustion and with the rate at which the heat is liberated, respectively. These two aspects are also interconnected to some extent.

   Some dusts, dependent on their chemical composition, will have a large heat of combustion per mole of O_2. This especially applies to non-organic dusts, such as aluminum. Consequently, non-organic dusts will emit a larger portion of thermal radiation than dusts that have a low heat of combustion per mole of oxidizer, and thereby increase both the maximum explosion pressure and the explosibility of explosions when performed adiabatically at constant volume.

   Depending on their chemical nature, the moisture content of dusts will affect the ignition sensitivity and explosion violence of dust clouds; the explosion violence is systematically reduced with increasing dust moisture content. As the moisture content increases in a dust sample, evaporating and heating of water in the combustion represents an inert heat sink. In addition, the water vapor mixes with the pyrolysis gases in the preheating zone of the combustion wave, thus making the mixture less reactive. Lastly, moisture content will enhance the degree of agglomeration in the dust and prevent it from dispersing into primary particles.

2. *Initial temperature and pressure of the gas phase.*

   From the ideal gas law, it is expected that as the initial temperature increases, the maximum explosion pressure, p_{max}, will decrease. This is due to decreasing oxygen concentration per unit volume of dust cloud at a given initial pressure, with increasing initial

temperature. The trend for the maximum rate of pressure rise, $(dp/dt)_{max,}$ is more complex and reflects the complicated kinetics involved.

In addition, the minimum explosible dust concentration decreases with increasing initial temperature.

As for the pressure, p_{max} is close to proportional to the initial pressure. The concentration that yields p_{max} is also nearly proportional to the initial pressure. Furthermore, the explosion violence, the K_{St}-value, seems to increase with increasing initial pressure [16].

3. *Particle size and specific surface area*

The degree of subdivision of the solid is called the specific surface area. Whether the flame propagation across a dust cloud is caused by pyrolysis or an oxidation process, described in section 2.2.1, the particle size plays an important role in the combustion process. For either mechanism, a finer dust size is likely to react faster than a larger particle of the same material. The finer fraction of the dust particles rises a larger threat because of their greater surface area per mass, and therefore react faster. The finer particles also disperse more easily and stay airborne longer. The shape of the particle and the porosity also affects the particle's surface area, and thereby the dust's maximum pressure and rate of pressure rise [16].

As the degree of agglomeration increases, the effective particle size becomes larger, and the effective specific surface area decreases, hence decreasing the explosibility characteristics (Figure 2.2).

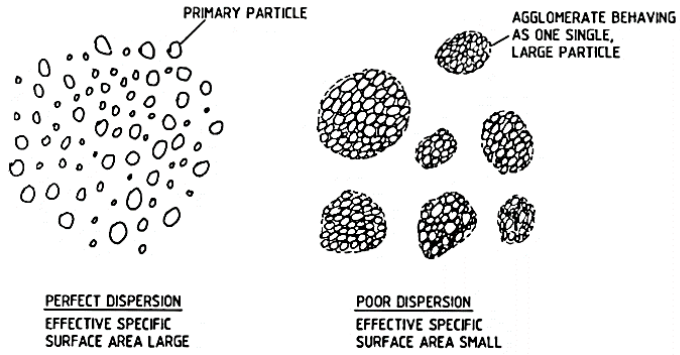

Figure 2.2: *Illustration of (a) a perfectly dispersed dust cloud and (b) a cloud consisting of agglomerations of much larger effective particles sizes than those of the primary particles, from Eckhoff [1].*

In real life situations a wide range of particle sizes can be expected to exist within a batch. Flame propagation will then occur in series; first the flame will propagate toward the smaller particles nearby, yielding a volatile flame. When the small particles are pyrolyzed, the flame will continue to heat the larger particles, establishing a local diffusion flame [17].

4. *Distribution of dust concentration and initial turbulence in an actual cloud.*

Initial turbulence is the turbulence generated by the dust production operations in one's equipment. When conducting a closed bomb dust explosion experiment, the dust cloud is formed by dispersing a given mass of dust by a short blast of air. In the early stages of dust dispersion the turbulence is quite high, and ceases with time as the air from the blast culminates.

A highly turbulent cloud will have more evenly distributed dust concentration, and if ignited will burn with a higher degree of violence. Hence, a higher initial turbulence gives a more violent explosion [4].

5. *Possibility of generation of explosion-induced turbulence in the still unburned part of the cloud and flame front distortion by mechanisms other than turbulence.*

There are two kinds of turbulence, where the first one is initial turbulence. The second kind of turbulence is generated during the combustion process after the dust cloud is ignited, and is induced by the expansion of the unburnt dust cloud ahead of the propagating flame. The turbulence is governed by the speed of the flow and the geometric structure, such as obstacles and vent openings. These structures will enhance the generation of turbulence, and is much greater than the initial turbulence [4].

6. *Radiative heat transfer*

Thermal motion is dependent on the temperature within a gas, and is due to unrestricted movement of particles that has different velocities. The higher the temperature, the greater thermal motion and hence higher intensity and energy of radiation [18]. Theoretically, as the temperature decreases to 0 K the substance now no longer radiates energy because the atomic motion has come to a complete halt.

Thermal radiation net intensity is described as

$$I = F\sigma\epsilon(T^4 - T_0^4) \tag{2.2}$$

Where I is intensity (W/m²), the σ Stefan Boltzmann's constant (W/(m²·K⁴)), ε the emissivity constant, T the absolute temperature of the radiating body, and T_0 the absolute temperature of the absorbing body, both in Kelvin. Eq. (2.2) describes the net heat flux one body with a certain temperature T, radiates another body with a lower temperature, T_0. The view factor, F, takes into account the two bodies' geometries and spatial arrangement of them with respect to each other. The emissivity is the effectiveness of a material's surface to emit energy as thermal radiation [19].

A body's behavior with regard to thermal radiation is characterized by its transmission τ, absorption α, and reflection r as illustrated in Figure 2.3. The sum of these three fractions equals unity, and can be written as

$$r + \alpha + \tau = 1 \tag{2.3}$$

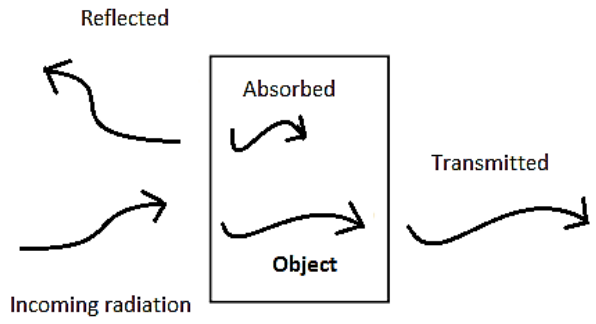

***Figure 2.3**: Radiation regarding an object*

A body that absorbs all radiation is called an absolute black body. A black body is a hypothetical and ideal object, where the transmissivity and reflectivity is zero, and the absorption equals unity according to Eq. (2.3). Real materials emit energy at a fraction of black-body energy levels. By definition, a black body in thermal equilibrium has an emissivity of $\varepsilon = \alpha = 1.0$. A source with lower emissivity independent of frequency is often referred to as a grey body [18]. The emissive power versus wavelength of a theoretical black body, a grey body with emissivity equal to 0.6 and a real body are illustrated in Figure 2.4.

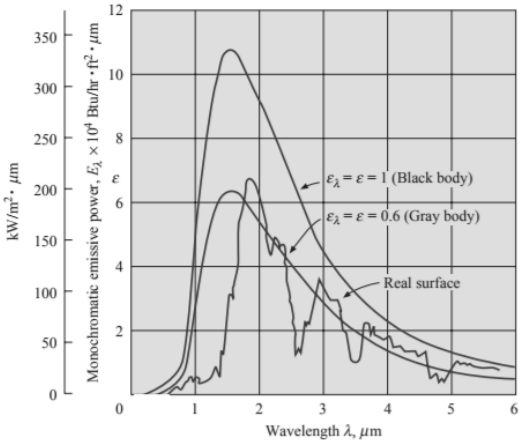

Figure 2.4: *Comparison of black body, grey body, and a real surface, from Holman [19].*

Because of the large heat of combustion per mole O_2 of metals compared to organic dusts, the temperature of the burning particles is significantly higher and the thermal radiation plays a pivotal role in the heat transfer in the combustion wave. Although radiative heat transfer is also supposed to play a role in for example coal dust flames, the effect would be much lower since thermal radiation is proportional to fourth power of the temperature [1].

Factors 1, 2 and 6 can be considered as basic parameters of the explosible dust cloud. Factors 3 through 5, however, depend on the dust cloud formation process and explosion development which in turn are dependent on the nature of the industrial process and the geometry of the system in which the dust cloud burns. The location of ignition point can also play an important role in deciding the course of the explosion.

2.2 Premixed Combustion

Dispersed combustible materials in air can only burn, in the presence of an ignition source, if the fuel concentration (in percentage) is between a defined range; the upper and lower flammability limits, denoted UFL and LFL respectively. A premixed flame is called stoichiometric if fuel and oxidizer consume each other completely, forming only carbon dioxide and water.

Many combustible dusts that are dispersed as a cloud in air and ignited, will allow a flame to propagate through the cloud in a way similar to that of flame propagation through a premixed

fuel-oxidant gas [1]. The correlation of the various parameters influencing a dust explosion pressure can be described by the equation of state

$$pV = nRT = \frac{m}{\overline{M}}RT \qquad (2.4)$$

where the absolute pressure, p, times the system volume, V, is proportional to the temperature, T. The proportionality constants are the number of moles, n, and the universal gas constant, R. Number of moles can be expressed as mass, m, of gaseous species over average molecular weight, $\overline{M}$, of such species. The increase of T due to heat development in the burning dust cloud has the determining influence on the explosion pressure. Consequently as heat of combustion per moles of oxygen consumed increases, so does the likelihood of a severe explosion [1].

2.2.1 Laminar Dust Flames

The information in this section is collected from *Dust Explosions in the Process Industries* by Eckhoff [1] unless stated otherwise.

As mentioned earlier a dust cloud is a system of fine particles dispersed by agitation, and are thereby rarely laminar. Studies of dust flames are customarily performed at two levels: Either the microscopic or the macroscopic level, i.e. combustion of single particles or combustion of an entire cloud of particles, respectively.

When studying the burning of a single particle, there can be made a distinction between two types of dust flames:

i) Nusselt flames

   Controlled by the diffusion of oxygen to the surface of individual solid particles, where the heterogeneous chemical reaction takes place. The greater thickness of the combustion zone in Nusselt type flames, compared with that of premixed gas flames, results from the slower rate of molecular diffusion, compared to diffusion in premixed homogenous gases.

ii) Volatile flames

   Pyrolysis is the controlling process and chemical reactions take place mainly in the homogeneous gas phase. In the volatile flame type, the greater flame thickness is due to the preheating zone, where volatiles are driven out of the particle ahead of the flame. When mixed with air, the gases and vapors burns almost as premixed gas. The combustion of the remaining solid char particles then occurs in the tail of the flame, at slower rate. Hence, the volatile flame in clouds of organic dusts is also in fact coupled to a Nusselt-type flame.

2.2.2 Turbulence

In contrast to laminar flows, turbulent flows are chaotic and unpredictable. They are characterized by continuous fluctuations in velocity, which in turn can lead to fluctuations in density, temperature and composition of the mixture. These fluctuations are a result of vortices, or eddies, generated by shear in the flow. When a transition from laminar to turbulent flow takes

place, the vortices grow as a result of competing forces between the generation process and the destruction process caused by viscous dissipation. For this reason, turbulence appears easier in low viscosity fluids. As the vortices continue to grow the flow becomes three-dimensional and develops to a fully turbulent flow, containing eddies in a large range of sizes. The transition is illustrated in Figure 2.5. Turbulence is needed for dispersion of dust, and turbulence will in turn be generated during combustion of the cloud [14]. If there is no initial turbulence, the dust would settle, and a dust explosion would not be able to take place. It is important to be aware of that turbulent is a property of the flow, not a property of the fluid, and that turbulent flows are hard to define.

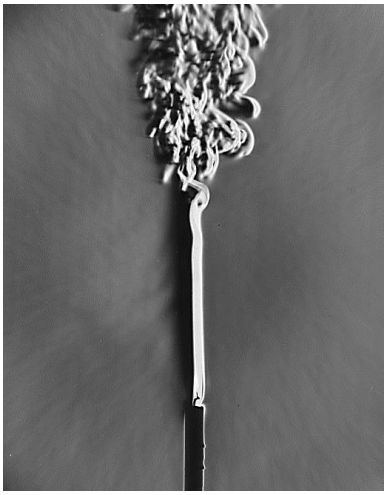

Figure 2.5: *The plume from an ordinary candle transitions from laminar to turbulent flow, from Wikipedia [20].*

In addition to assuming that turbulent flows are continuous and contain structures of eddies, it is possible to identify a few other characteristic properties of turbulent flows [21]:

i) *Irregularity.* Turbulent flows are highly unreliable, and it is therefore no way to describe the motion of the flow in detail. The inherent randomness of turbulent flows create chaos in an unpredictable system. For this reason, turbulence problems are often treated only statistically.
ii) *Diffusivity.* The turbulence in the flow increases the rate of mixing, and thereby enhances the rate of mass, momentum and energy transport.
iii) *Vorticity.* Turbulent flows are characterized by a three-dimensional vortex generation; vortex stretching. In general, this stretching causes thinning of the vortices, causing them to break up into smaller and smaller structures, until the smallest vortices disappear due to viscosity. For this reason, turbulence is always rotational and three-dimensional.
iv) *Dissipation.* To sustain a turbulent flow, there needs to be a transfer of kinetic energy from the flow to internal energy, or molecular motion, by the viscous shear stress. If no energy is added to the flow, the turbulence will disintegrate.

In addition it is often necessary to simplify the assumptions regarding the turbulent flow; the flow is presumed to be homogeneous, isotropic, stationary and incompressible. Since homogeneous and isotropic flows are free from external disturbances like rotation, mean share and magnetic fields, they are of particular significance. In reality all turbulent flows are inhomogeneous, thus making them non-isotropic, time dependent and compressible [21].

2.2.3 Maximum Explosion Pressure at Constant Volume

The European Committee for Standardization has composed a standard for determination of the maximum explosion pressure p_{max} of dust clouds [22]: The maximum explosion pressure determined in closed, spherical (or cubical) vessels with a central ignition source, is defined as the arithmetic mean of the maximum values of the explosion pressure p_{max} of each of the series conducted in an experiment, as shown in Eq. (2.5).

$$p_{max} = \frac{p_{max,[series\ 1]} + p_{max,[series\ 2]} + p_{max,[series\ 3]}}{3} \quad [bar] \tag{2.5}$$

Corrections of the measured explosion pressures in the 20 l sphere

- Correction of the measured explosion pressure $p_{max,\ 20\,l} \geq 5.5$ bar [22]

  A correlation must be made due to cooling effects:

$$p_{max} = 0.775 \cdot p_{max,20l}^{1.15} \quad [bar] \tag{2.6}$$

- Correction of the measured explosion pressure $p_{max,\ 20\,l} < 5.5$ bar [22]

  Due to the small volume in the 20 l sphere, the chemical igniters will have an effect on the pressure. This effect is accounted for in the following equation:

$$p_{max} = \frac{5.5 \cdot (p_{max,20l} - p_{ci})}{(5.5 - p_{ci})} \quad [bar] \tag{2.7}$$

$$p_{ci} = \frac{1.6 \cdot E_i}{10^4} \quad [bar] \tag{2.8}$$

Where p_{ci} is the pressure due to chemical igniters in bar and E_i the ignition energy in joules.

2.2.4 Maximum Rate of Pressure Rise (Explosion Violence)

As for p_{max} a standard has been developed for the determination of explosion violence of dust clouds [9]: The maximum rate of explosion pressure rise $(dp/dt)_{max}$ is defined as the arithmetic mean of the maximum values of the rate of explosion pressure rise $(dp/dt)_{ex}$ of each series as follows:

$$(dp/dt)_{max,20l} = \frac{(dp/dt)_{ex,[series\ 1]} + (dp/dt)_{ex,[series\ 2]} + (dp/dt)_{ex,[series\ 3]}}{3} \quad [bar \cdot s^{-1}] \tag{2.9}$$

$(dp/dt)_{max}$ depends on the volume, and decreases with increasing volume.

2.2.5 K_{St} and the 'Cube-Root Law'

The maximum explosion pressure and the maximum rate of pressure rise characterize the total energy release and the rate of reaction in dust explosions, respectively. As stated in the previous section, $(dp/dt)_{max}$ depends on the volume, and decreases as the volume increases, whereas K_{St} or K_{max} is employed to be volume independent [9]. In order to normalize the

maximum rate of pressure rise, scaling relationships are required. The most frequently used scaling law is the '*cube-root law*', introduced by Bartknecht in 1971 [23]:

$$(dp/dt)_{max} \cdot V^{\frac{1}{3}} = cons. \equiv K_{St} = K_{max} \quad [bar \cdot m \cdot s^{-1}] \tag{2.10}$$

For all practical purposes this means that one could obtain explosibilities for industrial enclosures by using small-scale test vessels.

Since air consists mainly of nitrogen, negligible change in number of moles of gas during combustion is assumed when applying the K_{St}-value. Hence, as an approximation of Eq. (2.4), a rapid combustion reaction in a closed system results in:

$$\frac{p_{max}}{p_0} = \frac{T_b}{T_0} \tag{2.11}$$

Where p_{max}, p_o, T_b and T_o are the maximum absolute explosion pressure, the initial absolute pressure, the absolute temperature of the burned gas and initial absolute temperature respectively. If the number of moles changes drastically, either due to chemical reactions in the combustion process or due to venting of the volume, so will the maximum explosion pressure [16].

The absolute pressure as a function of time, *p(t)*, in a spherical constant volume vessel is related to the fractional volume, *V(t)*, occupied by the fireball throughout the time of propagation, *t*, is written as:

$$\frac{p(t)-p_0}{p_{max}-p_0} = k\frac{V(t)}{V_0} \tag{2.12}$$

Where p_o is the same initial absolute pressure as in Eq. (2.11), V_o the volume of the vessel, and k a correction factor related to the difference in compressibility between the burned and unburned gases. If the flame propagates spherically from a point source, we have:

$$\frac{V(t)}{V_0} = \left[\frac{r(t)}{r_0}\right]^3 = \left[\frac{S_b t}{r_0}\right]^3 \tag{2.13}$$

where *r(t)* is the radius of the fireball, r_o the radius of the chamber and S_b the flame speed given by:

$$S_b = \frac{dr(t)}{dt} = \left(\frac{\rho_u}{\rho_b}\right) S_u \tag{2.14}$$

The flame speed, S_b, is relative to a stationary reference point, and $\frac{\rho_u}{\rho_b}$ is the density ratio between the unburned to burned gases at constant pressure. The burning velocity, S_u, is the rate of the flame propagation relative to the unburned gas in front of it. Both S_b and S_u are for turbulent conditions for dust explosions. As the Eq. (2.12) is to be solved with respect to time, it is rewritten as:

$$p(t) = k\frac{V(t)}{V_0}(p_{max} - p_0) + p_0 \tag{2.15}$$

Making use of the chain rule for Eq. (2.13), i.e. $dr(t)/dt = (r(t)^2/r_0^3) \cdot (dr(t)/dt)$ and substituting this and Eq. (2.14) into Eq. (2.15), which is now differentiated with respect to time, gives:

$$\frac{dp(t)}{dt} = 3k(p_{max} - p_0)\frac{r(t)^2\,\mathrm{d}r(t)}{r_0^3\ \ \mathrm{d}t} = 3k(p_{max} - p_0)\left(\frac{\rho_u}{\rho_b}\right)S_u\frac{r(t)^2}{r_0^3} \qquad (2.16)$$

For spherical propagation in a spherical vessel, the maximum pressure is reached just as the flame comes in contact with the wall. At that instant the correction factor, k=1, and the radius of the fireball is equal to the vessel radius:

$$r(t) = r_0 = (3V/4\pi)^{1/3} \qquad (2.17)$$

By the assumption that number of moles of gas will be constant for this ideal situation (Eq.2.11), one can also assume that

$$\frac{\rho_u}{\rho_b} \approx \frac{T_b}{T_0} \approx \frac{p_{max}}{p_0} \qquad (2.18)$$

We get

$$\frac{dp(t)}{dt} = 3(p_{max} - p_0)\left(\frac{p_{max}}{p_0}\right)S_u\frac{\left(\frac{3V}{4\pi}\right)^{\frac{2}{3}}}{\left(\frac{3V}{4\pi}\right)^{\frac{1}{3}}}$$

$$= 3\left(\frac{4\pi}{3}\right)^{\frac{1}{3}}(p_{max} - p_0)\left(\frac{p_{max}}{p_0}\right)S_u\left(\frac{1}{V}\right)^{\frac{1}{3}} \qquad (2.19)$$

And finally

$$K_{St} = \left[\frac{\mathrm{d}p(t)}{dt}\right]_{max}V_0^{1/3} = 4.84\left(\frac{p_{max}}{P_0} - 1\right)p_{max}S_u \qquad (2.20)$$

Eq. (2.20) is the deduced 'cube-root law', and the K_{St} is the size normalized maximum rate of pressure rise. The model on which the scaling law is based on, called the thin-flame model, assumes that the content of the vessel during an explosion consist of a completely burnt mixture surrounded by an outer region with completely unburnt mixture, separated by an infinitely thin spherical flame front [16]. Figure 2.6 illustrates this principle, where after ignition the flame front moves through the dust cloud with the flame speed, S_f. This velocity is the sum of the velocity due to expansion of the burnt mixture, S_e, the velocity due to due to the change in number of molecules from unburnt to burnt mixture, S_n, and the burning velocity, S_u. *r(t)* is the radius of the fireball as described in Eq. (2.13), propagating outwards [10]. Note that the thin-flame model is not for the ideal case since the number of molecules changes from unburnt to burnt mixture.

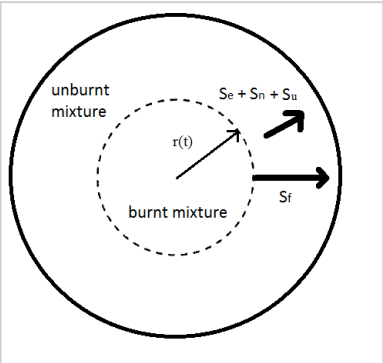

Figure 2.6: *The thin-flame model.*

The 'cube-root law' is only valid as a scaling correlation under hypothetical circumstances [21]:

i) The mass burning rate for the unburnt and burnt mixtures should be the same for both test vessels. This condition is satisfied when:
   a. The vessels are geometrically similar, preferably spherical.
   b. Point ignition at the center of the vessels with negligible energy input, followed by spherical flame propagation towards the walls.
   c. The flow properties should be identical in both vessels.
   d. Changes in temperature, pressure and turbulence have the same effect on the burning velocity in both vessels during the explosion.
   e. There should be no noteworthy net flow in the vessels at the time of ignition.

ii) The thickness of the flame should be negligible compared to the radius of the vessels.

If chemically identical mixtures are ignited in two different sized vessels holding identical conditions for temperature, pressure and turbulence, and changes in these conditions would be the same during the course of an explosion in these two vessels, one would measure identical maximum explosion pressures. Since the maximum rate of pressure rise is multiplied by the cube root of the vessel volume to yield the K_{St}-value, one can obtain the maximum rate of pressure rise of the other vessel (i.e. a plant unit) by dividing the found K_{St}-value by the cube root of its volume. This way of obtaining the maximum rate of pressure rise in different sized vessels is totally dependent on the validity of the 'cube-root law' [24].

Maize starch reacts with oxygen to form only water and carbon dioxide as follows [25]:

$$C_{27}H_{48}O_{20\,(S)} + 23O_{2\,(G)} + 86.5\,N_{2\,(G)} \rightarrow 12H_2O_{(G)} + 27CO_{2\,(G)} + 86.5\,N_{2\,(G)} \qquad (2.21)$$

This is an increase in number of moles of 15 %, but is still treated ideally the assumption made in Eq. (2.18).

2.2.6 Aluminum Dust Explosions

As mentioned before, all substances that holds a temperature above the absolute zero, emit thermal radiation. Aluminum is one of the dusts that has a large heat of combustion per moles of O_2, and will thereby emit more thermal radiation than those who have a low heat of combustion per mole of oxidizer. How much a matter or dust radiates, will affect the heat transfer in the combustion zone, the burning rate, and consequently the explosion violence. Since thermal radiation is proportional to the fourth power of the temperature, from Eq. (2.2), the overall increase of explosion violence for a radiating dust can be substantial. Although it does not seem to be particularly reactive, aluminum is considered a highly active metal.

The aluminum surface is protected by a layer of oxide (Al_2O_3), or alumina, which forms spontaneously in contact with air. This solid-phase layer protects the core, and will affect the ignition characteristics of aluminum [26].

The ignition and combustion processes of aluminum are complicated, and several studies have been conducted to try to find the answers. Although there are some similarities in their observation, it looks like the processes in question are strongly dependent on particle size and temperature.

For aluminum the assumption made in Eq. (2.18) is not valid for a non-ideal situation as the number of moles decreases by from 7 to 2 moles after combustion. The phases in which aluminum is consumed and alumina is formed depends on the combustion temperature. The balanced equations for aluminum are as follows [26]:

$$4Al_{(S,L)} + 3O_{2\,(G)} \rightarrow 2Al_2O_{3\,(S,L)} \tag{2.22}$$

$$Al_2O_{3\,(L)} \leftrightarrow Al_2O_{3\,(S)} \tag{2.23}$$

2.3 Previous Work

Up until 1985 the only internationally accepted apparatus for dust explosion testing was the ISO 1-m³ vessel [27]. This large vessel required much work and large quantities of powder. Siwek (1977) developed a smaller spherical vessel of 20 liters that would require much less maintenance and 50 times less powder. The problem however, was to obtain the same K_{St}-value in both vessels. Since dusts need to be airborne at the time of ignition to cause an explosion, both vessels had a blast system to initially suspend the particles, causing turbulence. Since the burning rate is dependent on turbulence, one needs different ignition delay times in the different sized vessels to gain the same magnitude of turbulence [24].

In 1989 Bartknecht [28] presented experimental results which showed that K_{St}-values found using the Siwek sphere was identical to those found for the 1-m³ vessel when using ignition delay times of 60 ms and 600 ms, respectively. Thus, greatly reducing the cost of dust explosion severity tests involving more expensive powders (such as pharmaceuticals).

Although Bartknecht and Siwek had presented experimental evidence for the validity of the 'cube-root law', other researchers have questioned the universality of it when it comes to different volumes, and different theories have been presented.

Proust et al. [29] tested several dusts to determine explosion indices in the 20-liter Siwek sphere and the ISO 1-m³ vessel, and compared the results. An outstanding observation was made;

a dust could have a significant explosion severity in the 20-liter vessel, while not even being explosible in the larger vessel. This could suggest that the ignition energy from the chemical igniters is forcing the explosion in the smaller vessel by increasing the initial temperature by several degrees.

2.3.1 Flame thickness

When using the thin-flame model, discussed in section 2.2.5, one of the assumptions for the model to be valid was the thickness of the flame should be negligible compared to the vessel radius. Numerical simulations have shown that the 'cube-root law' becomes inaccurate when the relative flame thickness surpasses 1 %. Reported flame thicknesses suggest a thickness up to 80 cm, which exceeds the radii of both the Siwek sphere and the 1-m³ vessel [10].

Dahoe et al. (1996) [10] developed a three-zone model that takes the flame thickness, δ, into account (Figure 2.7). The flame zone is assumed to be linear with position, ranging from completely burnt mixture to completely unburnt mixture.

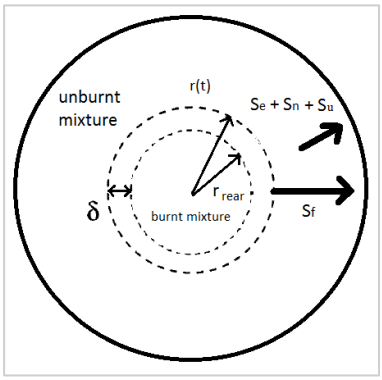

Figure 2.7: *The three-zone model.*

In general, simulations of explosions with increasing flame thicknesses alters both the time-pressure curves, and the curves for $(dp/dt)_{max}$, and consequently the K_{St}-values; as the flame thickness increases and the vessels get smaller, the K_{St}-value steadily declines (Figure 2.8 (a)). This indicates that explosion testing of dusts consisting of large particles with a low burning rate in small vessels, e.g. the 20-liter sphere, results in K_{St}-values which are too low [10]. Even though the conditions in the different vessels are identical, the K_{St}-value is not. Dahoe et al. suggest that usage of the 'cube-root law' is important, but that the effect of flame thickness should be taken into account. By plotting K_{St}-values as a function of the relative flame thickness δ/R, i.e. the flame thickness divided by the vessel radius, at constant burning velocities, this can be achieved (Figure 2.8 (b)).

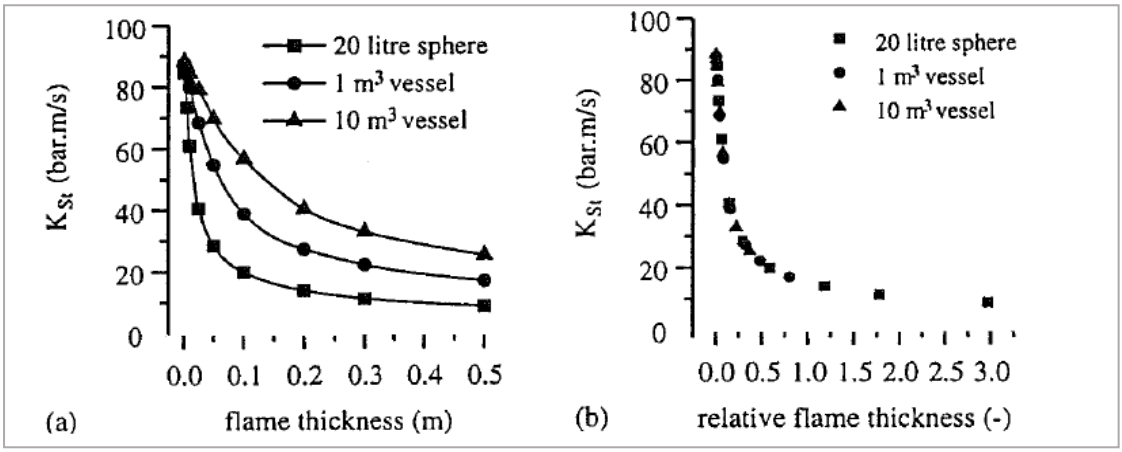

Figure 2.8: *(a) Kst-value as a function of the absolute flame thickness (b) K_{St}-value as a function of the relative flame thickness, from Dahoe et al. [10].*

Figure 2.8 (b) shows that that the values for the different sized vessels form a single curve. The figure now represents K_{St}-values which are independent of both flame thickness and vessel size.

2.3.2 Ignition delay time

Dahoe et al. [24] studied the decay of turbulence in the 20-liter explosion sphere using Laser Doppler anemometry, and compared it to the turbulence level in the 1-m³ vessel. The results showed that the K_{St}-value in the 20-liter sphere for ignition delay time of 60 ms was not in agreement with the K_{St}-value found in the 1-m³ vessel at 600 ms. However, they found that, although they did not measure it explicitly, similar turbulence existed in the two vessels when ignition delay time in the 20-liter sphere was 165 milliseconds.

A similar observation was made by van der Wel et al. [30] when they carried out turbulence measurements using hot-wire anemometry in the same two vessels. When using the 600 ms ignition delay in the 1-m³ vessel, they observed similar behavior in the 20-liter sphere at delay times of 150-180 ms, which is much longer than the 60 ms described in the standard.

Pu et al. [31] and Dahoe et al. [32], which used hot-wire anemometry and laser Doppler anemometry respectively, both found that the ignition delay time in the 20-liter sphere should be equal to 200 ms to match the turbulence level of the 1-m³ vessel (with ignition delay time of 600 ms).

Enright [33] conducted similar experiments in three closed vessels of different sizes. The same principles of dispersion systems were used in all vessels, and three different dusts were tested; lycopodium, wheat starch and aluminum powder. The same trend was observed for all dusts, with the lowest K_{St}-value found in the smallest volume of 1.2 liters, and the largest K_{St}-value was obtained in the largest volume of 20 liters.

Eckhoff [1] stresses that the K_{St}-value "remains an arbitrary measure of the explosion violence. K_{St} is not a specific dust constant but clearly also a function of the special test conditions in the ISO standard test. On the other hand, the K_{St}, as defined by the ISO, seems to provide a reasonable relative measure for ranking the explosion violence to be expected from various dusts in industrial dust explosions".

2.3.3 Dust dispersion systems

When determining explosibility characteristics a known mass of dust is dispersed into the test chamber by a blast of air. It is assumed that the dust cloud has a uniform concentration throughout the vessel, though this is hardly the case in real life situations. Since explosion properties are dependent on the turbulence level, it is important that the dispersion system and the ignition delay time is fitted to the vessel, so that the turbulence level at the time of ignition is known, not too high, but still high enough to keep the dust airborne at the time of ignition.

For the standard 1-m³ vessel, a semicircular spray pipe is mounted parallel to the wall. The spray pipe is fitted with holes of a diameter of 6 mm, or 5 mm, to disperse the dust. For coarse, voluminous or poorly flowing dust samples, the spray pipe may not be able to scatter the dust evenly throughout the volume, and special dust disperses, such as the rebound nozzle or dispersion cup, may be necessary [22]. The standard dispersion nozzle for the 20-liter vessel is the rebound nozzle. The initial flow patterns of the perforated semicircular pipe and the rebound nozzle are illustrated in Figure 2.9.

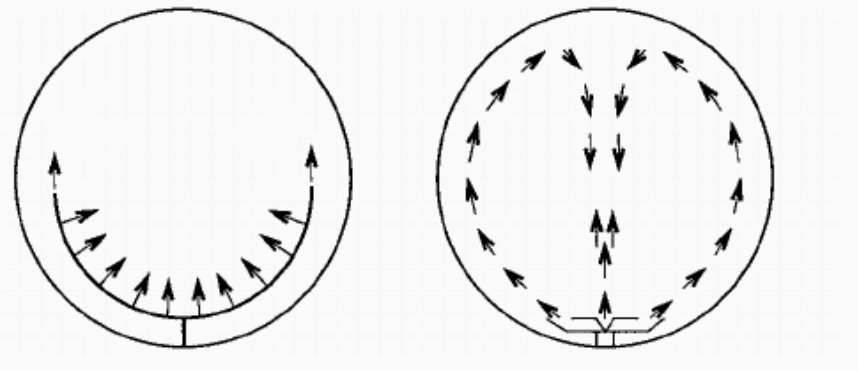

Figure 2.9: *Initial flow patterns of the perforated semicircular spray pipe (left) and the rebound nozzle (right), modified illustration from Dahoe et al. [24].*

2.3.4 Thermal Radiation

Moussa et al. [26] reviewed the combustion mechanisms in aluminum dust-air mixtures, and optical properties of burning aluminum particles and alumina were determined based on Mie scattering solutions. The results showed that both aluminum and alumina are weak emitters but exceptional scatterers, and they can thereby contribute to extensive thermal radiation.

Marion et al. [34] observed that the size of the aluminum particles after combustion were almost the same as the original size before combustion and that very high combustion temperatures can be attained. From this observation Moussa et al. [26] then states that the combustion and exploding of aluminum dust-air mixtures may be in the category of thermal radiation dominated flames.

Proust [35] showed that for dusts that gasify at low temperatures, laminar flame fronts exists and the propagation is similar to that of premixed gaseous flames. For these types of dusts, radiation plays little to no role since no particles are present in the combustion zone. Other powders that have high gasification temperatures, such as aluminum, have particles present in the burnt products that radiate towards the reactants, increasing the total heat exchange. These results are then in compliance with the observation made by Moussa et al.

Proust et al. [36] investigated radiation in dust flames using methane-air mixtures, to which they added different dusts. When inserting alumina, the radiative flux is reduced in proportion to the concentration of the dust added. This phenomena proposes that the particles are absorbing the heat from the flame, acting as heat sinks. Because of the much longer heating time of the particles compared to characteristic heating time in the gaseous phase, the particles are almost not heated in the flame front, and thereby the temperature may not increase sufficiently for the particles to radiate notably.

In the same study Proust et al. also added (rather coarse) aluminum particles to the methane-air mixture. Neither these particles seemed to radiate much, even less than stoichiometric methane-air mixtures [36].

3 Experimental set-up and procedure

In this chapter experimental set-up and procedures are described. Most of the equipment was already available at GexCon AS' facilities at Fantoft, Bergen, where the experiments were conducted. Specialized equipment such as the dispersion nozzle for the 0.5 m^3 vessel had to be acquired. The experimental results will be discussed in Chapter 4.

The experiments include two explosion vessels of volumes 20 and 500 liters. The dusts used in the experiments are the organic dust maize starch with two different moisture contents, as well as the metal aluminum.

3.1 Experimental set-up 20-liter sphere

The 20-liter sphere was already in place in a ventilated laboratory hood upon arrival in accordance with the European Standard [22], see Figure 3.1. The vessel had been cleaned and ventilated for a few days to avoid formerly used dust to influence the experiments.

3.1.1 Explosion chamber

The explosion chamber is a hollow sphere with a volume of 20 dm^3. The vessel is made of stainless steel and is designed to be explosion resistant. The chamber is equipped with a water jacket for cooling of the vessel between tests. The dust dispersion chamber is connected to the vessel via an inlet at the bottom, where pressurized air push the dust through a rebound nozzle. The fast acting valve for dispersion is opened and closed pneumatically, and the ignition source is positioned in the center of the vessel. For measuring the pressure development during an explosion, two pressure sensors are mounted on the chamber.

***Figure 3.1**: 20-liter explosion chamber, from Cesana-AG [37].*

3.1.2 Data acquisition and triggering system

The control system for the Siwek sphere is fully automated and is made up of two units; one control unit (KSEP 310) and a measurement and control system (KSEP 332), in addition to the acquisition and analysis software (KSEP 6). The system is provided by the manufacturer of the 20-liter sphere, Kühner AG.

The KSEP 332 controls the valves and ignition source, as well as receives signals from the pressure sensors. It is connected to the computer software, and relays signals between the software, the KSEP 310 unit and the explosion chamber. The two independent systems provide extra security to the measured results. KSEP 6 receives the signals form the KSEP 332 unit and analyses them. The software provides information about maximum pressure, maximum rate of pressure rise and explosivity for each test, as well as for a whole series. KSEP 6 draws curves for both p_{max} and (dp/dt) as a function of concentration as shown in Figure 3.2.

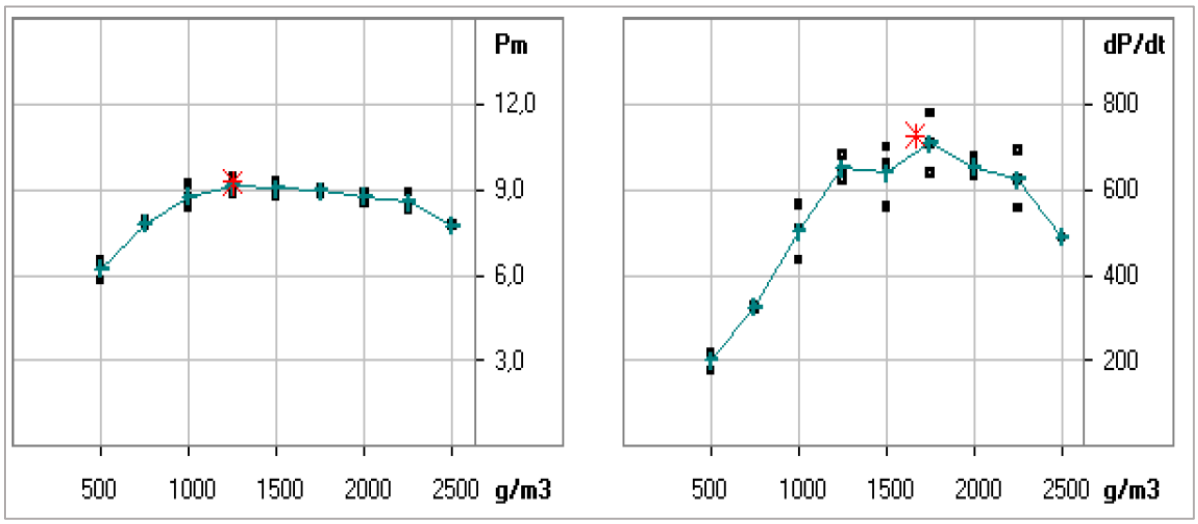

Figure 3.2: *Graphs obtained from the KSEP 6 software for three series of dehydrated maize starch in the 20-liter sphere.*

3.1.3 Dispersion system

The dispersion system consists of a dust container, inlet valve, connecting tube and dust disperser. The dust is loaded into the dust container having a volume of 0.6 dm³ and an aspect ratio of 3:1. The dust container is designed to tolerate an overpressure of at least 20 bar. A pneumatically activated valve separate the dispersion chamber from the vessel. Prior to dispersion, the explosion chamber is evacuated to 0.4 bar to ensure that the pressure in the sphere after dust dispersion is equal to the initial pressure (p_i = 1 013 bar). The dust exits the container through the connecting tube at the base, and is dispersed into the explosion chamber through a rebound nozzle (Figure 3.3).

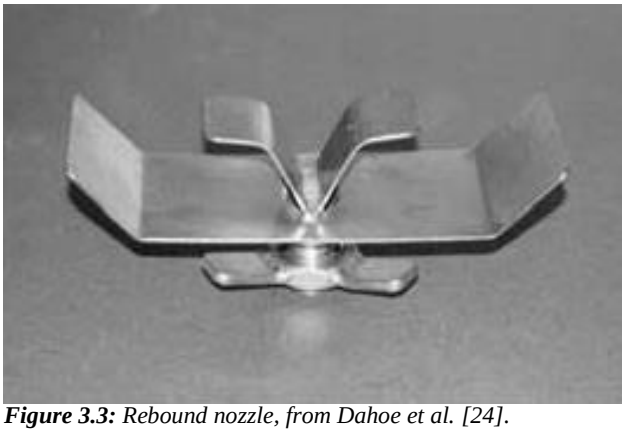

Figure 3.3: *Rebound nozzle, from Dahoe et al. [24].*

A schematic of the rebound nozzle can be viewed in Appendix B.

3.1.4 Ignition source

The ignition source includes two chemical igniters (EBBOS ChZ), each having an energy of 5 kJ, yielding a total mass of 2.4 g. The igniters are placed at the center of explosion chamber, firing in opposite directions. The power supply circuit is according to the European Standard [22] capable of firing the fuse heads in less than 10 ms. The igniters are delivered by Fr. Sobbe GmbH (Figure 3.4) [38].

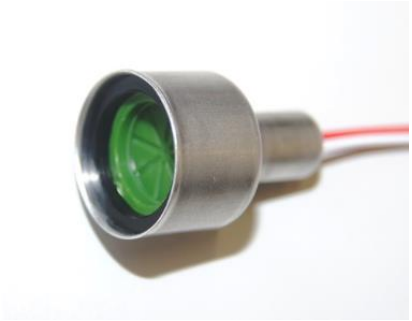

Figure 3.4: *EBBOS ChZ igniter used as ignition source in the 20-liter Siwek sphere, from Fr. Sobbe GmbH [38].*

3.1.5 Pressure measurement system

The two pressure transducers are fitted on the 20-liter sphere via a 30-mm flange. The tranducers are from Kistler (type 701A, with pressure range 0-250 bar). They generate an electrical signal as a function of the pressure exerted on the quartz crystal from the explosion chamber, and is given by force per unit area. The electrical signal is sent to the computer via the KSEP 332 unit and is converted back to pressure values. The Kistler 701A and the principal of a piezoelectric pressure transducer can be seen in Figure 3.5.

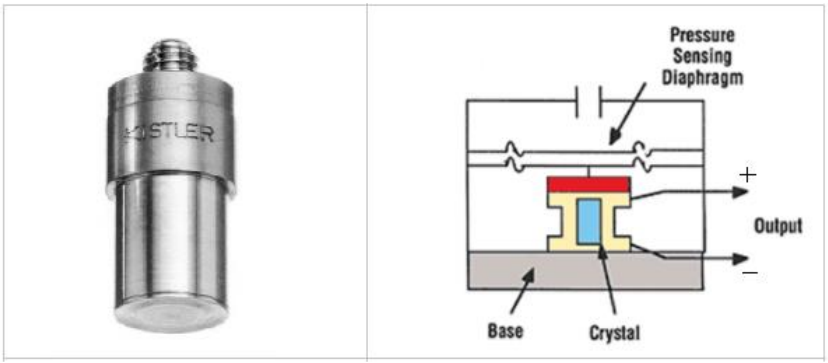

(a) *(b)*

Figure 3.5: *Piezoelectric pressure transducer. (a) Kistler type 701A, from Intertechnology Inc [39]. (b) Principal of pressure exerted on the quartz crystal which converts the force to an electrical output, from Sensormag [40].*

3.2 Experimental set-up 0.5 m^3 explosion chamber

The 0.5 m^3 have previously been used by Gault [41], and had an additional 0.7 m^3 add-on for testing of explosion vent panels. The equipment used by Gault had been dismantled and the system was built from scratch. The new set-up is shown in Figure 3.6.

Figure 3.6: *Experimental set-up of the 0.5 m^3 vessel.*

3.2.1 Explosion chamber

The explosion chamber used for the large-scale experiments is a 0.5 m^3 cylinder with an aspect ratio close to 1:1. There are several threaded and unthreaded holes in the chamber so that one may mount whatever equipment and measurement apparatus necessary for the experiments. The chamber is fitted with a dispersion system, two pressure sensors, a vacuum pump, ignition source holder, exhaust system and a digital pressure indicator.

3.2.2 Data acquisition and triggering system

A data acquisition system module of the type NI USB-6259 from National Instruments was set up for a systematic test sequence and data collection. The NI card is connected to a computer

via a USB port and the test sequence, i.e. the triggering and logging of the experiment, is set up in LabVIEW. Digital output ports on the card are used to control the triggering of the pressure measurements, dispersion and ignition. The data acquisition is done through analog input channels. The triggering signals are sent to a trigger box using 5 V BNC-cables which in turn triggers (through crydom relays) the explosive charge for dispersion and the chemical igniter with 24 V signals amplified via a 24 V power source. The trigger box also sends a signal to a Releco MR-C relay which in turn switches on the charge amplifiers for the pressure logging. The NI card, trigger box and the two types of relays used in the system are displayed in Figure 3.7.

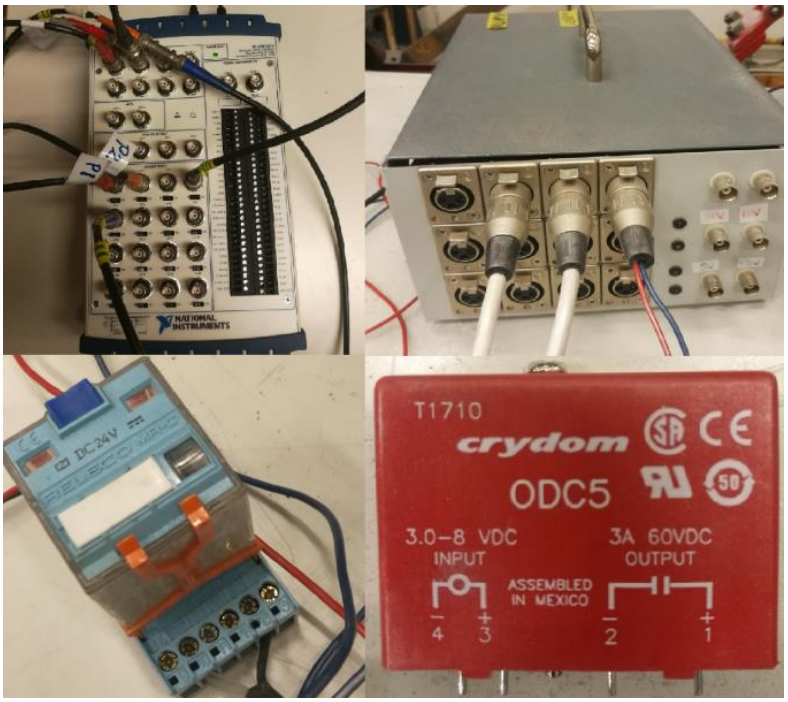

Figure 3.7: *Data acquisition and triggering system. From top left to bottom right: Data acquisition module, trigger box, relay for switching on the pressure loggings, relay used for switching on and off each of the channels inside the trigger box.*

3.2.3 Dust dispersion system

The dust dispersion system is built up of a dust container, fast acting valve, explosive charge, connecting tube and dust disperser.

The container in which the dust is to be loaded into, has a volume of 4.0 dm^3, with an aspect ratio of 3:1. Originally this was a Protractor-operated High Rate Discharge (PHRD) suppressor used in explosion protection and isolation systems [42]. As the area of use for these experiments was completely different, the container was stripped for unnecessary parts such as the blow-off cap and burst disc.

The dispersion vessel is designed to withstand an overpressure of at least 20 bar, and has a fast acting valve at the bottom through which the dust exits the container. The fast acting valve is shot open by an explosive charge, which is activated by an electrical signal from the triggering system described in section 3.2.2. As the charge is activated the valve will open in less than 10 ms due to the pressure inside the dispersion chamber. The dispersion chamber is connected to the explosion chamber by a 90° connecting tube, through which the dust will flow (Figure 3.8).

The previously installed dispersion system in the chamber consisted of two rebound nozzles, but it was discovered by Gault [41] that this system would not be able to disperse aluminum dust properly because of its density. Therefore a perforated semicircular spray pipe, was designed (according to specification in EN 14034-1/2) and sent to the workshop at the Department of Physics and Technology to be built. As the workshop did not have the necessary equipment to bend the pipe, they too had to outsource the job to a subcontractor resulting in a few weeks delay. The spray pipe has an internal diameter of 21 mm and is fitted with 13 holes, including one hole in each end cap, having a diameter of 6 mm (Figure 3.9). The design of the dispersion pipe can be seen in Appendix B.

(a) *(b)*

Figure 3.8: *(a) Dispersion chamber connected to the explosion vessel by a 90° connecting tube. The chamber is pressurized via the pipe on the left. (b) Fast acting valve at the bottom of the dispersion chamber.*

(a) *(b)*

Figure 3.9: *(a) Perforated semicircular spray pipe fitted into the 0.5 m^3 vessel and (b) a close up of the part of the tube connected to the dust container.*

Initially a dispersion test was performed with a Plexiglas-top to observe whether the new dispersion pipe was able to distribute the dust evenly throughout the volume. The original maize

starch with a concentration of 500 g/m^3 was used, and the experiment was filmed. When reviewing the recordings afterward, the nozzle seems to distribute the dust rather uniformly.

3.2.4 Ignition source

The same type of chemical igniters as used for the 20-liter sphere are also used for the 0.5 m^3 vessel.

During the test for the maize starch in the 0.5 m^3 vessel the ignition source was discovered to constantly receive a 24 V signal and not get switched off after the triggering was done. The source of error was the relay in the trigger box that got stuck in "on position" caused by shorting of the electrodes during the previous test, and extensive troubleshooting had to be performed in order to find the fault. New electrodes with more insulation was installed, and the relay replaced.

The same problem returned when testing aluminum dust and in addition there was a problem with the igniters not firing off during the tests. It is believed that the problem was the electrodes not conducting well enough and different electrodes were tested. Moreover the electrodes were burnt and shot out of the vessel during the tests and new ones had to be installed between each experiment.

3.2.5 Pressure measurement system

The pressure measurement system consists of two quartz pressure sensors, or piezo-electric pressure transducers, from Kistler (type 701A, with a pressure range 0-250 bar), and two charge amplifiers from Kistler (type 5011). During the testing of the aluminum dust the measurements were not satisfactory due to disturbances and frequent saturation on the measured signal, and it was decided to replace the transducers with another pair (Kistler type 7031, with a pressure range 0-250 bar), known to be more resistant to vibrations that might occur during explosion testing.

The transducers were calibrated to a pressure range of 0-25 bar and sensitivity in accordance to the guidelines for the transducers to yield the most accurate signals. The sensitivities were 82.5 ± 0.2 pC/bar for type 701A and 88.5 ± 0.0 pC/bar for type 7031, and were adjusted on the charge amplifiers. The procedure is explained in Appendix A.1.

A third transducer was originally connected to the dust dispersion chamber to get an indication of the dispersion rate from the chamber, but was then removed because of suspicion that the signal interfered the signals from the other transducers.

The transducers generate an electrical signal and is sent to the computer via charge amplifiers from Kistler (type 5011), which controls the transducer sensitivity, and is converted back to pressure values. The pressure is recorded with a sampling rate of 10^5 Hz with $5 \cdot 10^5$ samples from just prior to dispersion until 3.5 seconds after ignition, in order to get complete pressure-time measurements.

A pressure indicator was mounted to the explosion chamber to display the pressure in the tank manually. Mostly used to check the pressure when evacuating the vessel.

3.3 Experimental procedure

In general the test procedure described for the 1 m³ vessel in the European Standard [22] shall be applied to both the 20-liter sphere and the 0.5 m³ vessel, but since the set-up is somewhat different there will still be a few differences.

3.3.1 The 20-liter sphere

When conducting a test it is important that the vessel is cleaned and cooled to an initial temperature, T_i, of 20°C through (9) and (1) in Figure 3.10. The two chemical igniters are connected (6), the lid is sealed and the exhaust valve (10) is closed. The vessel is partially evacuated to a pressure of 0.4 bar absolute by a vacuum pump through a vacuum filter. The ball valve is closed, and the pressure inside the vessel is monitored with a digital pressure indicator. A dust sample of desired weight is discharged into the dispersion chamber (4) and the lid is sealed. The chamber is then pressurized to 20 barg from a 50 l compressed air bottle (5).

The point of the this partial evacuation is that the pressure in the vessel after dispersion of the dust from the pressurized dispersion chamber (but prior to ignition) is to be equal to the initial pressure pre-evacuation, p_i = 1013 bar.

The sequence begins when activating it in the KSEP 6 software. The fast acting valve (8) is opened by an electrical signal, and the dust is dispersed into the vessel by the overpressure in the reservoir. After dispersion, there is a 60 ms delay before the fuse heads on the chemical igniters are fired off (6).

Two pressure sensors (2) measures the pressure during the whole sequence.

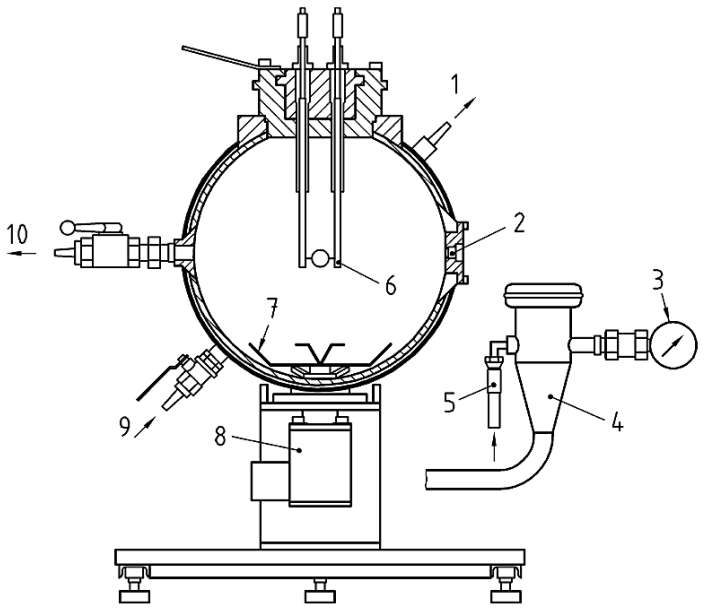

Key

1	Water outlet	6	Ignition source
2	Pressure sensors	7	Rebound nozzle
3	Manometer	8	Fast acting valve
4	Dust container (0,6 dm^3)	9	Water inlet
5	Air inlet	10	Outlet (air, reaction products)

Figure 3.10: *Test equipment 20-liter sphere, from the European Standard [15].*

The explosion pressure is determined over a wide range of concentrations, starting with a concentration of 250 g/m³ and increasing by steps of 250 g/m³. The explosion pressure, p_{ex}, for each of the concentrations is determined and plotted against the concentration until a maximum value of p_{ex} is found. This maximum value is considered the maximum explosion pressure, p_{max}, of the series. Two consecutive concentrations on both sides of the maximum value is to be carried out. The maximum value is the maximum explosion pressure $p_{max,[series\ 1]}$ in Eq. (2.6). After each test, the lid is opened and the vessel is cleaned.

p_{max} and $(dp/dt)_{max}$ are found for three series, all carried out as described above. The KSEP software provides all the information about the K_{St}-value obtained for each test and an average for the complete test series, as well as the curves for the explosion pressure development.

3.3.2 The 0.5 m³ vessel

The experimental procedure for the 0.5 m³ vessel is quite similar to the procedure for the 20-liter sphere. Before conducting an experiment, the vessel (1) and dispersion chamber (2) are cleaned, and the exhaust valve (3) in Figure 3.11 is closed. It is also important to inspect all cables, to check that the triggering sequence activates the signal for the dispersion and ignition, and that the relay for the pressure recordings is activated. This is done to prevent a failed test where we e.g. have an explosion, but no pressure recordings.

The chemical igniters are lowered into the vessel in a steel pipe so that they are placed in the center of the chamber (4), and the pipe is fastened. The dispersion chamber is loaded with the desired amount of dust, the valve (5) is closed, and the reservoir is mounted on top the connecting tube (6). The reservoir is then pressurized to 20 barg from a 50 l compressed air bottle (7), and the explosive charge is pinned to the valve. The ball valve between the dispersion chamber and the pressurized air (8) is closed. The explosion chamber is evacuated to an absolute pressure of 0.84 bar by a vacuum pump (9) through a vacuum filter, and the valve is closed. The electrodes, which are connected to the switching card (10) through terminal blocks, send signals to the ignition source and the explosive charge.

The software is now started, and the triggering sequence executed. The explosive charge is fired off by an electrical signal, and the dust is dispersed into the chamber through the semicircular spray pipe (11) by the overpressure in the reservoir. After dispersion, there is a given delay time before ignition occurs.

Two transducers measure the pressure in the explosion chamber during the whole sequence, and send the signal back to the computer software via amplifiers (12).

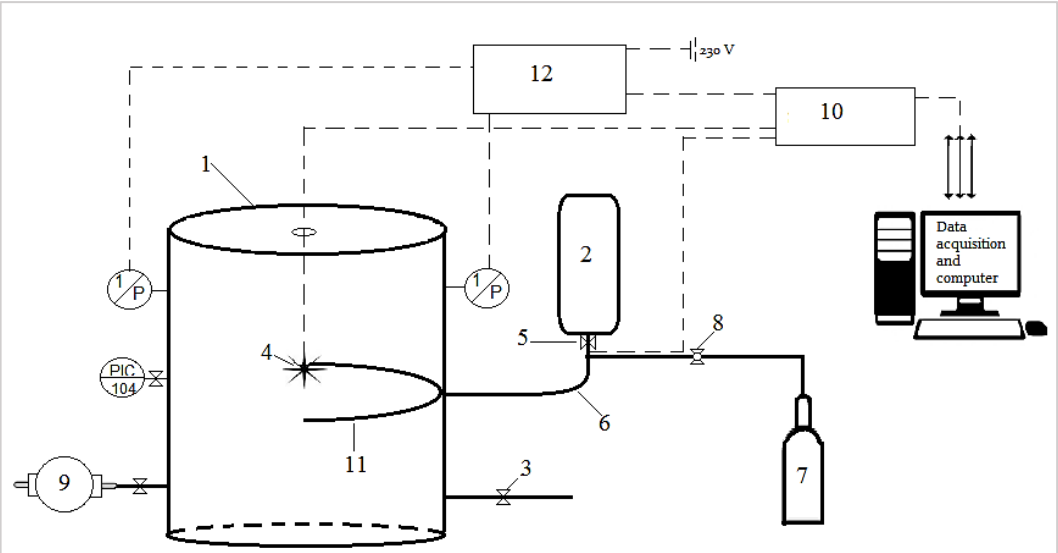

Figure 3.11: *Experimental set-up of the 0.5 m³ vessel, including all equipment.*

For the 0.5 m³ explosion chamber only one series is carried out per dust, according to the procedure in EN 14034-2.

Finding the ignition delay time of the 0.5 m³ vessel

The ignition delay time for the 0.5 m³ vessel was not predefined, since this volume is not specified in the standard. It was however expected to be between 60 ms and 600 ms, since those are the delay times for the 20-liter sphere and the 1 m³ vessel respectively.

When calibrating a non-standardized vessel, the approach is to do a test series in a standardized vessel, find the maximum explosibility, and try to get as close as possible to this value in the vessel that is not yet calibrated. The way to alter the explosion violence is to adjust the ignition delay time while keeping the concentration constant. When a non-standardized vessel is calibrated the explosibility for a given concentration, of e.g. 500 g/m³, should ideally be the same in both vessels.

Finding the maximum rate of explosion pressure rise

To find the maximum rate of explosion pressure rise, and hence the explosivity, the pressure-time curve obtained in each experiment comes to use. The steepest point on the pressure-time curve presents $(dp/dt)_{max}$ and its tangent is used to find the value (Figure 3.12 (a)). In order to find the maximum rate of explosion pressure rise, two pressure points and their associated time points on the tangent line are chosen and (dp/dt) is calculated by the following equation:

$$\left(\frac{dp}{dt}\right)_{max} = \frac{p_2 - p_1}{t_2 - t_1} \tag{3.1}$$

where $(p_2,t_2) > (p_1,t_1)$.

Figure 3.12 (b) illustrates the (dp/dt) curve for the same experiment, where the horizontal line represents the tangent from the pressure-time curve shown in (a). Since the signal is

unprocessed some noise can be observed. In order to obtain the correct value for $(dp/dt)_{max}$ a mean value of the higher and lower spikes are chosen as the true maximum rate of explosion pressure rise for the experiment.

The pressure-time curve and (dp/dt) curve in figure 3.10 are the true curves for maize starch of 10.24 % moisture content tested in the 0.5 m^3 vessel with a concentration of 1250 g/m^3, measured with transducer P1.

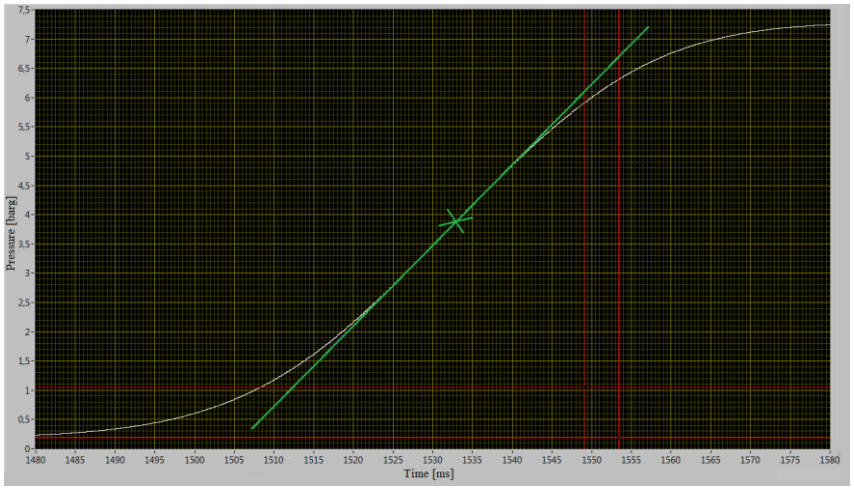

(a)

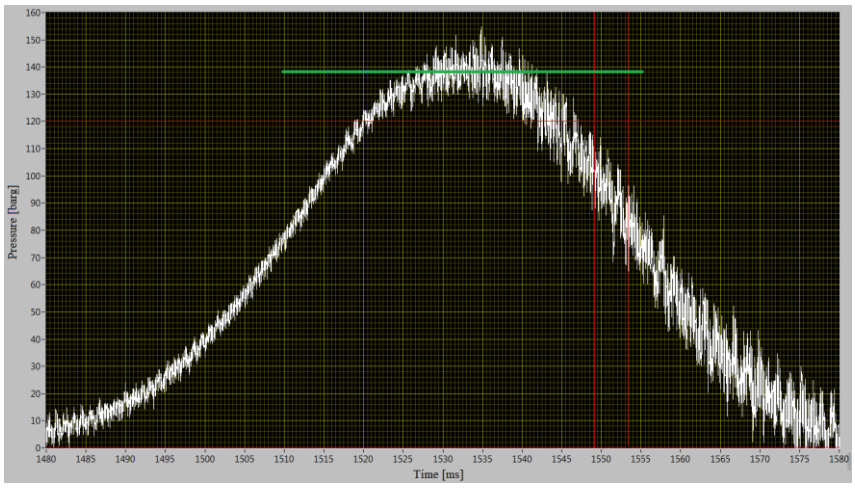

(b)

Figure 3.12: *(a) Pressure-time curve with tangent line to find* $(dp/dt)_{max}$ *and (b) curve for* $(dp/dt)_{max}$.

4 Experimental Results and Discussion

Several parameters influencing the explosion violence of a dust have been considered during the experiments. When conducting experiments in the 20-liter sphere, the effects of moisture content in maize starch was considered. As the volume increased, the effect of initial turbulence, i.e. ignition delay time was investigated. In addition it was studied whether the change in volume itself would change a dusts' explosion characteristics. Finally, the potential effects of thermal radiation was investigated.

4.1 The effect of moisture content

Maize starch from GexCon's batch of standard testing dust with two different humidities were tested. One of them tested as received containing 10.24 % moisture, while the second sample was dried in a heating cabinet overnight, and humidity was reduced to 0.83 %. Both dusts were tested in both volumes, but because of the time elapsed between conducting experiments in the two vessels, the moisture content had increased to approximately 3.5 % when the 0.5 m³ vessel was ready for testing.

The experiments in the 20-liter sphere were conducted with three series per sample, and the averaged values of the dust properties are presented in Table 4.1.

Table 4.1: *Explosion properties of maize starch with two different moisture contents. Tested in the 20-liter sphere.*

Dust sample	p_{max} **[bar]**	$(dp/dt)_{max}$ **[bar/s]**	$K_{St,\,max}$ **[m·bar/s]**
Maize starch, 0.83 % moisture content	9.3	728	198
Maize starch, 10.24 % moisture content	8.1	358	97

As clearly displayed in the table, all of the explosions properties decreased as moisture content increased, as expected. The maximum explosion pressure decreased by 1.2 bar when the moisture content was lowered. However, the maximum rate of pressure rise was reduced to half when moisture content was increased, and thus the explosibility of the dust decreased by the same magnitude.

As mentioned above the moisture content of the dried starch had increased to about 3.5 % when testing began in the 0.5 m³ vessel. It is then natural that the explosion properties was not altered to the same extent as for the newly dried dust. The experiments for the dust containing 10.24 % moisture was tested with two different ignition delay times, and the explosion properties are given in Table 4.2, in addition to the results obtained from the dried dust in the same vessel.

Table 4.2: *Explosion properties of maize starch with two different moisture contents. Tested in the 0.5 m^3 vessel.*

Dust sample	**Ignition delay time [ms]**	p_{max} **[bar]**	$(dp/dt)_{max}$ **[bar/s]**	$K_{St,\ max}$ **[m·bar/s]**
Maize starch, ~3.5 % moisture content	500	8.3	217.8	172.9
Maize starch, 10.24 % moisture content	500	7.9	153.3	121.7
Maize starch, 10.24 % moisture content	600	7.3	126.8	100.6

The effect of lowered moisture content in the 0.5 m^3 vessel is, as displayed in the table, not as big compared to the results from the 20-liter sphere. This was expected since the moisture content of the dried dust had increased from 0.83% to approximately 3.5 %. On the other hand, the explosion violence did increase significantly.

As explained in section 2.1.2 there are three main reasons for the lowered explosion violence as the moisture content is increased:

i) The heating and evaporation of water during combustion act like a heat sink. This cause the rate of pressure rise to decrease, hence making the slope, $(dp/dt)_{max}$, gentler.
ii) Water mixes with the oxidized gases in the preheating zone, thus making them less reactive.
iii) As moisture content increases, the degree of agglomeration will increase as well. These formed clusters of dust will prevent fine dispersion, and consequently the effective specific surface area decreases. As a result of this the particles will fall out of the cloud earlier.

In general the time from 10 % of p_{max} to p_{max} gives information about the steepness of the slope on a pressure-time curve, which again determines the explosion violence. A shorter time difference gives a steeper slope. If, when comparing two curves, the pressure difference between these two points are different, this will affect the slope even more. The pressure-time curves for the two different moisture contents of maize starch tested in the 20-liter sphere are illustrated in Figure 4.1.

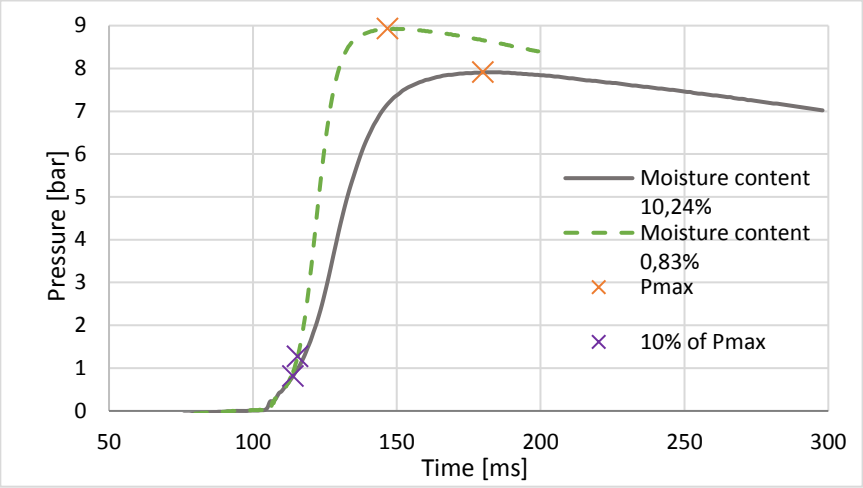

Figure 4.1: *Pressure-time curves for different moisture contents of maize starch. Tested in the 20-liter sphere.*

The curve for the dust containing 0.83 % moisture has a steeper slope, indicating a higher burning velocity and thus a faster rate of pressure rise, than for the dust containing 10.24 % moisture. The time from 10 % of p_{max} to p_{max} is shorter (about half) for the dried dust. In addition, the pressure is approximately 1 bar higher for the dried dust, which indicates the effect of extra moisture content acting as a heat sink. As a result of this, there will be a more rapid pressure rise and consequently a higher explosion violence for the dried dust.

4.2 The effect of turbulence

The ignition delay time determined for the 0.5 m³ vessel are based on the results obtained in the standardized 20-liter sphere. The delay determines the turbulence level in the explosion chamber at the time of ignition. It was expected that the ignition delay time for the 0.5 m³ vessel would lie between the delay times for the standardized vessels of volumes 20 liters and 1 m³, i.e. between 60 and 600 ms.

The first series of experiments were executed for maize starch of 10.24 % moisture content in the 20-liter sphere, and the maximum explosibility of the test series was used as a reference when finding the ignition delay time for the 0.5 m³ vessel. In addition, data from dust explosion experiments with the same maize starch, conducted in a 25 m³ silo at GexCon's test site at Sotra (Figure 4.2), helped shed some light on the explosibility one could expect.

Figure 4.2: *25 m³ test volume.*

Different ignition delay times were tested to find the same explosibility as the one obtained in the standard 20-liter sphere for the same 10.24 % moisture maize starch as used in this work. Three pressure-time curves from the calibration of the 0.5 m³ vessel are displayed in Figure 4.3. The concentration and all other conditions were kept constant, and the ignition delay times ranged from 300 ms to 900 ms.

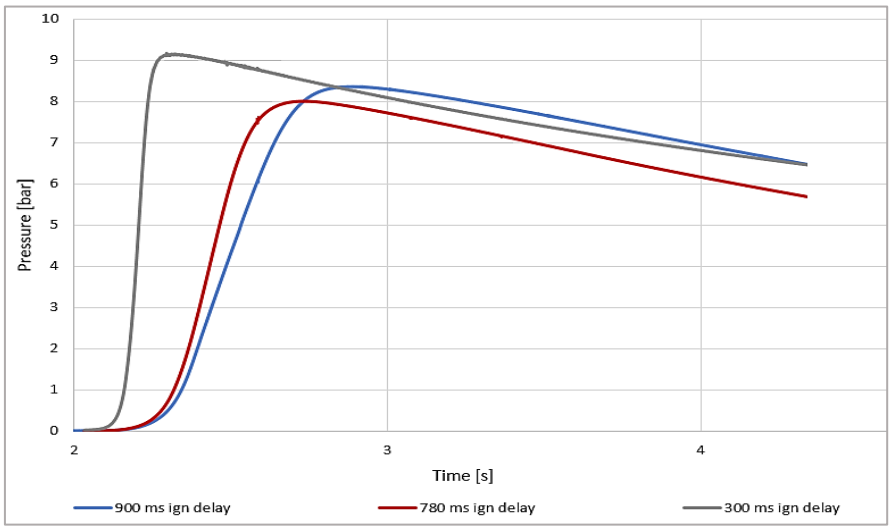

Figure 4.3: *Pressure-time curves for maize starch of 10.24 % moisture content of different ignition delay times, with the same concentration. Tested in the 25 m³ vessel.*

The associated maximum K_{St}-values for the pressure-time curves are listed in Table 4.3.

Table 4.3: *Explosibility data of maize starch from the large scale vessel of 25 m³.*

Ignition delay time [ms]	$K_{St,\,max}$ **[m·bar/s]**
300	345.89
780	93.80
900	64.49

The ignition delay time that corresponded to the same (or closest to the same) K_{St}-value as obtained in the 20-liter sphere was 780 ms. Keeping in mind that this is an organic dust with rather high moisture content (which yields a fairly low explosion violence in standardized and calibrated vessels), the K_{St}-value is increased by a factor of almost 5.4 by reducing the ignition delay time. This illustrates the great importance of calibration of the test vessel and the effect of ignition delay time, i.e. the level of turbulence and explosibility. This also highlights the importance of using the K_{St}-value with caution when designing mitigating safety measures, such as vents areas, in plants. Since the turbulence level for a given dust is not constant for different types of process equipment, it may not me adequately represented by standardized tests.

For the 0.5 m³ vessel a range of different ignition delay times were tested, starting with 900 ms, and decreasing in small time steps as shown in Table 4.4. At the time, the pressure decrease in the dispersion chamber, i.e. how fast the dust is dispersed into the vessel, had not been monitored successfully, and the dispersion time was therefore unknown. Thus, the calibration was done by guessing and testing with several different delay times both over and below the delay for the standard 1 m³ vessel.

Table 4.4: *Various ignition delay times with associated maximum pressures, maximum rates of pressure rise and explosibilities. Tested in the 0.5 m^3 vessel with a concentration of 500 g/m^3 of maize starch containing 10.24 % moisture.*

Ignition delay time [ms]	p_{max} **[bar]**	$(dp/dt)_{max}$ **[bar/s]**	K_{St} **[m·bar/s]**
400	7.84	179.90	142.78
500	7.15	109.39	86.82
600	7.04	84.06	66.72
750	7.78	66.59	52.85
900	6.80	54.98	43.63

As Table 4.4 portrays, an ignition delay of 500 ms, yielding a K_{St}-value of 86.82 m·bar/s, was initially the delay reflecting the maximum explosibilities in the 20-liter sphere and the 25 m³ vessel. On the basis of this, a series was carried out for the maize starch of 10.24 % moisture content at this delay. The results from the series are shown in Table 4.5.

Table 4.5: *Explosion characteristics of maize starch of 10.24 % moisture content tested in the 0.5 m^3 vessel with an ignition delay time 500 ms.*

Concentration [g/m³]	**p_{max} [bar]**	**$(dp/dt)_{max}$ [bar/s]**	**K_{St} [m·bar/s]**
250	4.61	26.70	21.19
500	6.56	109.39	86.82
750	7.92	153.34	121.70
1000	7.91	143.03	113.52
1250	7.36	141.01	11.92
1500	4.23	114.70	91.03

As the series was carried out, it was discovered that the explosivity increased a bit more than what was expected as the concentration was increased. Although the maximum rate of pressure rise does not deviate by more than the maximum permissible deviation of ± 20 % given by the standard [22], it was decided to change the ignition delay time. Since the turbulence, and thereby the maximum rate of pressure rise and explosion violence decrease with increasing ignition delay time, the delay was increased to 600 ms. The new K_{St}-values were obtained for the three highest explosions pressures in the previous series, and the results are displayed in Table 4.6.

Table 4.6: *Explosion characteristics of maize starch of 10.24 % moisture content in the 0.5 m^3 vessel. Ignition delay time 600 ms.*

Concentration [g/m³]	**p_{max} [bar]**	**$(dp/dt)_{max}$ [bar/s]**	**K_{St} [m·bar/s]**
750	7.12	123.99	98.41
1000	7.27	121.02	96.05
1250	7.34	126.78	100.63

By fine-tuning the ignition delay time, the maximum explosivity for the maize starch in the 0.5 m³ vessel is now almost the same as for the 20-liter sphere, 100.63 m·bar/s versus 97 m·bar/s. This new, and better calibrated, ignition delay time will be used when performing explosion violence tests for the aluminum dust.

It would seem a bit unexpected that the ignition delay time in the 0.5 m³ vessel should be the same as for a volume that is twice as large. Taking into account that the vessels have length-to-diameter ratio of 1:1, the radius, i.e. the distance from the ignition source to the vessel wall, can be found by using the equation for the volume of a cylinder:

$$V = \pi \cdot r^2 \cdot h \qquad (4.1)$$

Since the height is equal to the diameter, or *2r*, and the volume is known, the equation for the radius is:

$$r = \sqrt[3]{\frac{V}{2 \cdot \pi}} \qquad (4.2)$$

The radii for the 1 m³ and the 0.5 m³ are then 0.54 m and 0.43 m, respectively. Hence, the distance from the ignition source to the vessel wall of the explosion chamber used in this experiment is 80 % of the distance in the standardized 1 m³ vessel. In comparison the radius of the 20 liter vessel is only 0.15 meters, or 28 % of the radius in the 1 m³ vessel.

Because of the similarities of the standard 1 m³ volume and the 0.5 m³ vessel, the level of turbulence and the dust cloud distribution will be similar when using the same ignition delay time and dispersion system. Hence, the explosibility characteristics will be rather similar as well.

As only a delay of 500 ms was tested for the dust containing 3.5 % moisture, an attempt has been made to find the equivalent K_{St}-value for the ignition delay time of 600 ms for this dust. Considering the pressure-time curves (from 10 % of p_{max} to p_{max}) for both ignition delay times, there is a 27 % difference in their slopes, the slope for 500 ms being steeper. See Figure 4.4.

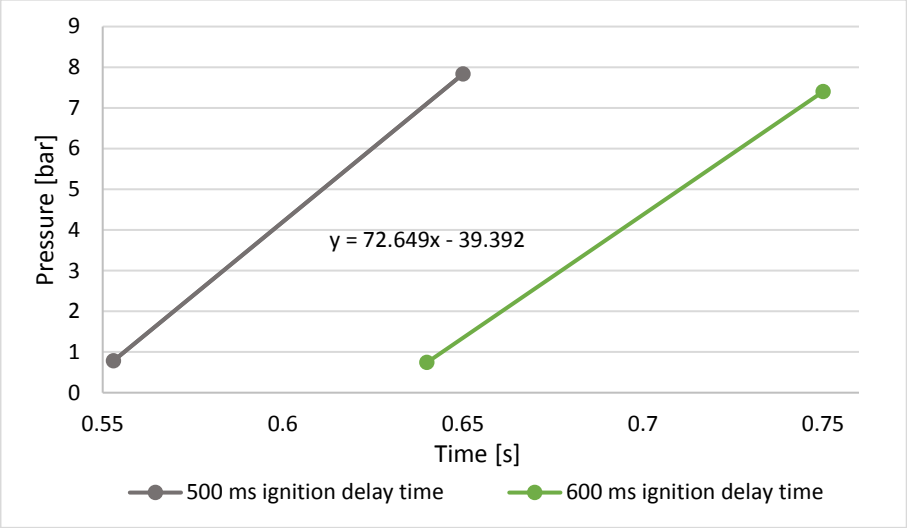

Figure 4.4: *Slopes of the pressure-time curves for the tests that gave $K_{St,\,max}$ for 500 ms and 600 ms ignition delay time.*

By applying the difference in their slopes to the relation between K_{St} and moisture content, one could extrapolate the K_{St}-value for the dust containing 3.5 % moisture with an ignition delay time 600 ms as shown in Figure 4.5.

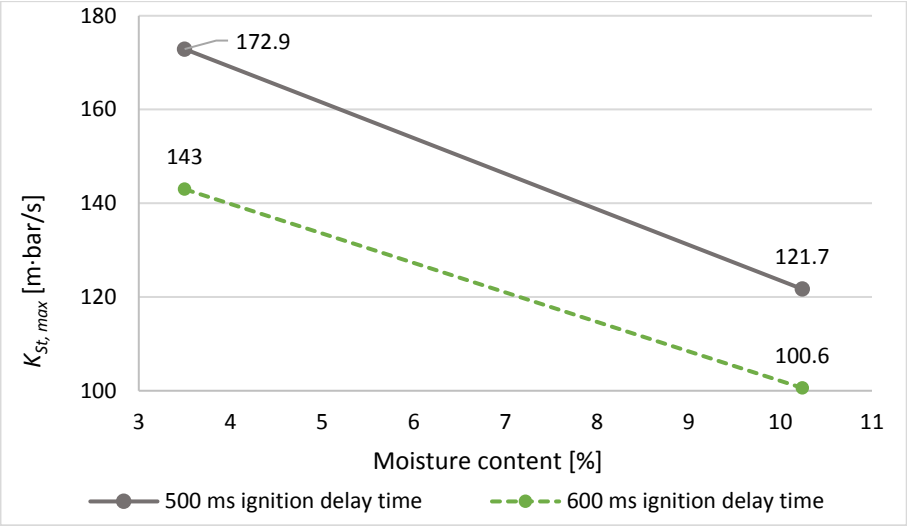

Figure 4.5: *Extrapolation for the maximum explosion violence for the test of 3.5 % moisture content and an ignition delay time of 600 ms, based on the values from the 500 ms tests conducted in the 0.5 m³ vessel.*

Doing so yields a $K_{St,\,max}$-value for the dust containing 3.5 % moisture (600 ms ignition delay) of 143 m·bar/s. This gives the same explosibility as one would get by assuming that the effect of reducing the moisture content from 10.24 % to 3.5 % is the same for an ignition delay of 600 ms (42 %) as for 500 ms.

When comparing these K_{St}-values to the ones found for the dried dust in the 20-liter sphere (198 m·bar/s) it is reasonable to assume that these results are sensible. A small increase in moisture content, will somewhat reduce the explosibility of the dust.

Looking at the maximum explosion pressures and explosion violence for the 10.24 % moisture starch, a few things can be highlighted. To get a clear view of the properties, they are summarized in Table 4.7.

Table 4.7: *Maximum explosion pressure and explosion violence for maize starch containing 10.24 % moisture. Tested in the 20-liter sphere and the 0.5 m³ vessel with both ignition delay times.*

Vessel	p_{max} **[bar]**	$K_{St,\,max}$ **[m·bar/s]**
20 liter sphere	8.1	97.00
0.5 m³ vessel, 500 ms ign. delay	7.9	121.70
0.5 m³ vessel, 600 ms ign. delay	7.3	100.63

When comparing the maximum pressure in the 20-liter sphere and the 0.5 m³ vessel with delay 500 ms, they are fairly consistent, which entails that an equivalent dust concentration is present in the dust cloud in both vessels at the time of ignition. But looking at the explosion violence, this suggests that the turbulence level in the larger vessel is higher, and hence the dust in the cloud will burn faster.

As the ignition delay time in the 0.5 m³ vessel was prolonged the explosion violence coincided with the one obtained in the Siwek sphere, which implies that the turbulence levels during the initial phase of the explosion are quite similar. Looking at the maximum pressure however, this has gone down by almost 10 %, which suggests that a larger portion of the dispersed dust has settled out of the cloud.

Taking these observations into account, the ideal ignition delay time could lie somewhere in between 500 and 600 ms for the 0.5 m³ vessel. Bearing in mind that the standard classifies all dust with a K_{St}-value between 0 and 200 m·bar/s as dust class 1, the obtained results are reasonable.

4.3 Particle size distribution

When measuring the particle size distribution a sieve analysis was conducted by fixing a stack of sieves to a mechanical shaker, as shown in Figure 4.6. A representative weighed sample of dust was placed onto the top sieve which has the largest mesh size. For each level of sieves the mesh size is reduced, and at the base there is a receiver pan. Four mesh sizes of 250, 125, 63 and 32 µm were used for these measurements. The difference in weight of each sieve before and after sieving is the accumulated dust that is small enough to pass through the mesh of the overlying sieve, but too large to pass through the mesh of the current one.

(a) *(b)*

Figure 4.6: *Sieving equipment for determination of particles size distribution in a dust sample. (a) Stack of sieves on mechanical shaker. (b) Close-up of mesh on sieve.*

The particle size distribution can give information about a dust's explosibility if data for the same material is already available, and is often given by the mean particle size. In reality the particle size distribution within a batch can be quite wide, and the expected explosibility may be misleading. A dust that seems to have a large particle size (by the mean particle diameter) and not be explosible in air, can still be so if they contain a significant "tail" of fine particles [1].

In applications where surface area is important the Sauter mean diameter (SMD) is frequently used and is given by

$$d_{3,2} = \frac{\sum_i d_i^3}{\sum_i d_i^2} \qquad (4.3)$$

where all size measures refer to the diameter of the equivalent spheres. SMD is defined as the diameter whose ratio of volume to surface area is the same as that of the entire droplet sample [43].

Particle size distribution for maize starch tested during the current work is listed in Table 4.8, and mass % and cumulative mass % illustrations are displayed in Figure 4.7.

Table 4.8: *Particle size distribution of maize starch.*

Particle size [μm]	**Particle mass [%]**	**Particle mass accumulation [%]**
< 32	3.53	3.53
32 - 63	58.98	62.51
63 - 125	33.71	96.23
125 - 250	2.87	99.10
> 250	0.90	100.00

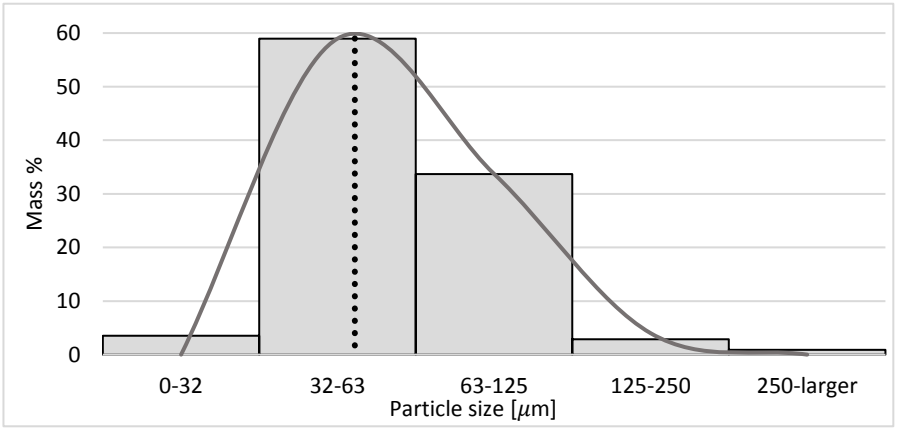

(a)

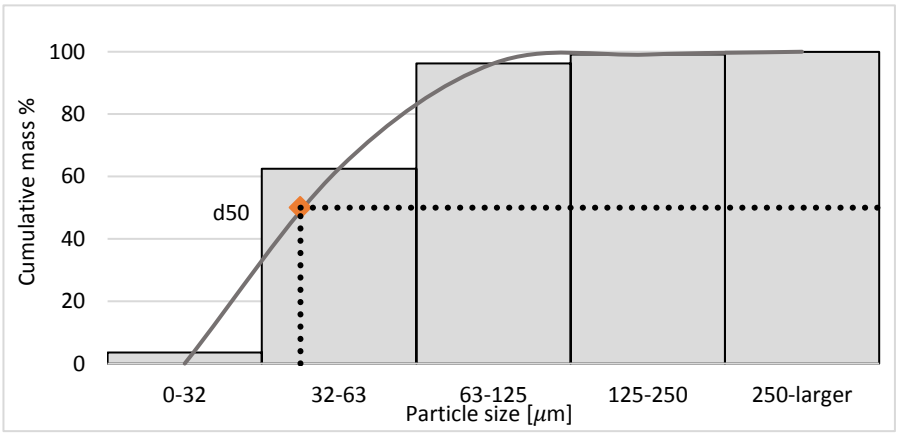

(b)

Figure 4.7: *Particle size distribution of maize starch by (a) mass % and (b) cumulative mass %.*

The particle size distribution of mass % (Figure 4.7 (a)) gives information about how frequent a particle size (or a particle size range) occur within the sample. The top of the curve represents the mode of the particle size distribution. The mode gives the particle size which occurs most frequently in the distribution, and is 71 μm for the maize starch.

96 % of the particle mass are in the range between 32 µm and 125 µm, without any significant "tail" of particles.

The cumulative mass % plot gives information about how many percent of the particles that are under a given particle range. The mass median diameter, denoted d_{50} divides the frequency of the particles in half. 50 mass % of the particles then have a larger diameter and 50 mass % have a smaller diameter. The mean diameter, SMD and mass median for maize starch are displayed in Table 4.9.

Particle size distribution for aluminum are listed in Table 4.9, and mass % and cumulative mass % illustrations are displayed in Figure 4.8.

Table 4.9: *Particle size distribution of aluminum.*

Particle size [*µm*]	**Particle mass [%]**	**Particle mass accumulation [%]**
< 32	0.39	0.39
32 - 63	44.16	44.55
63 - 125	48.44	93.00
125 - 250	4.47	97.47
> 250	2.53	100.00

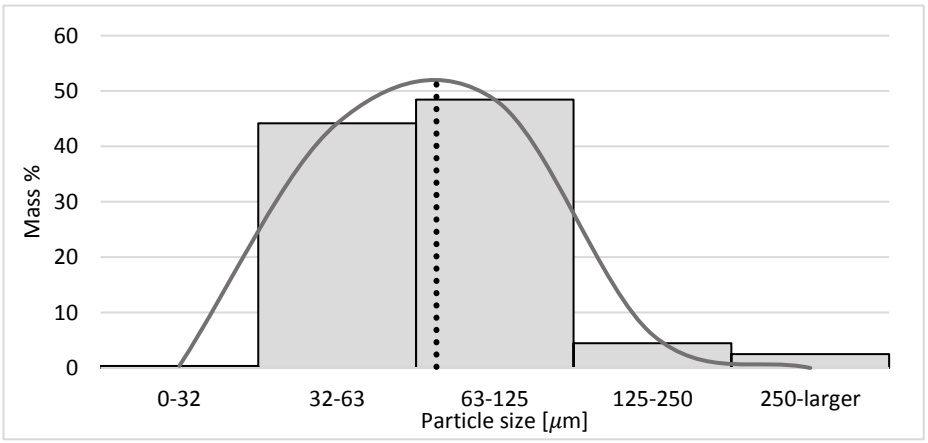

(a)

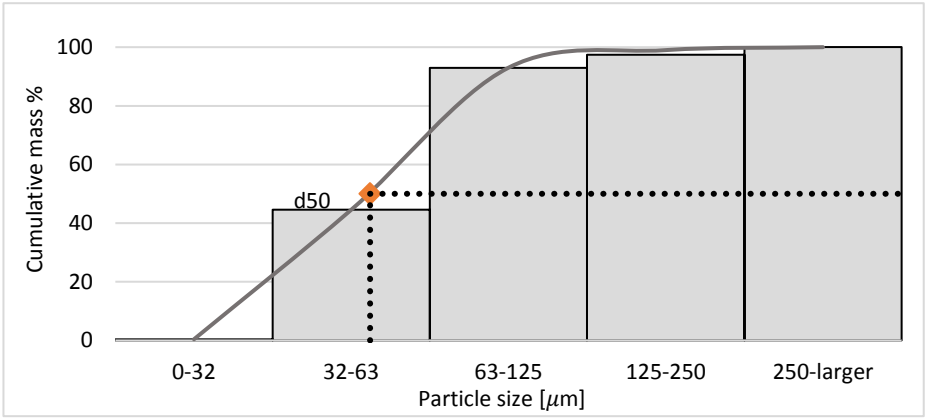

(b)

Figure 4.8*: Particle size distribution of aluminum by (a) mass % and (b) cumulative mass %.*

As for the maize starch the majority mass % for aluminum is given by particles having diameters between 32 µm and 125 µm. Neither the particle size distribution of aluminum dust nor maize starch has a "tail" that would decrease the overall surface area of the dust to any extensive degree.

Summation of the mass weighted particle sizing for maize starch and aluminum are displayed in Table 4.10.

***Table 4.10**: Mass weighted particle sizing for maize starch and aluminum.*

	Maize starch	**Aluminum**
Mean [µm]	46	56
Sauter mean [µm]	53	46
Mass median [µm]	40	52
Mode [µm]	51	71

The Institute for Occupational Safety and Health of German Social Accident Insurance has gathered information about explosibilites of aluminum dusts for various particle size distributions. The samples that are closest to the aluminum used in these experiments when it comes to particle size distribution are displayed in Table 4.11.

***Table 4.11:** Properties of recorded samples of aluminum dust for comparison, from GESTIS DUST-EX [44].*

	Sample 2433	**Sample 672**
Median value [µm]	85	36
Maximum explosion overpressure, p_{max} [bar]	11.4	12.0
K_{St} [m·bar/s]	319	750
Explosibility Class	St 3	St 3

As these two samples are the closest ones in particle size distribution to the aluminum used in these experiments, a few thing can be taken away from this. It is clear that samples with relatively similar sized dust, can give completely different explosion violence. Thus, the particle size itself is probably not the crucial parameter when different samples with similar particle size distributions yield different explosibilities. Other factors such as different geometries and surface-area-to-volume ratios, which are important factors for the reactivity as explained in section 2.1.2, will however have an impact. Different samples may also have different purities, which also affects the explosion properties. In addition, although the K_{St}-values are very different, the samples are both classified as explosibility class 3. This underlines the fact that the K_{St}-value is an approximate classification of the threat that a dust poses.

4.4 Effect of change in volume

In Figure 4.9 are the maximum explosion pressure and K_{St}-values for maize starch of 10.24 % moisture content, tested in the 20-liter sphere and the 0.5 m³ vessel (for both ignition delay times) displayed.

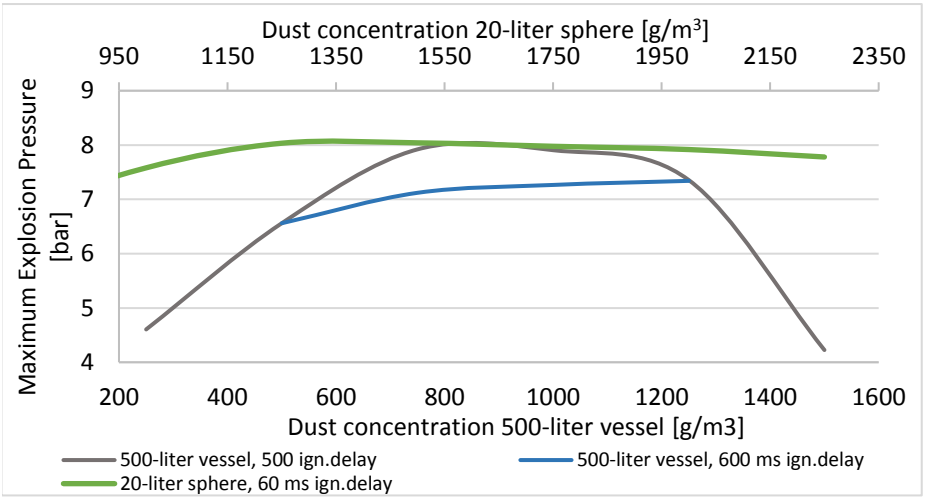

(a)

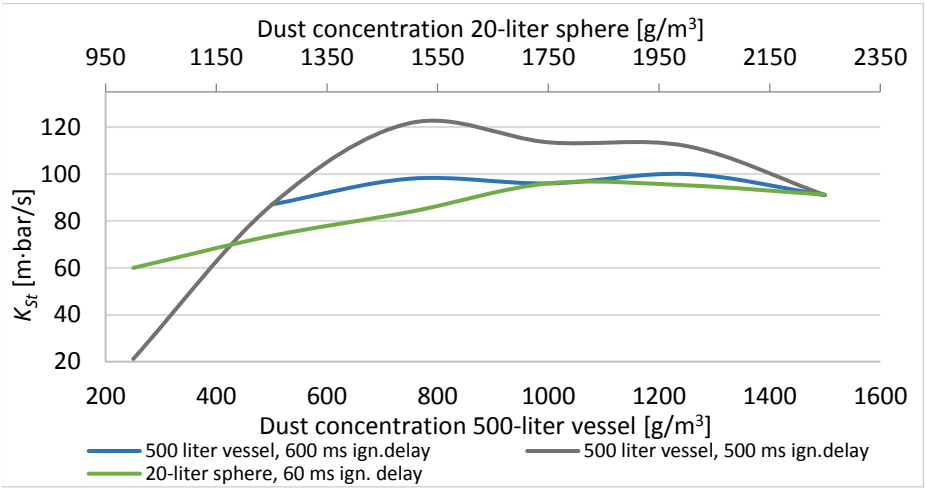

(b)

***Figure 4.9**: (a) Maximum explosion pressure and (b) explosibility curves for maize starch of 10.24 % moisture content tested in the 20-liter sphere and the 0.5 m³ vessel. Concentration scale for results from the 20-liter sphere on the secondary axis to match the curves from the 0.5 m³ vessel.*

By using a secondary axis for the concentrations used in the 20-liter sphere in Figure 4.9, it is possible to visualize how the change of ignition delay time in the larger vessel fits with the p_{max} and K_{St}-values obtained in the 20-liter vessel.

A decrease in the maximum pressure is observed in the 0.5 m³ when the ignition delay time is changed from 500 to 600 ms, from 7.92 bar to 7.34 bar respectively, ref. Figure 4.9 (a). This indicates that a smaller portion of the dispersed dust is combusted during the explosion. As the ignition delay time increases, the turbulence decreases and the dust starts to settle out of the cloud. An ignition delay time of 500 ms in the 0.5 m³ vessel seems to correlate better with the maximum explosion pressures obtained in the Siwek sphere. Yet, an ignition delay time of 600

ms is in better compliance with the explosibility obtained in the 20-liter sphere, which is the parameter that the ignition delay time was calibrated after (Figure 4.9 (b)).

The same pressure drop as a function of ignition delay time can be observed for the 25 m³ vessel; when the ignition delay time is 300 ms a maximum explosion pressure of just over 9 bars is measured, while for 780 and 900 ms the pressure has gone down by circa 1 bar as shown in Figure 4.3.

A defined range of maximum explosion pressures can be observed for the 0.5 m³ vessel over the range of concentration, while in the 20-liter sphere the maximum explosion pressure is more similar for the different concentrations inside the explosibility range. Due to the small volume and the powerful igniters of 10 kJ in the 20-liter sphere, the whole volume will be ignited at the same time. Hence, the dust cloud would fully ignite and an explosion could occur in the 20-liter sphere for a given concentration, while the cloud would hardly burn at the same concentration in the 0.5 m³ vessel. The pressure decrease in the 20-liter sphere is then only due to the increased fuel-to-oxygen ratio, while in the 0.5 m³ the effect of dust settling out of the dust cloud and the heat sink phenomena will also contribute to the pressure drop.

Figure 4.9 (b) illustrates that as the volume increases, a lower concentration is needed to obtain the maximum explosibility value, $K_{St,\ max}$. This could be due to the large surface area compared to the volume in the 20-liter sphere. A larger portion of the dust will adhere to the surface of the walls in this vessel, in comparison to the 0.5 m³ vessel which has a smaller surface to volume-ratio. The rebound nozzle in the 20-liter sphere disperses the dust toward the walls, and as the maize starch has a relatively high moisture content it will easily adhere to the walls (while the nozzle in the 0.5 m³ vessel disperses the dust inwards). Thus, a larger concentration is needed in the dispersion chamber in 20-liter sphere to get the same concentration in the dust cloud at the time of ignition. Table 4.12 shows that the worst-case concentration is reduced even further when the volume increases from 0.5 to 25 m³.

Table 4.12: *Maximum explosion violence with associated concentrations for maize starch of 10.24 % moisture content, tested in the 20-liter sphere, the 0.5 m³ vessel, and the external 25 m³ vessel*

Volume	$K_{St,\ max}$ **[m·bar/s]**	**Concentration at** $K_{St,\ max}$ **[g/m³]**
20-liter sphere	97.0	1750
0.5 m³ vessel	101.0	1250
25 m³ vessel	93.8	500

Even though a larger concentration is needed to obtain the maximum explosibility when the volume increases, the maximum value itself does not seem to be altered.

The KSEP software for testing in the 20-liter sphere does corrections in the measured pressure values in order to make up for the chemical igniters and cooling effects (see section 2.2.3 for the correlations). In addition, the software filtrates possible noise in the measurements. However, the results and graphs obtained from the explosions in the 0.5 m³ vessel are completely unprocessed. Figure 4.10 shows a pressure-time curve from each of the vessels. (a) The processed pressure-time curve obtained from KSEP 6, and (b) pressure-time curve obtained from the 0.5 m³ vessel.

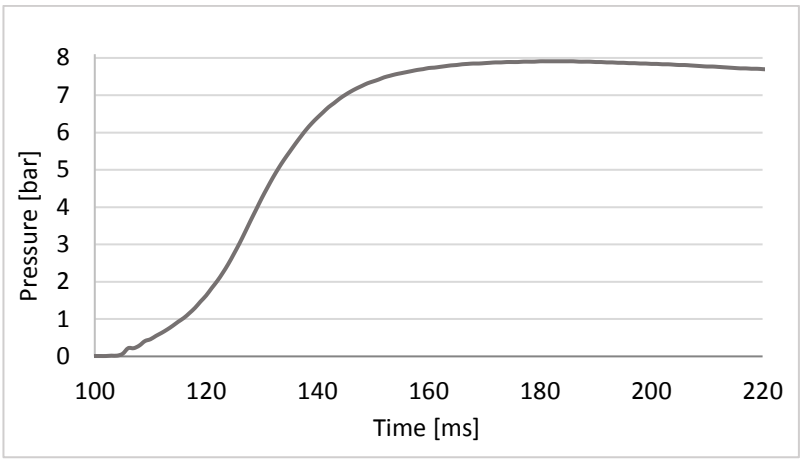

(a)

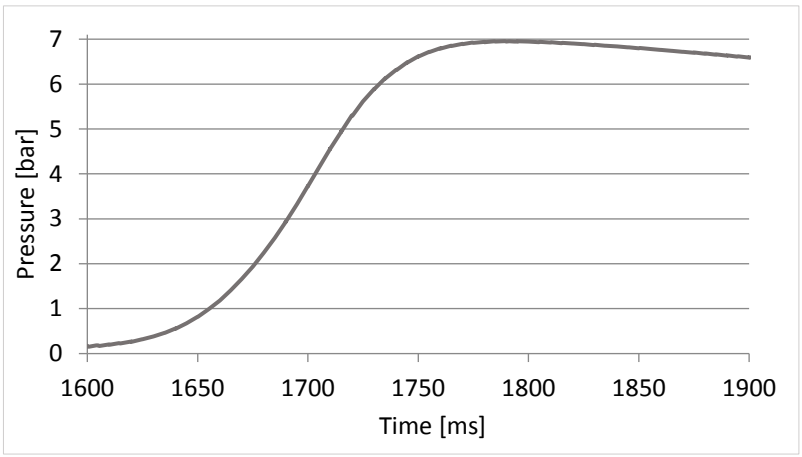

(b)

Figure 4.10: *Pressure-time curves for maize starch holding 10.24 % moisture. (a) Post-processed KSEP-curve from the 20 liter sphere and (b) non-filtrated curve from the 0.5 m^3 vessel.*

As can be seen from the curve obtained from the 0.5 m^3 vessel (Figure 4.10 (b)) has a bit of noise and disturbances, but not as much as one might expect. Since the curve is quite smooth, the maximum pressure and maximum rate of pressure rise can easily be found. It is, however, possible to smooth the curve in the LabVIEW software by using Savitzky-Golay or Butterworth filters, which make frequency response as flat as possible.

When starting to conduct experiments for aluminum in the 0.5 m^3, the recorded pressure-time curves became faulty. Aluminum, which is a metal, has low resistivity and high conductivity, i.e. it has a high ability to conduct electric current. As the aluminum was dispersed with a relatively high turbulence, a flow field of electric current was present, as illustrated in Figure 4.11 (b). As the transducers were activated, the dust in the vessel and on vessel walls was immediately attracted to the earthed connection between the transducers and the amplifiers, and caused the signal to fail. The first experiment for aluminum with a concentration of 750 g/m^3 is shown in Figure 4.11 (a) in grey.

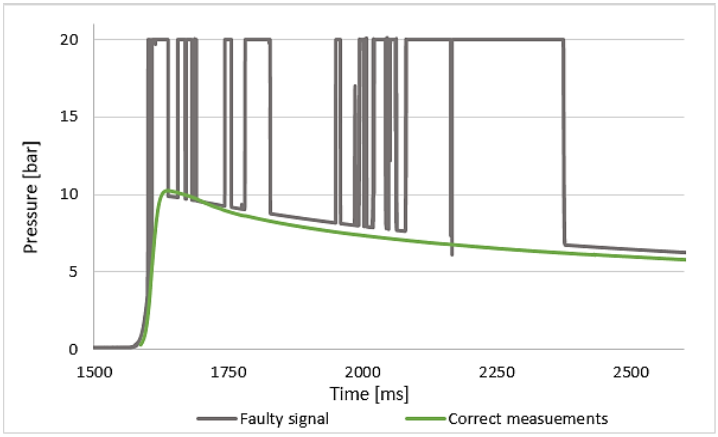

(a)

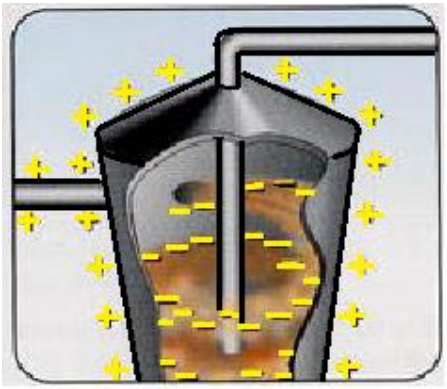

(b)

Figure 4.11: *(a) Pressure-time curves for aluminum in the 0.5 m³ vessel giving faulty signal and correct measurements. (b) Illustration of a vessel containing a turbulent charged powder, from NEK [45].*

To solve the problem both pressure transducers were replaced, and both the explosion vessel and NI card was earthed. After these actions had been taken, new experiments were conducted for the same concentration, and is represented by the green (smooth) curve in Figure 4.11 (a).

4.5 The effect of thermal radiation

The effect of moisture content has already been discussed in section 4.1, and the experimental results showed that the maximum pressure, maximum rate of pressure rise, and thereby the explosivity increased as the moisture content was reduced. When comparing the results obtained in the 20-liter sphere for maize starch with the explosion pressure development from the test series for aluminum, the increase in explosivity is even higher.

Looking at Figure 4.12 (a) the maximum explosion pressure for aluminum dust as a function of concentration is rapidly increasing for concentrations up to 500 g/m³. After reaching p_{max} for the series at 1000 g/m³ the maximum explosion pressure is relatively constant throughout the rest of the test series with only a slight decrease as the concentration is increased. The test series with aluminum dust yielded approximately the same maximum pressures as the dried maize for concentrations above 1500 g/m³.

For the maximum rate of pressure rise a vast increase is observed for the aluminum dust up to a concentration of 1000 g/m³ (Figure 4.12 (b)). The $(dp/dt)_{max}$ is approximately three times higher for aluminum than for the dried maize for concentrations above 1000 g/m³. This level of explosibility characterizes aluminum as a St 3, which is the highest dust explosion class and thus the most dangerous.

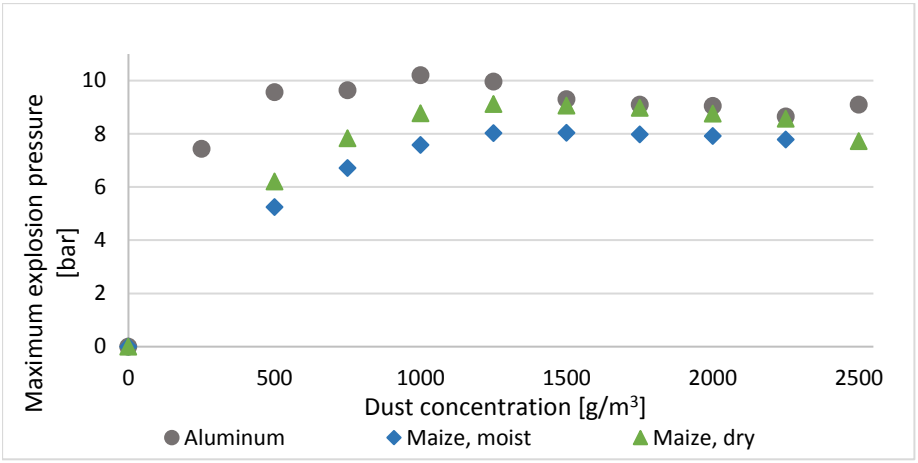

(a)

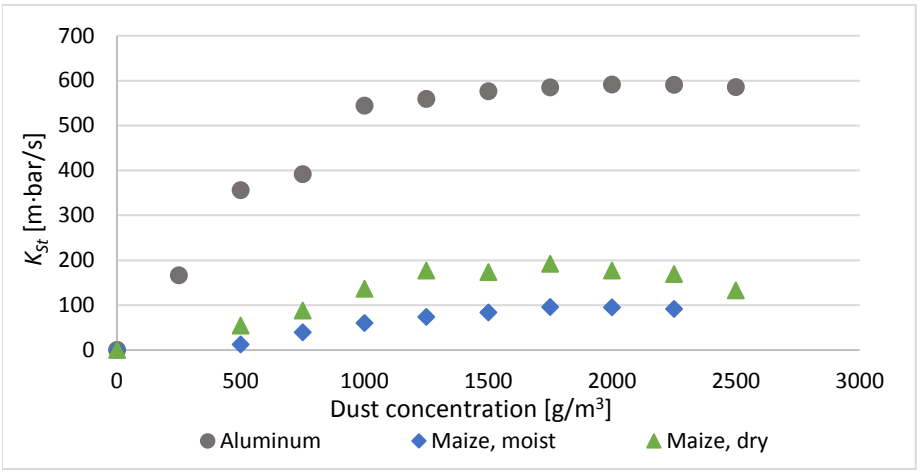

(b)

Figure 4.12: *(a) Maximum explosion pressure as a function of dust concentration, (b) maximum rate of pressure rise as a function of dust concentration. Maize starch with two different moisture contents and aluminum dusts, all tested in the Siwek 20-liter sphere.*

In Table 4.13 an overview of various fuels with their associated adiabatic flame temperatures can be found. Adiabatic temperature refers to the combustion process where no heat loss takes place, and is an ideal system since some degree of heat loss always occurs. Metals have adiabatic flame temperatures ranging from 1830 K for lead to 4060 K for aluminum. Most organic dusts have an adiabatic flame temperature around 2000 K.

Table 4.13: *Adiabatic flame temperatures for various fuels, from Cashdollar and Zlochower [46] and DeRose [47].*

Fuel	**Maximum adiabatic flame temperature [K]**
Aluminum (Al)	4060
Chromium (Cr)	3170
Iron (Fe)	2490
Lead (Pb)	1830
Magnesium (Mg)	3610
Organic dusts	~2000

Based on the results obtained in the 20-liter sphere and that aluminum burns at a higher temperature than maize, ref Table 4.13, it could be assumed that the effect of thermal radiation would increase the explosion violence of aluminum significantly more than for maize starch when increasing the test volume. This considering that heat transfer due to thermal radiation is proportional to the fourth power of the temperature as well as depending on the flame area and the view factor described in section 2.1.2.

Figure 4.12 (a) shows that aluminum reaches the maximum explosion pressure at a lower concentration than maize starch, 500 g/m^3 versus 1250 g/m^3 respectively. The maximum rate of explosion pressure rise (Figure 4.12 (b)) increases for all dusts until a maximum concentration of 1750 g/m^3 for maize starch and 2000 g/m^3 for aluminum is reached. The worst-case concentration often seems to occur at higher concentrations for metal dusts than for organic dusts [1]. Beyond these concentrations, moving towards the upper explosible limit, the amount of fuel in the explosion chamber at the time of ignition is so large that the flame is starting to get quenched due to the heat sink effect.

The series conducted in the 0.5 m^3 vessel is not complete (according to EN 14034-2). Due to the brutality of the aluminum dust, equipment used during the explosion testing were damaged more for every conducted test. Since a trend could be observed for aluminum without carrying out a full series, it would not be beneficial to continue. When comparing the maximum explosion pressures and explosibilities found in the 0.5 m^3 vessel to the values obtained in the 20-liter sphere, some similarities are observed as shown in Figure 4.13 and Table 4.14.

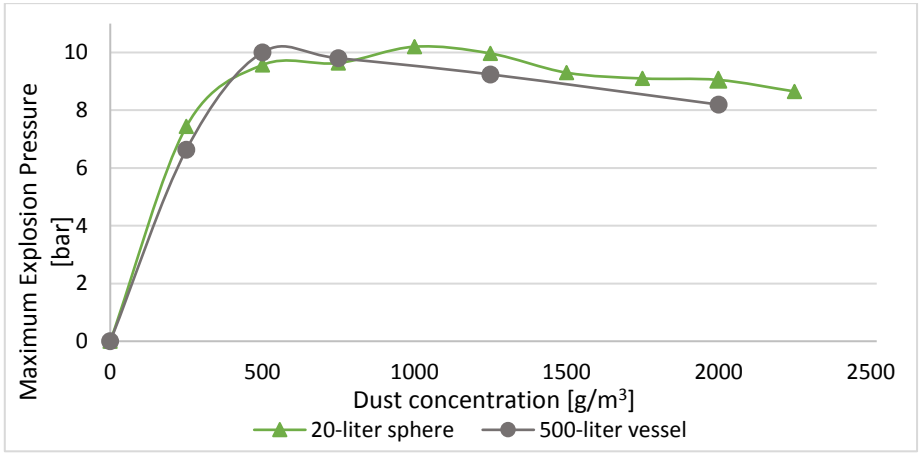

(a)

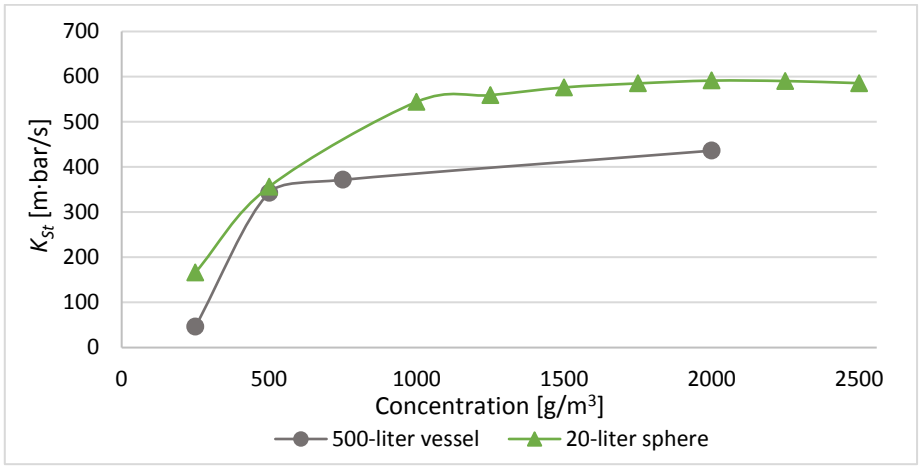

(b)

Figure 4.13: *Comparison of explosion data obtained for aluminum dust in the 20-liter sphere and the 0.5 m³ vessel. (a) Maximum explosion pressure and (b) explosibility as a function of concentration.*

Figure 4.13 (a) displays the maximum explosion pressure for aluminum dust in both test vessels. The maximum explosion pressure as a function of concentration is very similar

In both the 20-liter vessel and the 0.5 m³ sphere, and could imply that an equivalent dust concentration is present in the dust cloud in both vessels at the time of ignition. Since this is not the case for maize starch (Figure 4.9) this suggests a different dispersion pattern for aluminum dust. Aluminum does not have the same adhesion properties as maize starch, and a smaller portion of the dust would adhere to the walls prior to ignition in the 20-liter sphere.

Because of aluminums' high density, dust farther from the ignition source would have time to settle out of suspension before the flame has propagated to that same point in the 0.5 m³ vessel, thus decreasing the actual concentration in the volume. These two factors combined would make the actual concentrations in the two vessels more similar, and thereby a similar pattern for the maximum explosion pressure can be observed. Maximum explosion pressures and explosibilities for aluminum dust in the 20-liter sphere and 0.5 m³ vessel are listed in Table 4.14.

Table 4.14: *Explosion properties for aluminum dust. Tested in both the 20-liter sphere and the 0.5 m^3 vessel.*

Volume	p_{max} **[bar]**	$K_{St,\ max}$ **[m·bar/s]**
20-liter sphere	10.20	591.20
0.5 m^3 vessel	10.00	436.00

When increasing the concentration beyond the worst-case concentration (~500 g/m^3) the aluminum particles starts acting like heat sinks, and the maximum explosion pressure will decrease. At the same time the ratio between fuel and oxidizer increases, and a more ideal concentration will be reached earlier in the explosion, i.e. dt becomes smaller. A turbulent and rapid combustion process will then take place in the early stage of the explosion, resulting in a higher $(dp/dt)_{max}$, and thus a higher K_{St}-value (Figure 4.13 (b)). As the flame propagates outwards, the amount of dust present will be so large that the flame temperature decreases and a lower p_{max} is obtained, from Eq. (2.4). The principle can be seen in Figure 4.14.

As the heat transfer due to thermal radiation is dependent on the temperature to the fourth power, the heat transfer will decrease significantly as the flame propagates outwards and the amount of dust increases. The view factor in Eq. 2.2 which is dependent on the concentration, will decrease as the concentration is increased. As the concentration increases past stoichiometric, more dust will shade for a heated particle in the combustion zone trying to radiate a particle in the unburnt region, and the particles are not able to "see" each other. Since the heat transfer is reliant on the area of the flame front, which is larger in the 0.5 m^3 vessel than in the 20-liter sphere, this would be an opposing force to the decrease in heat transfer due to the lowered temperature and view factor. A larger concentration may also contribute an increase in initial turbulence, which will increase $(dp/dt)_{max}$. However, the effect of the larger flame front in the 0.5 m^3 vessel (and the potential increase in turbulence) does not seem to have enough influence to cause a net increase in the heat transfer.

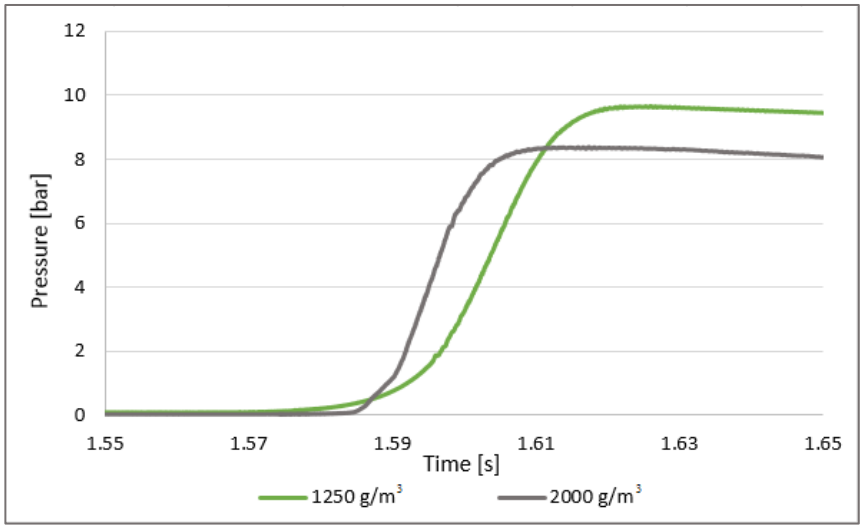

Figure 4.14: *Pressure evolution as a function of time for aluminum dust with two different concentrations. Tested in the 0.5 m^3 vessel.*

The difference in explosion severity in the 20-liter sphere and the 0.5 m^3 vessel, is relatively small in comparison to the effect of altering the ignition delay. The same explosivity of 591.20 m·bar/s as obtained in the 20-liter sphere could be acquired in the 0.5 m^3 vessel by decreasing the ignition delay time. As mentioned, since aluminum has a higher density than maize starch, more dust will have settled out of the dust cloud at the given ignition delay. Thereby by decreasing the time between dispersion and ignition, more dust would be present in the cloud when flame propagation from the ignition source is initiated, and the explosion violence would increase.

The trends for the explosibility in both vessels are quite similar in the sense that they level out as the concentration is increased. A severe breach is observed on the K_{St}-graph for the 0.5 m^3 vessel since a concentration of 250 g/m^3 yields a lower K_{St}-value in comparison to the 20-liter sphere. The turbulence level may be too low, since an optimal turbulence level for maize starch, may not be optimal for aluminum dust. Hence, higher concentrations of aluminum dust would not increase the explosion severity.

As the aim was to look at how the standard would handle metal dusts, no altering of the ignition delay time has been carried out for aluminum. Thus a weakness in the standard can be observed since the standardized vessels are calibrated for dusts which possesses different physical properties than aluminum and other high density dusts.

The K_{St}-value for aluminum dust tested in the 0.5 m^3 vessel does not seem to exceed that of the 20-liter sphere. Nor is it likely that the explosivity in the 0.5 m^3 will increase much further if the concentration increases due to heat sink effects and the reduced view factor related to radiation (Figure 4.13 (b)). When comparing explosion violence of aluminum in the two vessels between concentrations 500 g/m^3 and 2000 g/m^3, there is a larger increase of K_{St} in the 20-liter sphere than in the 0.5 m^3 vessel. Even though the series in the 0.5 m^3 vessel is not complete, the results show that the explosion severity for aluminum does not necessarily increase with increasing vessel size. Thereby, it is not possible to generalize that this is the case for metal dusts, i.e. it cannot be stated that thermal radiation contribution increases the explosibility as the volume increases.

5 Application of Test Results

As explained in section 1.1, there are several techniques for mitigating dust explosions. When designing a plant it is important to keep in mind that one or more mitigation safety measures could be necessary for each vessel. It is therefore vital to be aware of the maximum explosion pressure and maximum rate of explosion pressure rise for the dusts that are handled at the plant. In addition, parameters such as moisture content in the dust and turbulence levels in different parts of the plant are relevant, because these impact the K_{St}-value.

From an economical aspect is not necessary to design all equipment to withstand the worst case explosibility, because turbulence levels may vary from enclosure to enclosure. For example, a plant may have a ventilation system that is both connected to the free space in the factory, as well as separate enclosures, such as built in conveyor belts. The main outlet of the system commonly has a filter where the turbulence level tend be very high due to suction through the system and obstacles in the filter. If all enclosures are designed to withstand the same explosion pressure and rate of pressure rise as the filter, the costs would be enormous. In the enclosure around a conveyor the turbulence level will be much lower, and hence a smaller vent area or weaker walls can be applied.

If a plant is built without considering mitigating measures, the costs could be even bigger as the necessary actions may not be practically possible to integrate in the completed plant. For example if it is discovered that a silo needs to be able to withstand a larger rate of pressure rise, it would be cheaper to increase the vent area than to strengthen the whole vessel. At this time it may no longer be possible to increase the vent area due to of lack of space or due to the safety of personnel.

Vent areas are a widely employed, cost effective mitigation measure, and will now be discussed in more detail.

5.1 Designing vent areas

Explosion venting does not prevent or quench an explosion, but is a mitigation measure which limits the explosion overpressure. Venting shall not be performed if the dust in question or its combustion products are classified as dangerous or damaging to either people or the environment and could be released in unacceptable amounts.

The most important aspect of designing vents is accurate sizing, and is dependent on the explosion characteristics of the dust, the state of the dust cloud, i.e. the concentration, turbulence and distribution, as well as the geometry of the enclosure. Especially the length-to-diameter ratio of an enclosure is important since the rate of the flame propagation increases as the ratio increases [12].

For enclosures the required vent area, A_v, can be calculated from the following equations:

a) 0.1 bar overpressure $\leq \underline{p_{red,max}} <$ 1.5 bar overpressure

$$A = B(1 + C \cdot log\ L/D\ ) \quad [m^2] \tag{5.1}$$

with

$$B = [3.264 \cdot 10^{-5} \cdot p_{max} \cdot K_{St} \cdot p_{red,max}^{-0.596} + 0.27 \cdot (p_{stat} - 0.1) \cdot p_{red,max}^{-0.5}] \cdot V^{0.753} \quad (5.2)$$

$$C = (-4.305 \cdot log\ p_{red,max} + 0.758) \quad (5.3)$$

$$A_v = A/E_f \qquad E_f\text{: venting efficiency} \quad (5.4)$$

b) 1.5 bar overpressure ≤ $p_{red,max}$ < 2.0 bar overpressure

$$A = B \quad (5.5)$$

$$A_v = A/E_f \qquad E_f\text{: venting efficiency} \quad (5.6)$$

When assuming the efficiency factor is equal to 1, the effective venting area is equal to the physical one and A will be the volume that needs to be fitted to the enclosure. If the venting efficiency is less than 1, the required venting area A_v shall be larger than the geometric vent area A.

The above equations need to fulfill several conditions to be valid, such as atmospheric conditions of the surrounding medium. For the complete set of conditions see the European Standard EN 14491 [12]. The most relevant condition for this work however, is the maximum explosion overpressure which is dependent on the K_{St}-value. p_{max} shall be between 5 and 10 bar for 10 m·bar/s ≤ K_{St} ≤ 300 m·bar/s and 5 to 12 bar for 300 m·bar/s ≤ K_{St} ≤ 800 m·bar/s.

The equations will estimate the required vent areas correctly for most practical purposes. However, if the turbulence in the dust cloud is either low or particularly severe, the necessary vent area can be over or understated, respectively [12].

To demonstrate the effect of p_{max} and K_{St} on vent area, a hypothetical enclosure of 50 m³ has been given the conditions displayed in Table 5.1. By using the maximum explosion pressures and explosibilities found for the maize starch and aluminum in both the 20-liter sphere and 0.5 m³ vessel, the required vent areas for this hypothetical enclose is calculated.

Table 5.1: *Hypothetical enclosure volume for vent area calculation.*

Enclosure volume [m³]	50.0
Static activation overpressure of the venting device, p_{stat} [bar]	0.2
Maximum reduced explosion overpressure, $p_{red,\ max}$ [bar]	1.0
Efficiency factor, E_f	1.0
Length-to-diameter ratio, L/D	1.0

Since the maximum reduced explosion overpressure is chosen to be 1.0 bar, Eq. (5.1) is used. Still, when using a length-to-diameter ratio of 1, A = B, and Eq. (5.5) can be applied as well. The explosion properties used for the calculations and the resulting vent areas for maize starch and aluminum in both test vessels are presented in Table 5.2.

Table 5.2: *Explosion properties for maize starch of 10.24 % moisture content and aluminum (obtained in the 20-liter sphere and 0.5 m³ vessel) with required vent area for the enclosure presented in Table 5.1.*

Real volume [m^3]	**Explosion properties**	**Maize starch**	**Aluminum**
0.02	Maximum explosion overpressure, p_{max} [bar]	8.10	10.20
	Explosibility, K_{St} [m·bar/s]	97.00	591.20
	Required vent area, A_v [m^2]	**1.00**	**4.26**
0.5	Maximum explosion overpressure, p_{max} [bar]	7.28	10.50
	Explosibility, K_{St} [m·bar/s]	100.63	371.45
	Required vent area, A_v [m^2]	**0.97**	**2.91**

For the maize starch the required vent area only differs by 0.03 m² when using the explosion properties found in the 20-liter sphere and 0.5 m³ vessel, which implies that the scaling law which is the K_{St}-value, is consistent for organic dusts. For aluminum on the other hand, the vent area differs by 32 % when using the two different explosion properties. This could imply that the vent area required for the 50 m³ vessel containing aluminum dust is overestimated when using the standard 20-liter sphere for explosion testing and that in reality the severity of the explosion is not as high in a large scale industrial enclosure.

The required vent area for the same hypothetical enclosure with the same parameters (Table 5.1) for the different ignition delay times used in the 25 m³ vessel are calculated and displayed in Table 5.3. The dust used in this vessel is the same maize starch of 10.24 % moisture content as used in the experiments in this work.

Table 5.3: *Explosion properties for maize starch (obtained in the 25 m³ vessel) with required vent area for the enclosure presented in Table 5.1.*

Explosion properties	**Ignition delay time [ms]**		
	900	**780**	**300**
Maximum explosion overpressure, p_{max} [bar]	8.40	8.20	9.10
Explosibility, K_{St} [m·bar/s]	64.49	93.80	345.89
Required vent area, A_v [m^2]	**0.84**	**0.99**	**2.47**

As mentioned earlier the maize starch is not very explosible, and is a class 1 dust. By changing the initial turbulence at the time of ignition, the K_{St}-value increases vastly and now yields an explosibility associated with dust class 3 (ignition delay time of 300 ms).

When comparing the K_{St}-value for maize starch for the shortest ignition delay, it is almost as high as for the aluminum dust tested in the 0.5 m³ vessel. This illustrates the great importance of ignition delay time and its effect on explosibility and thus the vent area required to successfully mitigate an explosion. This once again shows that the K_{St}-value is an approximate value that may not alone be suited for mitigating measures.

Maize starch of different moisture contents shows that this too alters the required vent area because of it yielding quite different explosivity values (Figure 5.4).

Table 5.4: *Explosion properties for maize starch of two different moisture contents (obtained in the 20-liter sphere) with required vent area for the enclosure presented in Table 5.1.*

Explosion properties	**Moisture content [%]**	
	10.24	**0.83**
Maximum explosion overpressure, p_{max} [bar]	8.10	9.30
Explosibility, K_{St} [m·bar/s]	97.00	358.00
Required vent area, A_v [m^2]	**1.00**	**1.66**

When altering the parameters volume, moisture content and ignition delay time, they do not have the same impact on the required vent areas. This implies that the different factors influence the explosibility to different extents. From Tables 5.2 through 5.4, it is clear that the factor altering the explosibility and hence the vent area the most, is moisture content and the ignition delay time, or the level of turbulence at the time of ignition.

5.1 CFD Simulations

Full scale testing is time consuming and very expensive, and is one of the reasons that standardized testing in small volumes have been developed. CFD software packages are developed in order to simulate the course of industrial dust explosions in complex geometries from the explosion properties obtained in standardized tests.

It is not only the K_{St}-value from Eq. 2.20 that can be used when considering pressure development and dust explosions. The burning velocity, S_u, which is the rate of the flame propagation relative to the unburned gas in front of it, is also used in CFD simulations. A widely applied CFD software is the FLACS-DustEx delivered by GexCon AS [48]. By using K_{St}-values and burning velocities obtained in 20-liter test vessels and by using Eq. (2.20), realistic representations of industrial plants and enclosures can be simulated along with e.g. worst-case explosion scenarios and necessary mitigation safety measures.

6 Conclusions

Pressure development in dust explosions have been considered in the standardized 20-liter Siwek sphere and a non-standardized 0.5 m^3 vessel. The K_{St}-value or the dusts' explosion violence, which is said to be independent of vessel volume, have been challenged by altering various dust properties.

A change in volume seemed to affect the maize starch in the sense that a larger dust concentration was necessary in the 20-liter sphere to obtain the same explosion properties, i.e. maximum explosion pressure and explosion violence, as in the 0.5 m^3 vessel. Aluminum however, did not seem to be affected by a change in vessels size.

As the moisture content of the maize starch was reduced, an increase in both maximum pressure and explosion violence, i.e. the maximum rate of explosion pressure rise, was observed.

When comparing the experimental results from the aluminum used in this work to other samples with similar particle size distributions, it can be seen that they might yield completely different explosion properties. However, other parameters such as purity of the sample and the shape of the particles (which the particle size distribution says nothing about), may be the reason for the deviations.

The effect of change in turbulence is probably the most important parameter when it comes to explosion violence. It was observed that a shorter ignition delay time (and hence a higher turbulence intensity) increased the explosibility to a large extent. In the 0.5 m^3 vessel the K_{St}-value increased more than three times when changing the ignition delay time from 900 to 400 ms. An even greater increase in initial turbulence and hence explosion violence was observed in the 25 m^3 vessel where an ignition delay time from 900 to 300 ms increased the K_{St}-value more than 5 times.

When testing aluminum dust the effect of thermal radiation did not seem to increase with volume, i.e. when the area of the flame front increased. When increasing the concentration beyond the concentrations that yields the worst-case explosion scenario for aluminum, the particles started acting like heat sinks rather than contributing to an increase in the temperature. Due to these observations, it not possible to proclaim that thermal radiation contribution increases the explosibility as the volume increases for metal dusts in general.

When it comes to designing mitigation safety measures, it is clear that all properties of the dust, such as moisture content, particle shape and size distribution and concentration, must be considered. The standard method for determining explosibility, in particular the 20-liter sphere, may not provide accurate enough results, as the model for the K_{St}-value is quite simplified. Especially, one must consider the turbulence levels that may occur inside enclosures, in order to predict the worst-case scenario.

The standard for obtaining a dusts' explosibility may be used more as an aid when considering mitigating safety measures, rather than as a specific dust constant.

7 Further Work

There is no doubt that further study on the field and optimization of the 0.5 m^3 vessel is necessary to get conclusive results. As neither the dispersion nor ignition systems are airtight, the evacuated pressure before dispersion could not be kept constant, and needs to be improved. An upgraded trigger box with relays that can withstand the current that is sent through it is also highly recommended. In addition, to save time, the dispersion chamber should be replaced with a stationary one that is always mounted to the vessel and which is charged with dust from the top.

It may also be useful to install thermocouples in order to provide information about the temperature inside the vessel, as well as a water jacket to cool down the vessel to the initial temperature between each experiment.

Each test series for the maize starch and aluminum should be carried out at least three times to get satisfactory explosivity values in the 0.5 m^3 vessel, which has not been done yet. Furthermore several other dusts should be tested in the 0.5 m^3 volume in order to prove conformity and be able to use it as an alternative to the standard explosion chambers.

As previously mentioned the K_{St}-value is a highly approximate term when characterizing a dust's explosion violence. Another model that considers the effect of flame thickness and turbulence should definitely be developed in order to design proper mitigation safety measures.

In general the focus should be addressed the turbulence level. Other properties like moisture content, particle size distribution and concentration can easily be measured, while the turbulence level stays undetermined. By using CDF tools, realistic simulations can be obtained when it comes to both initial turbulence and pressure development. Via these simulations it may be possible to assess the K_{St}-value in a different manner by dividing it into different categories.

The current standard may be realistic for low turbulence levels, which occur in equipment such as silos and conveyor belts. However, for enclosures where the turbulence can get very high, the K_{St}-value itself may not be sufficient. A further developed standard may be crucial for these types of enclosures if the K_{St}-value is to be used when designing mitigating safety measures in the future.

References

[1] R. Eckhoff, *Dust Explosions in the Process Industries* - 3rd ed., Amsterdam: Gulf Professinal Publishing, 2003.

[2] Skjold, T., Larsen, Ø. & Hansen, O.R., Possibilities, limitations, and the way ahead for dust explosion modelling, *IChemE Symposium Series,* vol. 151, pp. 282-297, 2006.

[3] T. Skjold, *Flame propagation in dust clouds, Numerical simulatuion and experimental investigation*, Dr thesis, University of Bergen, 2014.

[4] Abbasi, T., Abbasi, S.A., Dust Explosions - Cases, causes, consequences, and control, *Journal of Hazardous Materials,* vol. 140, no. 1-2, pp. 7-44, 2007.

[5] Cloney, C., www.mydustexplosionresearch.com, [Online]. Available: http://www.mydustexplosionresearch.com/explosion-incidents/. [Accessed 16 05 2018].

[6] Cloney, C., 2017 Combustible Dust Incident Report - Version #1, Retreived from http://www.myDustExplosionResearch.com/2017-Report, 2018.

[7] Amyotte, P.R., Eckhoff R.K., "Dust explosion causation, prevention and mitigation: An overview," *Journal of Chemical Health and Safety,* vol. 17, no. 1, pp. 15-28, 2010.

[8] "Minimum requirements for improving the safety and health protection of workers potentially at risk from explosive atmospheres", *Official Journal of the European Communities,* vol. 15th individual Directive within the meaning of Article 16(1) of Directive 89/391/EEC, 1999.

[9] European Standard EN 14034-2, *Determination of explosion characteristics og fust clouds - Part 2: Determination of the maximum rate of pressure rise (dp/dt)max of dust clouds,* Brussels: European Committee for Standardization (CEN), 2006.

[10] Dahoe, A.E., Zevenbergen, J.F., Lemkowitz, S.M., Scarlett, B., Dust explosions in spherical vessels: The role of flame thickness in the validity of the 'cube-root law', *Journal of Loss Prevention in the Process Industries,* vol. 9, no. 1, pp. 33-44, 1996.

[11] U.S. Department of Labor, Hazard Communication Guidance for Combustible Dusts, *Occupational Safety and Health Administration (OSHA 3371-08),* 2009.

[12] European Standard EN 14491, *Dust explosion venting protective systems*, Brussels: European Committee for Standardization (CEN), 2006.

[13] Bidabadi, M., Zadsirjan, S., Mostafavi, S.A., Radiation heat transfer in transient dust cloud flame propagation, *Journal of Loss Prevetion in the Process Indursties,* vol. 26, no. 4, pp. 862-868, 2013.

[14] Warnatz, J. , Maas, U., and Dibble, R.W., *Combustion*, 4th ed., Berlin: Springer, 2006.

[15] Youmans, E.L., *The Popular Science Monthly,* vol. X, 1876.

[16] K. Cashdollar, Overview of dust explosibility charactersitics, *Journal of Loss Prevention in the Process Industries,* vol. 13, pp. 183-190, 2000.

[17] Gao, W., Mogi, T., Sun, J., Yu, J., Dobashi, R., Effects of particle size distributions on flame propagation mechanism during octadecanol dust explosions, *Powder Technology,* vol. 249, pp. 168-174, 2013.

[18] Lillestøl, E., Hunderi, O., Lien, J.R., *Generell fysikk for universiteter og høgskoler, bind 2 varmelære og elektromagnetisme*, Oslo: Universitetsforlaget, 2001.

[19] Holman, J.P., *Heat Transfer* - 10th ed., McGraw-Hill, 2010.

[20] "Wikipedia", 7 March 2007. [Online]. Available: https://en.wikipedia.org/wiki/Laminar%E2%80%93turbulent_transition. [Accessed 05 03 2018].

[21] T. Skjold, *Selected aspects of turbulence and combustion in 20-litre explosion vessels: development of experimental apparatus and experimental investigation*, MSc Thesis, University of Bergen, 2003.

[22] European Standard EN 14034-1, *Part 1: Determination of the maximum explosion pressure Pmax of dust clouds*, Brussels: European Committee for Standardization (CEN), 2004.

[23] Bartknecht, W., *Brenngas- und Staubexplosionen*, Forschungsbericht F45. Koblenz: Fedeeral Republic of Germany: Bundesinstitut fur Arbeitsschutz., 1971.

[24] Dahoe, A.E. Cant, R.S. Scarlett, B., On the Decay of Turbulence in the 20-Liter Explosion Sphere, *Flow, Turbulence and Combustion,* vol. 67, no. 3, pp. 159-184, 2001.

[25] "www.pubchem.ncbi.nlm.nih.gov", National Center for Biotechnology Information, U.S. National Library of Medicine, 11 07 2008. [Online]. Available: https://pubchem.ncbi.nlm.nih.gov/compound/24836924#section=Top. [Accessed 07 06 2018].

[26] Moussa, R.B., Proust, C., Guessasma, M., Saleh, K., Fortin, J., Physical mechanisms involved into the flame propagation process through aluminum dust-air clouds: A review, *Journal of Loss Prevention in the Process Industries,* vol. 45, pp. 9-28, 2017.

[27] International Standard ISO 6184-1, *Explosion protection systems Part 1: Determination of explosion indices of combustible dusts in air*, International Organization for Standardization (ISO), 1985.

[28] Bartknecht, W., *Dust Explosions: Course, Prevention, Protection*, Berlin: Springer-Verlag [Translation of Staubexplosionen, by Bruderer, R.E. and Siwek, R.], 1989.

[29] Proust, C., Accorsi, A., Dupont, L., Measuring the violence of dust explosions with the "20 l sphere" and with the standard "ISO 1m³ vessel". Systematic comparison and analysis of the discrepancies, *Journal of Loss Prevention in the Process Industries,* vol. 20, no. 4-6, pp. 599-606, 2007.

[30] van der Wel, P.G.J., van Veen, J.P.W., Lemovitz, S.M., Scarlett, B., van Wingerden, C.J.M., An interpretation of dust explosion phenomena on the basis of time scales, *Powder Technology,* vol. 71, pp. 207-215, 1992.

[31] Pu, Y.K., Jarosinski, J., Johnson, V.G., Kauffman, C.W., Turbulence effects on dust explosions in the 20-l spherical vessel, *Symposium (International) on Combustion,* vol. 23, no. 1, pp. 843-849, 1991.

[32] Dahoe, A.E., Cant, R.S, Pegg, M.J., Scarlett, B., On the transient flow in the 20-liter explosion sphere, *Journal of Loss Prevention in the Process Industries,* vol. 14, no. 6, pp. 475-487, 2001.

[33] Enright, R.J., Experimental Evaluation of the 1.2, 8 and 20 Litre Explosion Chambers, *Proceedings of the First International Colloquium on Explosiveness of Industrial Dusts,* pp. 52-62, November 1984.

[34] Marion, M., Chauveau, C., Gökalp, I., Studies on the ignition and burning of levitates aluminum particles, *Combustion Science and Technology,* vol. 115, no. 4-6, pp. 369-390, 1996.

[35] Proust, C., A few fundamental aspects about ignition and flame propagation in dust clouds, *Journal of Loss Prevention in the Process Industries,* vol. 19, no. 2-3, pp. 104-120, 2006.

[36] Proust, C., Moussa, B.R., Mphamed, G., Khasahayar, S., Jérôme, F., Thermal radiation in dustflame propagation, *Journal of Loss Prevention in the Process Industries,* vol. 49, no. Part B, pp. 896-904, 2017.

[37] Cesana-AG, "cesana-ag.ch", Adolf Kuhner AG, 2016. [Online]. Available: http://www.cesana-ag.ch/20_L_Apparatus.shtml. [Accessed 22 05 2018].

[38] Fr. Sobbe GmbH, "sobbe-zuender.de", SOBBE, 2017. [Online]. Available: http://www.sobbe-zuender.de/en/product-ranges/pyrotechnical-igniters/. [Accessed 19 05 2018].

[39] "www.intertechnology.com", Kistler Instrumente AG Winterthur, [Online]. Available: https://intertechnology.com/Kistler/pdfs/Pressure_Model_701A.pdf. [Accessed 31 05 2018].

[40] "www.sensorsmag.com", 01 01 2003. [Online]. Available: https://www.sensorsmag.com/components/pressure-measurement-principles-and-practice. [Accessed 31 05 2018].

[41] Gault, K., Internship Resport: Unknown Aspects of Metal Dust Explosions, *Institut National des Sciences Aplliquées (INSA)*, 2014.

[42] IEP technologies, HOERBIGER Safety Solutions, PHRD Suppressor Operating Manual, MC-592 Rev AA, Cheltenham.

[43] Crowe, C.T., Schwatzkopf, J.D., Sommerfeld, M., Tsuji, Y., *Multiphase flows with droplets and particles*, 2nd ed., Boca Raton: CRC Press, Taylor & Francis Group, 2012.

[44] "www.staubex.ifa.dguv.de" Institute for Occupational Safety and Health of German Social Accident Insurance, [Online]. Available: http://staubex.ifa.dguv.de/exploergebnis.aspx?lang=e. [Accessed 08 05 2018].

[45] CLC/TR 50404, Statisk elektrisitet i eksplosjonsfarlige områder, Brussels: Comité Européen de Normalisation Electrotechnique, CENELEC. (Translation of Electrostatics – Code of practise for the avoidance of hazards due to static electricity by Norsk Elektroteknisk Komite, NEK, 2003.

[46] Cashdollar K.L., Zlochower, I.A. Explosion temperatures and pressures of metals and other elemental dust clouds, *Journal of Loss Prevention in the Process Industries,* vol. 20, no. 4-6, pp. 337-348, 2007.

[47] DeRose, S., "www.derose.net" 06 04 2005. [Online]. Available: http://www.derose.net/steve/resources/engtables/flametemp.html. [Accessed 06 06 2018].

[48] "www.gexcon.com" Gexcon AS, 13 10 2017. [Online]. Available: https://www.gexcon.com/flacs-software/article/FLACS-DustEx. [Accessed 06 05 2018].

[49] Kalejaiye, O., Amyotte, P.R., Pegg, M.J., Cashdollar K.L., Effectiveness of dust dispersion in the 20-L Siwek chamber, *Journal of Loss Prevention in the Process Industries,* vol. 23, no. 1, pp. 46-59, 2010.

[50] Cloney, C., "www.mydustexplosionresearch.com" 2017. [Online]. Available: http://www.mydustexplosionresearch.com/dust-equivalence-ratio/#aluminum. [Accessed 25 03 2018].

[51] Li, Y., Xu, H., Wang, X., Experimental Study on the Influence of Initial Pressure on Explosion of Methane-coal Dust Mixtures, *Procedia Engineering,* vol. 62, pp. 980-984, 2013.

Appendix A Calibration and Certificates

In order to obtain precise measurements it is important that calibrated equipment is used when conducting the experiments. The pressure transducers used to measure the pressure evolution during the explosions were calibrated as explained in Appendix A.1. In order to calibrate the pressure transducers a digital manometer was used, and the certification off calibration is attached in Appendix A.2.

Appendix A.1 *Pressure Transducers*

Before setting up the system for the 0.5 m^3 vessel the transducers had to be calibrated. This was done by connecting the transducers to a 3.37 liter reservoir with a manometer and a pressure indicator. The transducers were further connected to the charge amplifiers, the acquisition module and computer. A manometer was used as the reference pressure indicator. The transducer sensitivity on the charge amplifiers were adjusted to get as accurate pressure readings from the transducers as possible.

The test is performed by filling the reservoir to a given pressure using compressed air. By opening the valve between the pressurized volume and the connected transducers (which are at atmospheric conditions), a rapid increase in pressure occurred and was measured by the sensors. The pressure values detected by the transducers are sent to the LabVIEW program and compared to the reference manometer. The tests were executed with pressures ranging from 2 to 7 barg as illustrated in Figure A.1.

As the explosion testing started for the aluminum dust it was discovered that the pressure measurements was not as they should be, and it was decided to switch out the transducers with another pair, also these from Kistler, but now of the type 7031, having the same pressure range as the previous ones. The new transducers were calibrated as described above. The transducer serial numbers, IDs and sensitivities on the charge amplifiers are given in Table A.1.

Table A.1: *Pressure transducers used to record the pressure in the 0.5 m^3 explosion vessel.*

Transducer serial number	**Transducer ID**	**Transducer sensitivity on charge amplifier [pC/bar]**
SN1212291	P1	82,5
SN1546628	P2	82,3
SN4351126	P1, after 02.05.2018	88,5
SN4315128	P2, after 02.05.2018	88,5

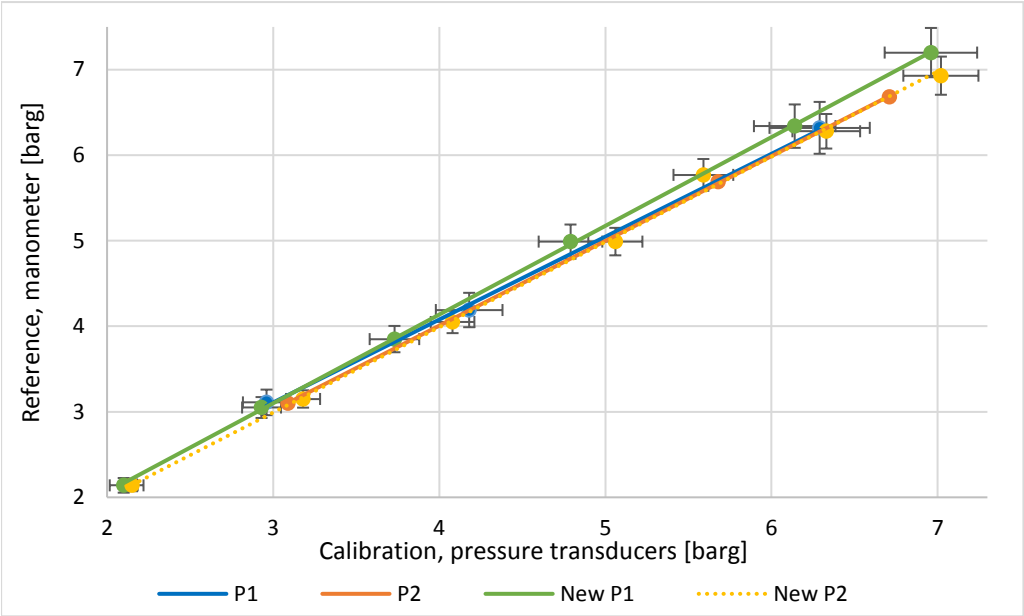

Figure A.1: *Calibration of pressure transducers.*

The transducers were calibrated to a maximum of 5 % deviation from the reference manometer.

Appendix A.2 *Manometer*

A digital manometer from Instrutek, model DMT1, ID: TI108102 was used for calibration of the pressure transducers. The certificate of calibration is supplemented below.

Kalibreringsbevis
Certificate of calibration

Oppdragsgiver/*Client* *GexCon AS* *Postboks 6015 Postterminalen* *5892 BERGEN*	**PO:** *060417* **Location:**	**Bevisnr.**/*Certificate no.*	**17-396167**
		Kalibreringsdato/*Date of calibration*	25.04.2017
		Utskriftsdato/*Date of issue*	25.04.2017
		Anb. ny kal./*Recommended due date*	25.04.2018
		Antall sider/*No. of pages*	1 av 1

Kalibrert utstyr/*Calibrated equipment*

Kundens ID *Clients ID*	**Fabrikat** *Manufacturer*	**Modell** *Model*	**Objekt** *Object*	**Serienr.** *Serial no*	**TI ID** *TI ID*
TI108102*	Instrutek	DMT1	Digital gauge	14829	TI108102

Kalibreringsnormaler/*Calibration standards*

404488, 408032, 405013, TI117665, 500001

Kalibreringsdata/*Calibration data*

Status/*Status*	Kalibrert med merknad / Cal. with remarks
Kalibreringsprosedyre/*Calibration procedure*	Ref. vedlegg / Ref. attachment
Temperatur og fuktighet/*Temperature and humidity*	20°C±2°C, 45%RH±25%RH

Merknader/*Comments*

The calibration certificate is not valid unless the following attachment is fully represented: 17-396167-1

Kalibrert av/*Calibration performed by*

Evelyn Kvamme

Calibration engineer

Evelyn Kvamme

Instrumentet er kalibrert i henhold til dokumenterte prosedyrer som kan forevises på forespørsel, og mot målenormaler som er sporbare til nasjonale eller internasjonale normaler.

This instrument is calibrated according to documented procedures which will be available upon request, and against measuring standards traceable to national or international standards.

Kiwa Teknologisk Institutt as

Postadresse: Pb. 141 Økern, 0509 Oslo
Besøksadresse: Kabelgaten 2, 0580 Oslo
Telefon: 22 86 50 00
Telefaks: 22 72 45 02
E-post: firmapost@ti.no
Web: www.teknologisk.no
Org.nr. 942 340 680
Kongsberg: Pb. 1019, NO-3601 Kongsberg
Stavanger: Forusparken 22, NO-4031 Stavanger
Haugesund: Pb. 93, NO-4299 Avaldsnes
Bergen: Pb. 23, NO-5346 Ågotnes

Kalibreringsbevis
Certificate of calibration

Attachment no. 17-396167-1

Kalibrert av *Calibrated by:*
Evelyn Kvamme

Kalibreringsdato *Date of Calibration :*
25.04.2017

Range:	-1 to 10 bar	Serial number:	14829
Output signal:	-1 to 10 bar	Fluid:	nitrogen

Kommentarer / merknader. *Comments / remarks:*

Reading of the output signal is done by the use of the internal display unit.
The output signal readings are direct in the appropriate pressure unit.
Pressure is applied to the pressure sensor in accordance with prosedure KH2-9-1 AG.
The pressure sensor is further calibrated in accordance with procedures KH 2-9-1 A.

The instrument is calibrated in a vertical position, with pressure connection downwards,
Reference level: At pressure connection

Kalibreringsbevis
Certificate of calibration

kiwa

Attachment no.: 17-396167-1

Range	*bar*	*Signal reading in:*	*bar*	*Resolution, bar*
Min. pressure:	-1	Min. signal reading:	-1,0	0,01
Max pressure:	10	Max. signal reading:	10,0	0,01
			Scale division shift at:	
Specified accuracy:	*bar*	*Abs. value in bar*	*% av FS*	*% av RDG*
Lowest pressure:	-1,0		0,2	
To and from pressure:	10,0		0,2	
To next pressure range:				

Results of calibration, pressure measurements.

Applied pressure **bar**	*Applied pressure* **bar**	*Reading increasing* **bar**	*Reading decreasing* **bar**	*Uncertainty of measurment* **bar**
-0,951	-0,951	-0,94	-0,94	±1,3E-02
0,000	0,000	0,00	0,00	±1,3E-02
2,502	2,502	2,51	2,51	±1,3E-02
5,005	5,005	5,01	5,01	±1,3E-02
7,508	7,508	7,51	7,52	±1,8E-02
10,012	10,012	10,03	10,03	±1,3E-02

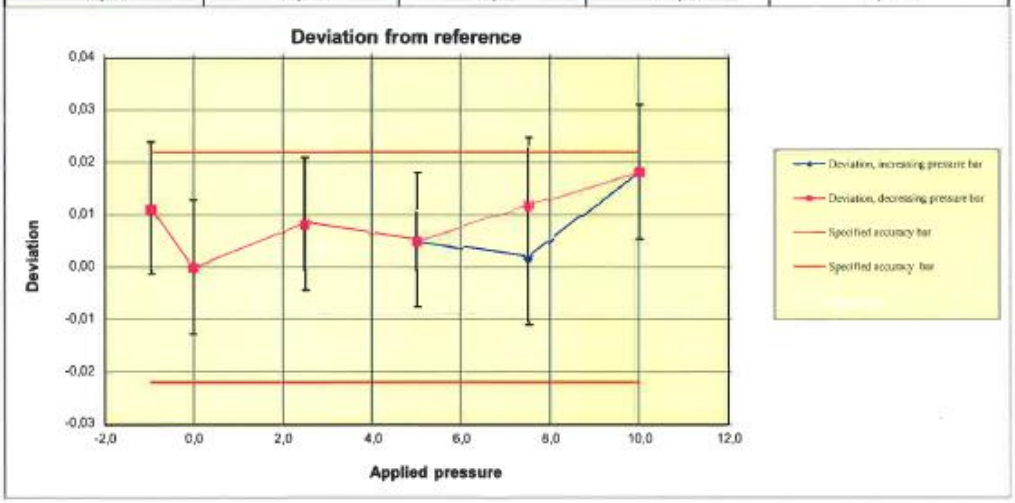

Appendix B Schematics

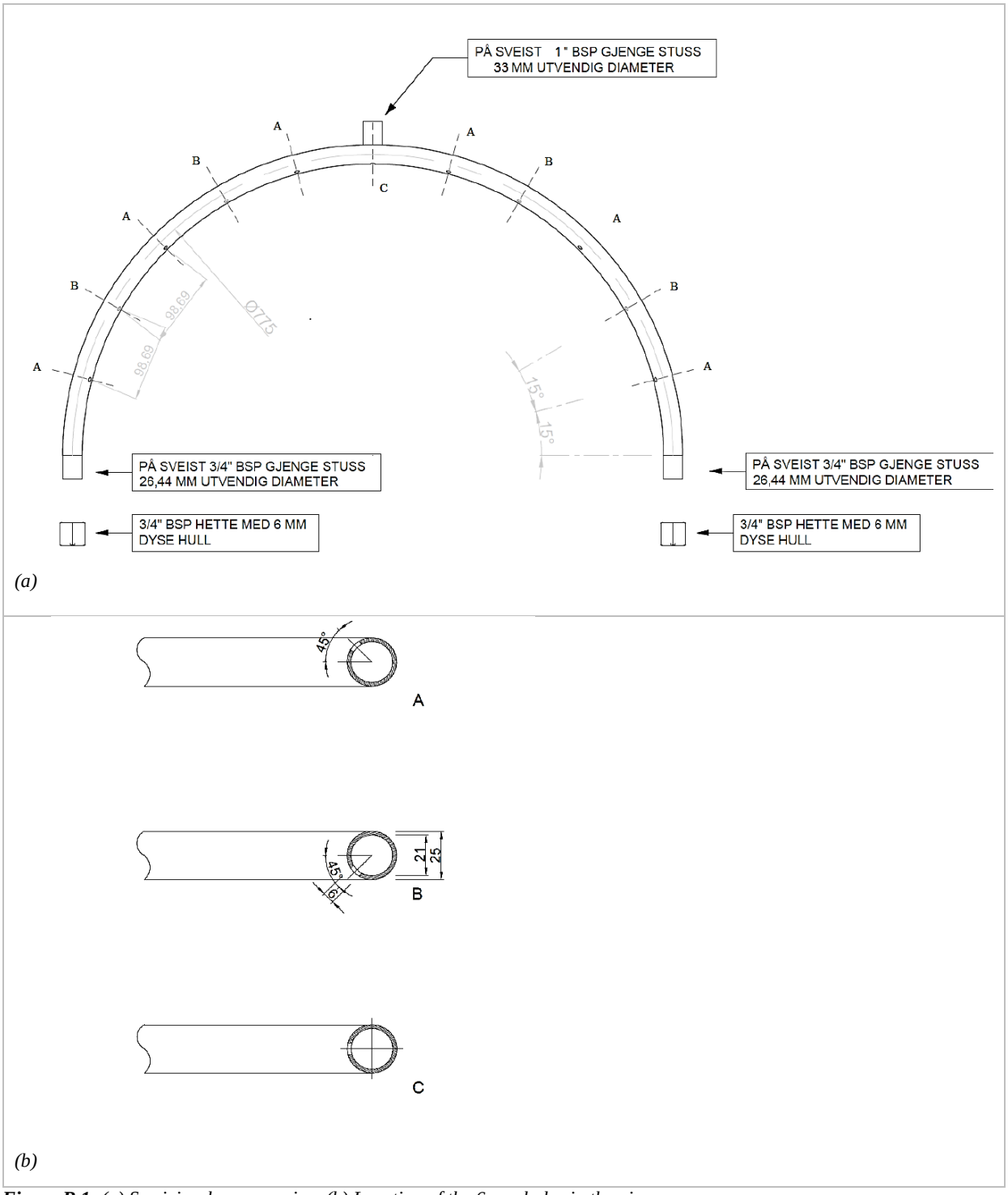

Figure B.1: *(a) Semicircular spray pipe. (b) Location of the 6 mm holes in the pipe.*

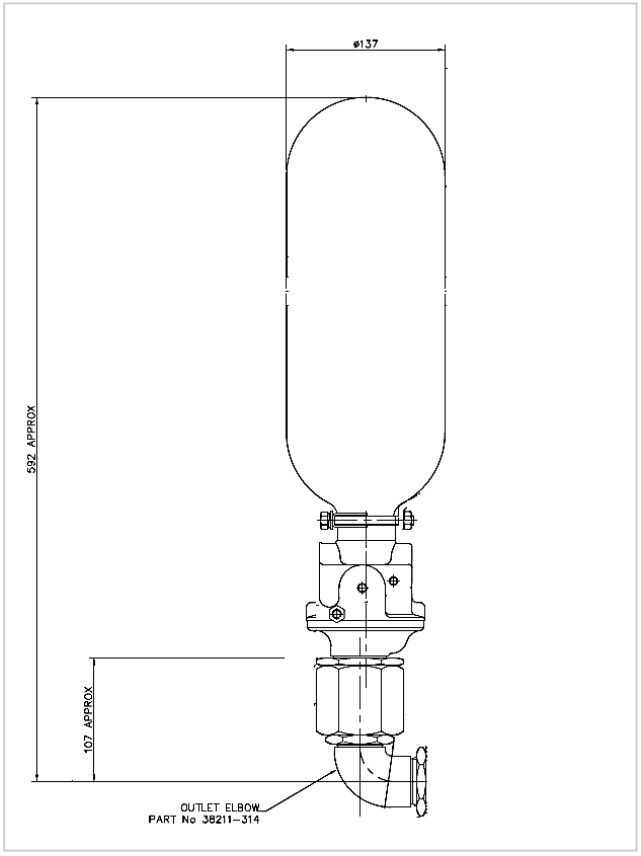

Figure B.2: *Dispersion chamber. Modified Protractor-operated High Rate Discharge (PHRD) suppressor used in explosion protection and isolation systems, from IEP technologies [42].*

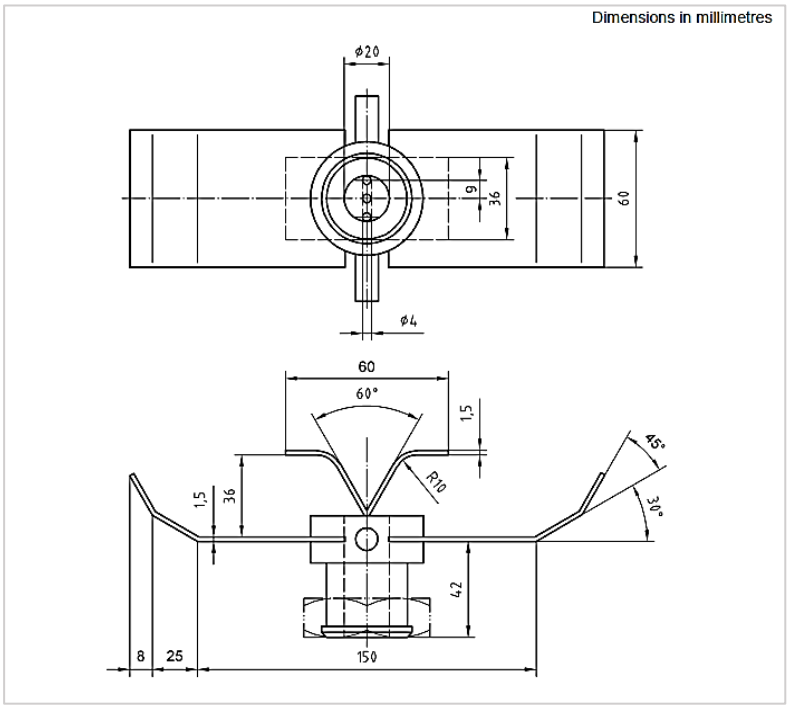

Figure B.3: *Rebound nozzle used in the standard 20-liter Siwek sphere.*

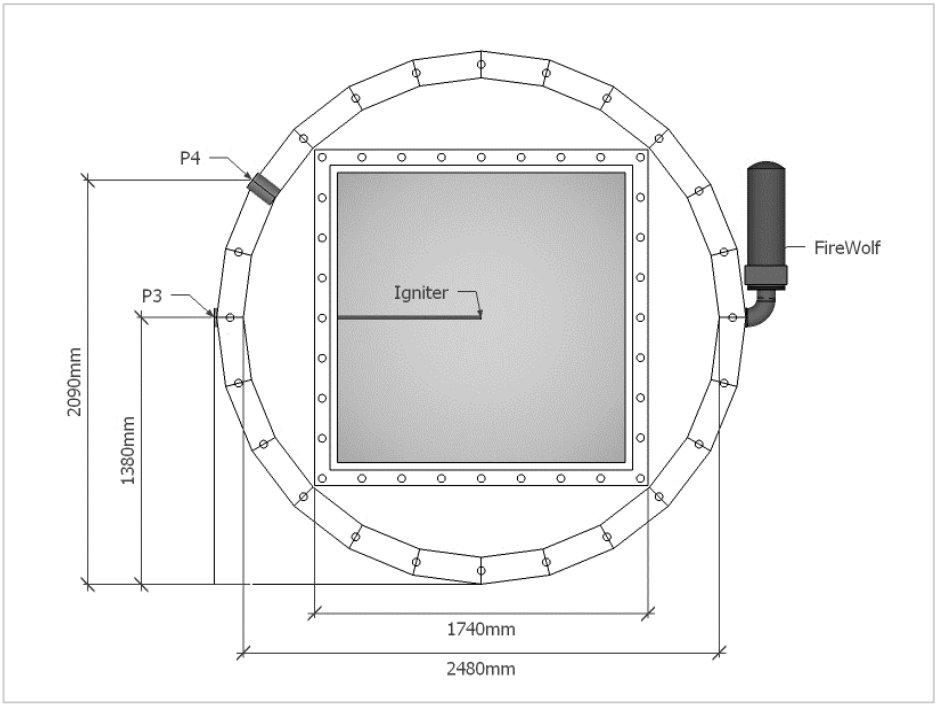

Figure B.4: *25m^3 vessel at Sotra.*

Appendix C LabVIEW Triggering Sequence

The trigger sequence for explosion testing in the 0.5 m³ is set up in a LabVIEW program as shown in Figure C.1.

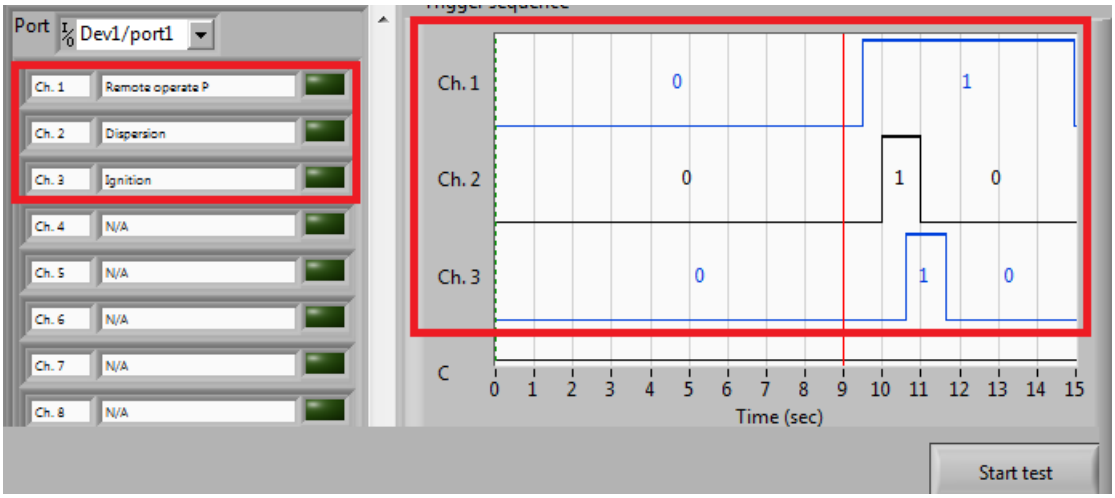

Figure C.1: *Trigger sequence in LabVIEW for explosion testing in the 0.5 m³ vessel.*

Only the first tree channels are in use, each connected to a digital output ports on the NI-card. The logging starts 9 seconds after the sequence is started, denoted by the red line. This yields time to retreat from the vessel and prepare for the experiment. Channel 1, which is connected to the relay that switches on the charge amplifiers for pressure logging is the first channel to be activated. Next up is Channel 2 which sends a signal to the explosive charge that opens the fast acting valve in the dispersion chamber, and the dust is dispersed into the vessel. 600 ms after dispersion the ignition source receives 24 V signal and is fired off.

Appendix D KSEP 6 Software

The KSEP 6 software is used to determine explosion properties for dusts in the 20-liter Siwek sphere. KSEP 6 is the acquisition and analysis software which receives signals from the control and measurement systems. The pressure development for each test (and test series) is analyzed and the software provides information about maximum pressure, maximum rate of pressure rise and explosivity, and curves are drawn as a function of concentration as shown in Figure 3.2.

Figure D.1 (a) shows all the tests that have been conducted for the given dust, which series it belongs to, the concentration and the associated explosion properties of KSEP 6. Figure D.1 (b) shows the details of test number 32. The two pressure sensors measure slightly different pressure evolution, and the tangent of the pressure-time curve can be fitted to yield the average of these two, and thereby an averaged K_{St}-value.

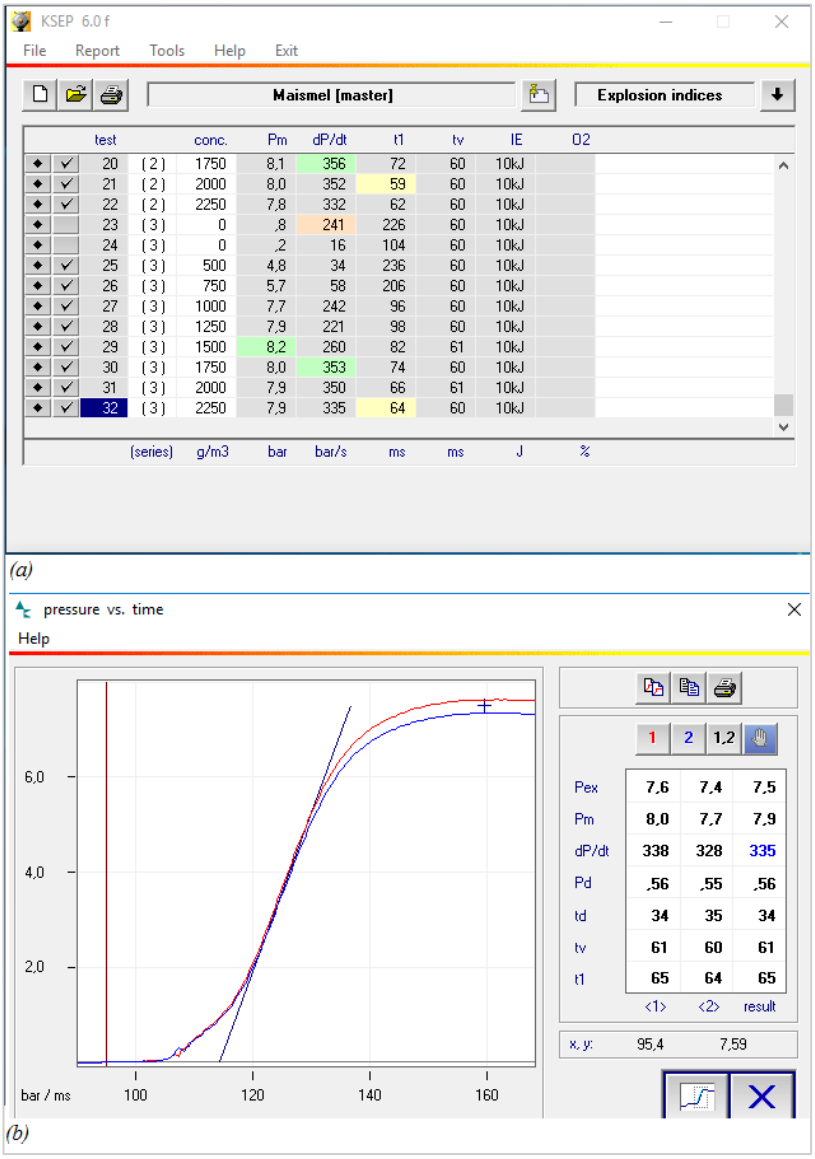

Figure D.1: *KSEP 6 (a) all the tests conducted for maize starch with associated explosion indices and (b) detailed explosion properties for test*

Appendix E Dust Explosion Data

All tables and figures for the maximum explosion pressures, maximum rates of explosion pressure rise and explosion violence are enclosed in this section. Maize starch tested as received (of 10.24 % moisture content) and dried, as well as aluminum dust are tested in volumes of 20-liter and 0.5 m³. Maize starch is also tested with different ignition delay times in the 0.5 m³ vessel.

Table E.1: *Averaged series for maize starch containing 10.24 % moisture content tested in the 20-liter sphere.*

Concentration [g/m³]	p_{max} **[bar]**	$(dp/dt)_{max}$ **[bar/s]**	K_{St} **[m·bar/s]**
500	5.25	45	12.31
750	6.71	145	39.27
1000	7.58	221	59.99
1250	8.03	271	73.65
1500	8.04	309	83.88
1750	7.98	354	90.00
2000	7.92	351	95.19
2250	7.78	336	91.20

Table E.2: *Averaged series for maize starch containing 0.83 % moisture content tested in the 20-liter sphere.*

Concentration [g/m³]	p_{max} **[bar]**	$(dp/dt)_{max}$ **[bar/s]**	K_{St} **[m·bar/s]**
500	6.21	199	54.02
750	7.83	324	87.95
1000	8.78	503	136.54
1250	9.12	651	176.71
1500	9.06	639	173.45
1750	8.97	708	192.18
2000	8.75	652	176.98
2250	8.57	624	169.38

Table E.3: *Averaged series for aluminum dust tested in the 20-liter sphere.*

Concentration [g/m³]	p_{max} **[bar]**	$(dp/dt)_{max}$ **[bar/s]**	K_{St} **[m·bar/s]**
250	7.43	612.67	166.30
500	9.57	1311.67	356.04
750	9.63	1442.33	391.51
1000	10.20	2004.67	544.15
1250	9.97	2059.00	558.90
1500	9.30	2122.33	576.09
1750	9.10	2155.00	584.96
2000	9.05	2178.00	591.20
2250	8.65	1274.50	590.25
2500	9.10	2157.00	585.50

Table E.4 *Explosion characteristics of maize starch of 10.24 % moisture content tested in the 0.5 m³ vessel. Ignition delay time 500 ms.*

Concentration [g/m³]	p_{max} **[bar]**	$(dp/dt)_{max}$ **[bar/s]**	K_{St} **[m·bar/s]**
250	4.61	26.70	21.19
500	6.56	109.39	86.82
750	7.92	153.34	121.70
1000	7.91	143.03	113.52
1250	7.36	141.01	11.92
1500	4.23	114.70	91.03

Table E.5: *Explosion characteristics of maize starch of 10.24 % moisture content tested in the 0.5 m³ vessel. Ignition delay time 600 ms.*

Concentration [g/m³]	p_{max} **[bar]**	$(dp/dt)_{max}$ **[bar/s]**	K_{St} **[m·bar/s]**
750	7.12	123.99	98.41
1000	7.27	121.02	96.05
1250	7.34	126.78	100.63

Table E.6: *Explosion characteristics of maize starch of ~3.5 % moisture content tested in the 0.5 m^3 vessel. Ignition delay time 500 ms.*

Concentration [g/m³]	p_{max} **[bar]**	$(dp/dt)_{max}$ **[bar/s]**	K_{St} **[m·bar/s]**
250	5.55	59.49	47.22
500	7.72	148.25	117.67
750	8.33	193.76	153.79
1000	7.82	209.41	166.20
1250	8.08	217.84	172.90
1500	7.34	180.88	143.56
1750	7.01	197.33	156.62
2000	6.52	110.94	88.05

Table E.7: *Explosion characteristics of aluminum tested in the 0.5 m^3 vessel. Ignition delay time 600 ms.*

Concentration [g/m³]	p_{max} **[bar]**	$(dp/dt)_{max}$ **[bar/s]**	K_{St} **[m·bar/s]**
250	6.63	58.85	46.71
500	10.00	431.87	342.77
750	9.80	457.10	362.80
1000	8.60	460.08	365.17
1250	9.24	459.01	364.37
2000	8.20	549.33	436.00

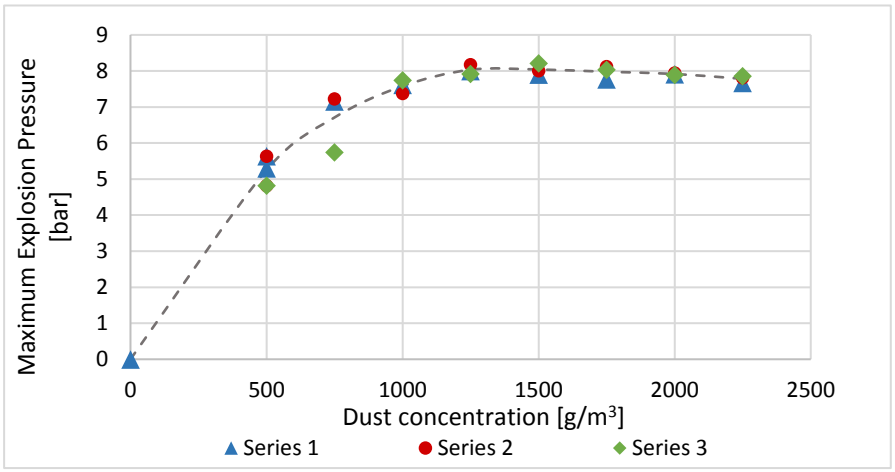

(a)

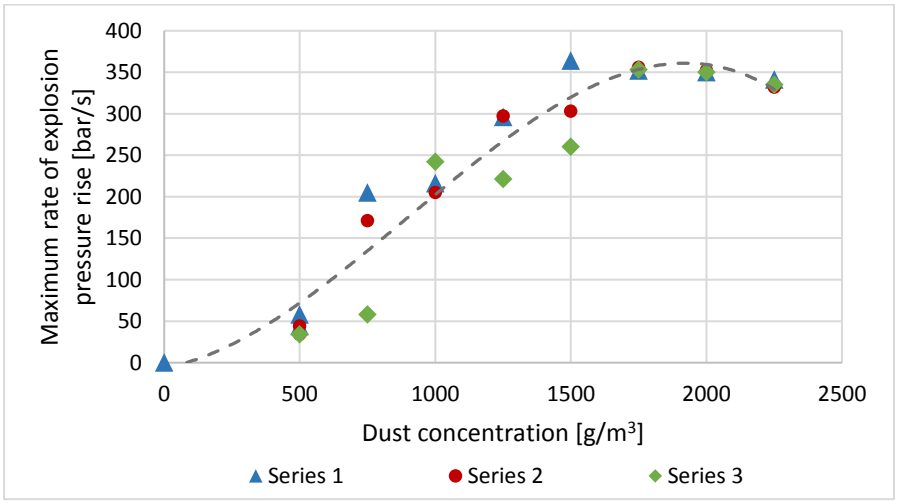

(b)

Figure E.2: *Series for maize starch containing 10.24 % moisture content. (a) Maximum explosion pressure and (b) maximum rate of explosion pressure rise. Tested in the 20-liter sphere.*

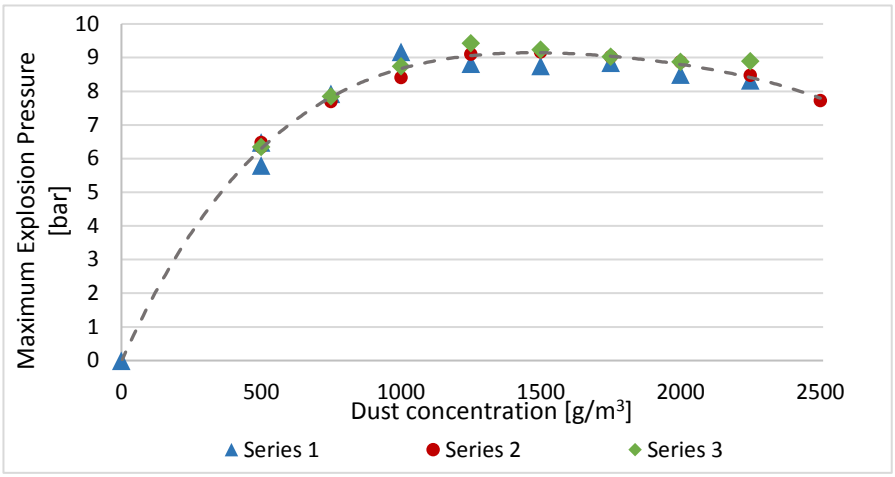

(a)

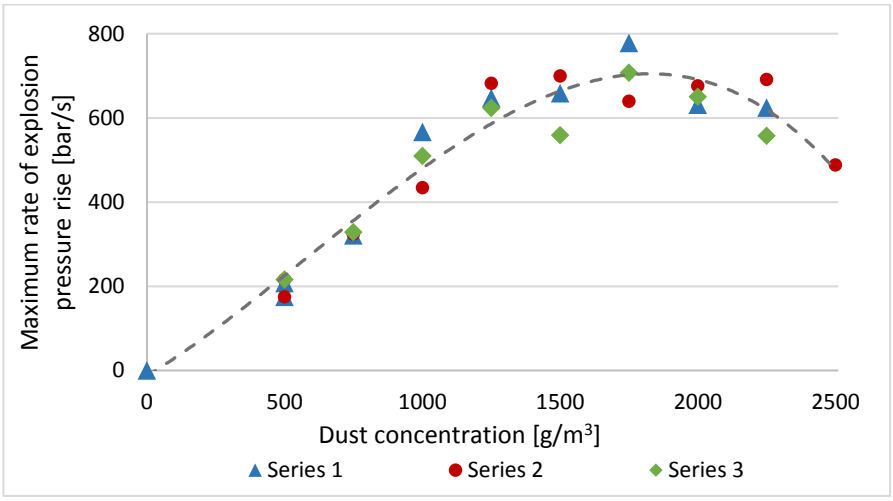

(b)

Figure E.2: *Series for maize starch containing 0.83 % moisture content. (a) Maximum explosion pressure and (b) maximum rate of explosion pressure rise. Tested in the 20-liter sphere.*

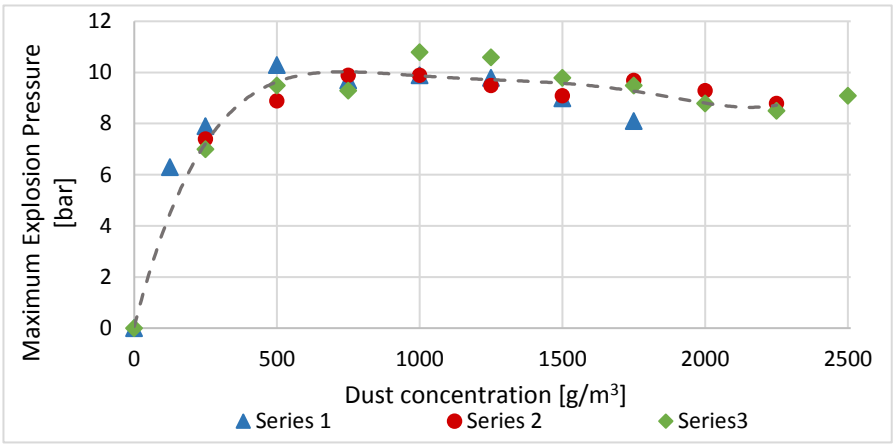

(a)

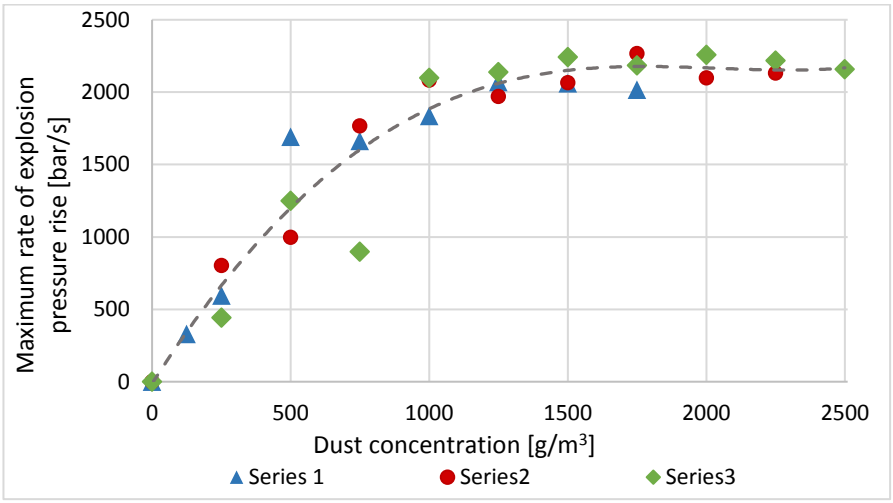

(b)

Figure E.3: *Series for aluminum. (a) Maximum explosion pressure and (b) maximum rate of explosion pressure rise. Tested in the 20-liter sphere.*

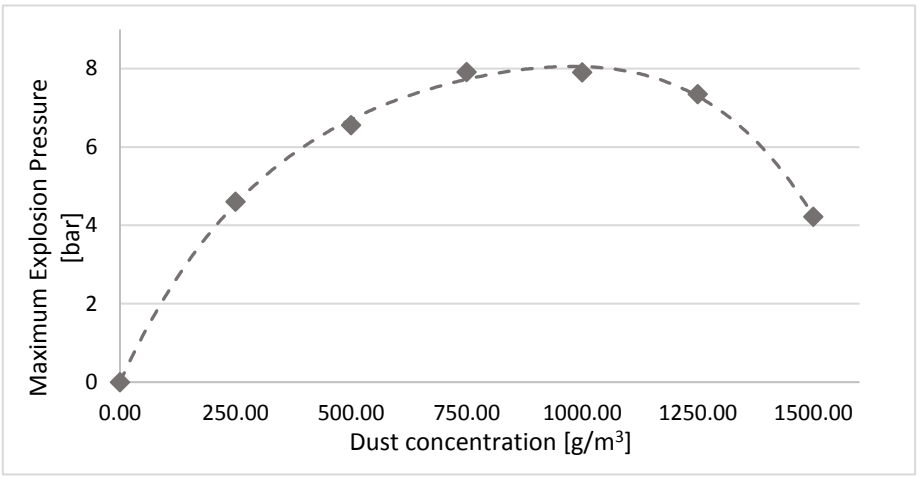

(a)

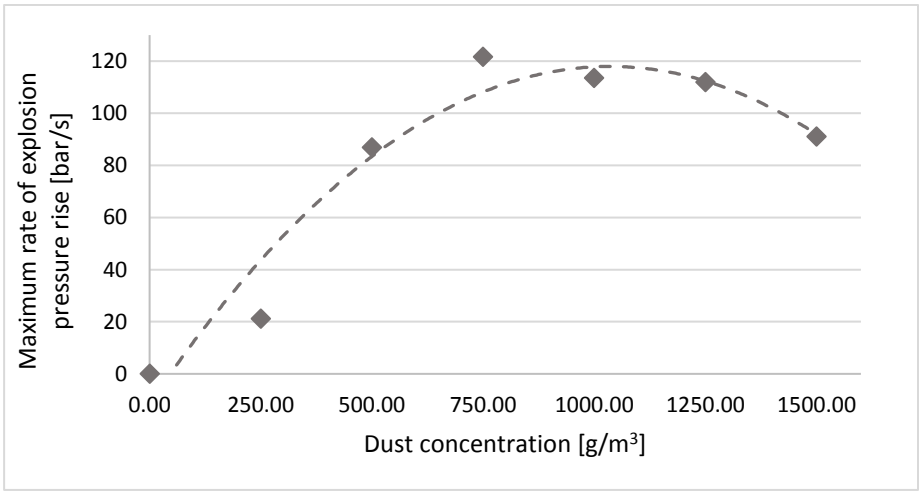

(b)

Figure E.4:

Series for maize starch containing 10.24 % moisture content. (a) Maximum explosion pressure and (b) maximum rate of explosion pressure rise. Tested in the 0.5 m^3 vessel.

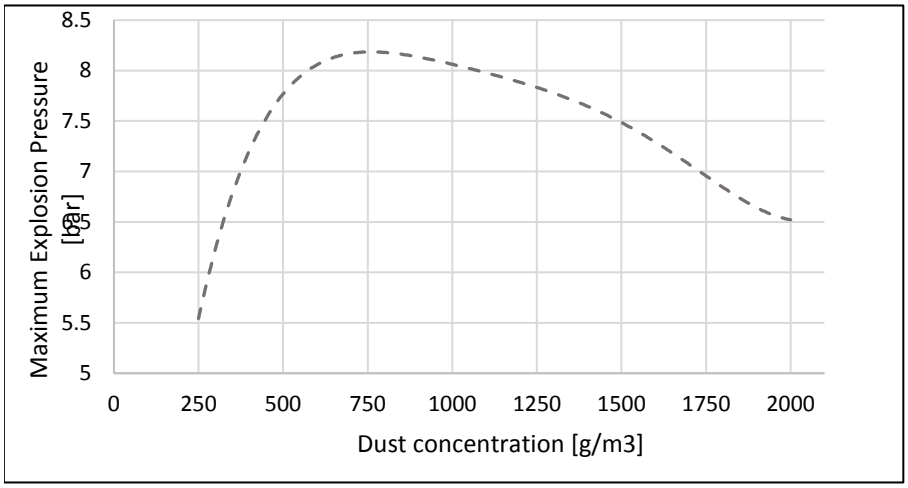

(a)

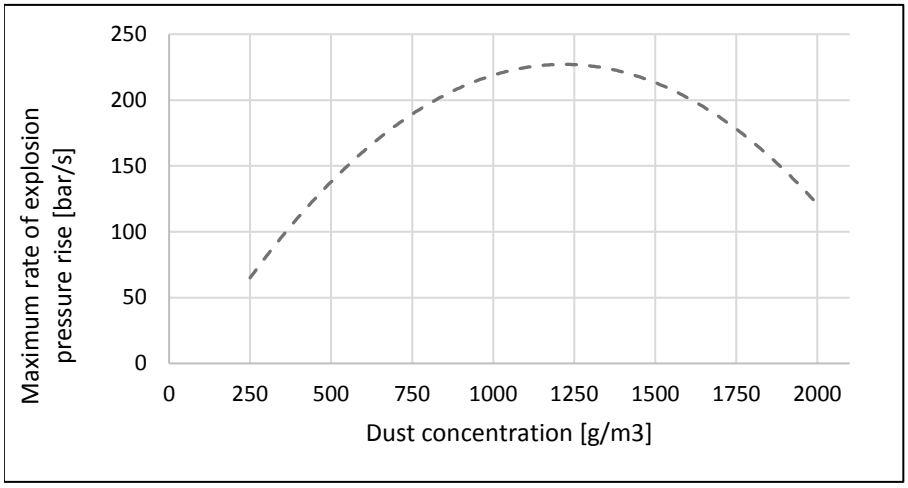

(b)

Figure E.5: *Series for maize starch containing ~3.5 % moisture content. (a) Maximum explosion pressure and (b) maximum rate of explosion pressure rise. Tested in the 0.5 m^3 vessel.*

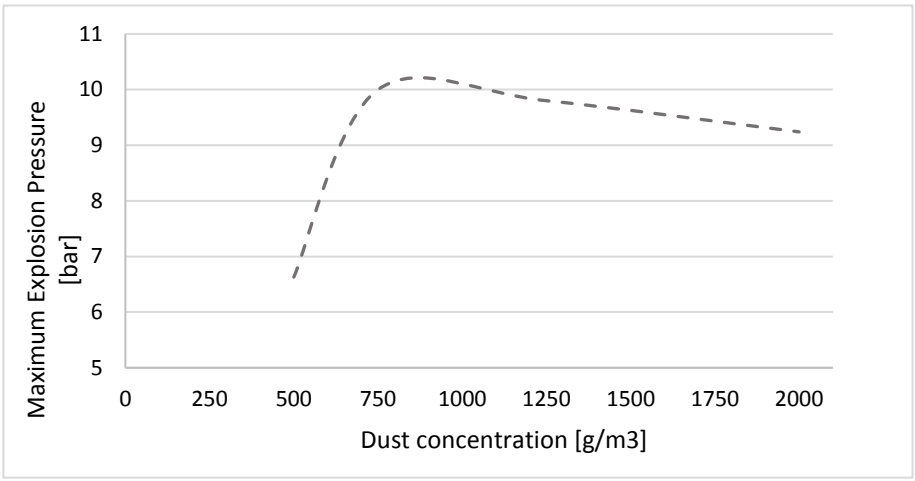

(a)

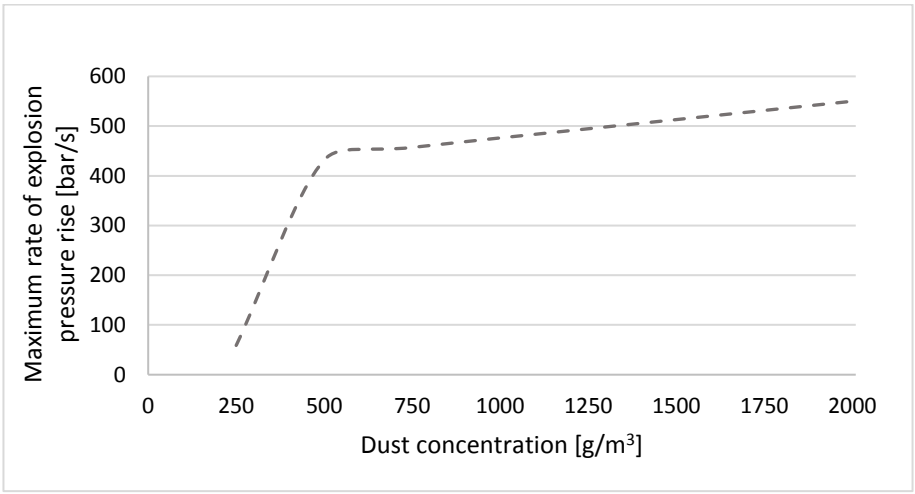

(b)

Figure E.6: *Series for aluminum. (a) Maximum explosion pressure and (b) maximum rate of explosion pressure rise. Tested in the 0.5 m^3 vessel.*

Appendix F Symposium WiPP Presentation

During the 37th International Symposium on Combustion in Dublin, Ireland, 29 July – 3 August 2018, a poster presentation of this thesis will be exhibited. The following abstract is sent to and approved by the Combustion Institute.

ID: 16779

EVALUATION OF FLAME PROPAGATION IN DUST CLOUDS IN 500-LITER AND 20-LITER SPHERICAL VESSELS

C. Engström Skavland [2], I.B. Kalvatn [1], B.J. Arntzen [2]

[1]*GexCon*

[2]*University of Bergen*

The maximum normalized pressure rise, $K_{St} = (\mathrm{d}p/\mathrm{d}t)_{\max} \cdot V^{1/3}$, is an experimental value obtained from combustion of dust clouds in spherical vessels with volume, V, together with the maximum pressure, p_{max}. These two values are seen to be representative for the burning velocity and the energy release of a specified dust and are used in design of dust explosion protection measures and equipment. The K_{St}-value depends on a range of factors like chemical composition, dust concentration, particle size distribution and turbulence intensity, but is assumed to be independent of volume, the so-called 'cube-root law'.

The aim of this study was to investigate the validity of the 'cube-root law' with regard to combustion of dusts from powders where thermal radiation is thought to be important. This is typically metal dusts like alumina which has a much higher flame temperature than organic dusts like maize starch. Thermal radiation can heat up particles faster and farther away from the reaction zone than thermal convection. This may lead to an increase of flame propagation velocity with radius. Standardized combustion tests were conducted in both 20-liter and 500-liter spherical vessels, for both maize starch and aluminum dust clouds, for a range of dust concentrations.